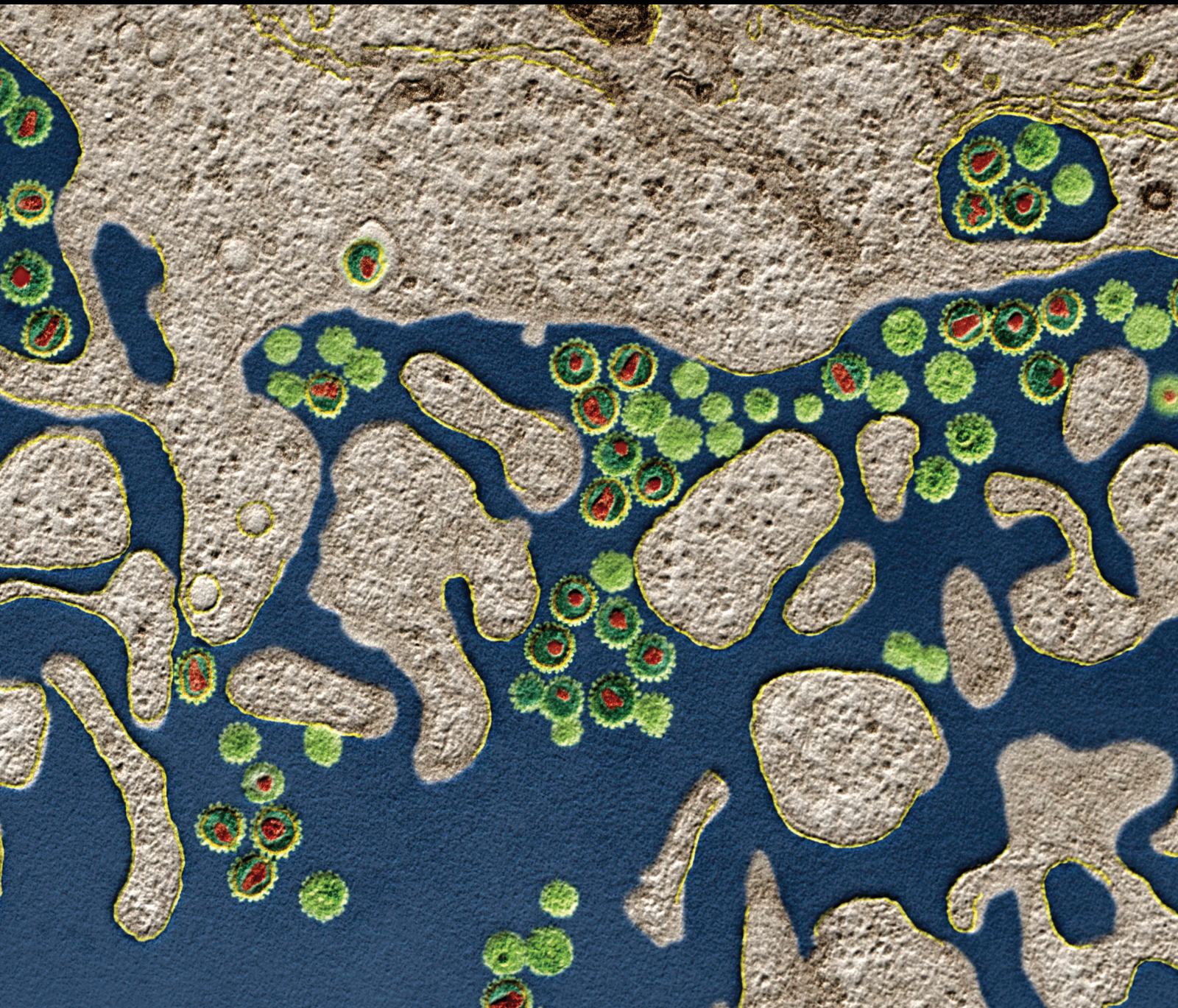


The Immune Microenvironment in Kidney Diseases

Lead Guest Editor: Cheng Yang

Guest Editors: Bin Yang and Liming Lu





The Immune Microenvironment in Kidney Diseases

Journal of Immunology Research

The Immune Microenvironment in Kidney Diseases

Lead Guest Editor: Cheng Yang

Guest Editors: Bin Yang and Liming Lu



Copyright © 2021 Hindawi Limited. All rights reserved.

This is a special issue published in "Journal of Immunology Research." All articles are open access articles distributed under the Creative Commons Attribution License, which permits unrestricted use, distribution, and reproduction in any medium, provided the original work is properly cited.

Associate Editors

Douglas C. Hooper , USA
Senthamil R. Selvan , USA
Jacek Tabarkiewicz , Poland
Baohui Xu , USA

Academic Editors

Nitin Amdare , USA
Lalit Batra , USA
Kurt Blaser, Switzerland
Dimitrios P. Bogdanos , Greece
Srinivasa Reddy Bonam, USA
Carlo Cavaliere , Italy
Cinzia Ciccacci , Italy
Robert B. Clark, USA
Marco De Vincentiis , Italy
M. Victoria Delpino , Argentina
Roberta Antonia Diotti , Italy
Lihua Duan , China
Nejat K. Egilmez, USA
Theodoros Eleftheriadis , Greece
Eyad Elkord , United Kingdom
Weirong Fang, China
Elizabeth Soares Fernandes , Brazil
Steven E. Finkelstein, USA
JING GUO , USA
Luca Gattinoni , USA
Alvaro González , Spain
Manish Goyal , USA
Qingdong Guan , Canada
Theresa Hautz , Austria
Weicheng Hu , China
Giannicola Iannella , Italy
Juraj Ivanyi , United Kingdom
Ravirajsinh Jadeja , USA
Peirong Jiao , China
Youmin Kang , China
Sung Hwan Ki , Republic of Korea
Bogdan Kolarz , Poland
Vijay Kumar, USA
Esther Maria Lafuente , Spain
Natalie Lister, Australia

Daniele Maria-Ferreira, Saint Vincent and the Grenadines

Eiji Matsuura, Japan
Juliana Melgaço , Brazil
Cinzia Milito , Italy
Prasenjit Mitra , India
Chikao Morimoto, Japan
Paulina Niedźwiedzka-Rystwej , Poland
Enrique Ortega , Mexico
Felipe Passero, Brazil
Anup Singh Pathania , USA
Keshav Raj Paudel, Australia
Patrice Xavier Petit , France
Luis Alberto Ponce-Soto , Peru
Massimo Ralli , Italy
Pedro A. Reche , Spain
Eirini Rigopoulou , Greece
Ilaria Roato , Italy
Suyasha Roy , India
Francesca Santilli, Italy
Takami Sato , USA
Rahul Shivahare , USA
Arif Siddiqui , Saudi Arabia
Amar Singh, USA
Benoit Stijlemans , Belgium
Hiroshi Tanaka , Japan
Bufu Tang , China
Samanta Taurone, Italy
Mizue Terai, USA
Ban-Hock Toh, Australia
Shariq M. Usmani , USA
Ran Wang , China
Shengjun Wang , China
Paulina Wlasiuk, Poland
Zhipeng Xu , China
Xiao-Feng Yang , USA
Dunfang Zhang , China
Qiang Zhang, USA
Qianxia Zhang , USA
Bin Zhao , China
Jixin Zhong , USA
Lele Zhu , China

Contents

An Immune Atlas of Nephrolithiasis: Single-Cell Mass Cytometry on SIRT3 Knockout and Calcium Oxalate-Induced Renal Injury

Wei Zhang , Ling Li, Ti Zhang, Xiaomin Gao, Zeyu Wang, Shaoxiong Ming, Ziyu Fang, Min Liu, Hao Dong, Baoyi Zhu, Junhao Liao, Jianwen Zeng , Yonghan Peng , and Xiaofeng Gao 
Research Article (15 pages), Article ID 1260140, Volume 2021 (2021)

Perilipin 2 Impacts Acute Kidney Injury via Regulation of PPAR α

Sujuan Xu , Edward Lee , Zhaoxing Sun , Xiaoyan Wang , Ting Ren , Zhouping Zou , Jifu Jin , Jie Li , Jian Zhang , Yingxiang Li , Qiang Yang , Yang Zhang , Man Guo , Yi Fang , and Xiaoqiang Ding 
Research Article (12 pages), Article ID 9972704, Volume 2021 (2021)

Uterine Sensitization-Associated Gene-1 in the Progression of Kidney Diseases

Xiaohu Li , Wenlong Yue , Guiwen Feng , and Jinfeng Li 
Review Article (6 pages), Article ID 9752139, Volume 2021 (2021)

A Novel Insight into the Role of PLA2R and THSD7A in Membranous Nephropathy

Pingna Zhang , Weijun Huang, Qiyang Zheng, Jingyi Tang, Zhaocheng Dong , Yuhua Jiang, Yuning Liu , and Weijing Liu 
Review Article (12 pages), Article ID 8163298, Volume 2021 (2021)

Predictive Significance of the Prognostic Nutritional Index (PNI) in Patients with Severe COVID-19

Wei Wei , Xingyue Wu , Chaoyuan Jin , Tong Mu , Guorong Gu , Min Min , Sucheng Mu , and Yi Han 
Research Article (11 pages), Article ID 9917302, Volume 2021 (2021)

HMSC-Derived Exosome Inhibited Th2 Cell Differentiation via Regulating miR-146a-5p/SERPINB2 Pathway

Jing Zhou, Yi Lu, Wei Wu, and Yunhai Feng 
Research Article (11 pages), Article ID 6696525, Volume 2021 (2021)

Research Article

An Immune Atlas of Nephrolithiasis: Single-Cell Mass Cytometry on SIRT3 Knockout and Calcium Oxalate-Induced Renal Injury

Wei Zhang ¹, Ling Li,¹ Ti Zhang,² Xiaomin Gao,¹ Zeyu Wang,¹ Shaoxiong Ming,¹ Ziyu Fang,¹ Min Liu,¹ Hao Dong,¹ Baoyi Zhu,³ Junhao Liao,³ Jianwen Zeng ³, Yonghan Peng ¹, and Xiaofeng Gao ¹

¹Department of Urology, Changhai Hospital, Naval Medical University, Shanghai 200433, China

²National Clinical Research Center of Kidney Diseases, Jinling Hospital, Nanjing University School of Medicine, Nanjing, 210002 Jiangsu, China

³Department of Urology, The Sixth Affiliated Hospital of Guangzhou Medical University, Qingyuan People's Hospital, Qingyuan, 511518 Guangdong, China

Correspondence should be addressed to Jianwen Zeng; zengjwen@gzhmu.edu.cn, Yonghan Peng; yonghanyhtl@163.com, and Xiaofeng Gao; gxfdoc@sina.com

Received 6 July 2021; Revised 25 September 2021; Accepted 23 October 2021; Published 20 November 2021

Academic Editor: B. Yang

Copyright © 2021 Wei Zhang et al. This is an open access article distributed under the Creative Commons Attribution License, which permits unrestricted use, distribution, and reproduction in any medium, provided the original work is properly cited.

Background. As a common urological disease with a high recurrence rate, nephrolithiasis caused by CaOx may elicit a strong immunologic response. We present a CyTOF-based atlas of the immune landscape in nephrolithiasis models to understand how the immune system contributes to, and is affected by, the underlying response caused by SIRT3 knockout and CaOx inducement. **Materials and Methods.** We performed a large-scale CyTOF analysis of immune cell abundance profiles in nephrolithiasis. The immunophenotyping data were collected from four different mouse models, including the SIRT3 wild-type or knockout, including and excluding CaOx inducement. Unsupervised analysis strategies, such as SPADE and viSNE, revealed the intrarenal resident immune components and the immune alterations caused by SIRT3 knockout and CaOx-induced renal injury. **Results.** An overview analysis of the immune landscape identified T cells and macrophages as the main immune cell population in nephrolithiasis models. Highly similar phenotypes were observed among CD4⁺ and CD8⁺ T cell subsets, including cells expressing Ki67, Ly6C, Siglec-F, and TCR β . Macrophages expressed a characteristic panel of markers with varied expression levels including MHC II, SIRP α , CD11c, Siglec-F, F4/80, CD64, and CD11b, indicating more subtle differences in marker expression than T cells. The SIRT3^{KO}/CaOx and SIRT3^{WT}/CaOx groups exhibited global differences in the intrarenal immune landscape, whereas only small differences existed between the SIRT3^{KO}/CaOx and SIRT3^{KO}/Ctrl groups. Among the major immune lineages, the response of CD4⁺ T cells, NK cells, monocytes, and M1 to CaOx inducement was regulated by SIRT3 expression in contrast to the expression changes of B cells, DCs, and granulocytes caused by CaOx inducement. The panel of immune markers influenced by CaOx inducement significantly varied with and without SIRT3 knockout. **Conclusion.** In a CaOx-induced nephrolithiasis model, SIRT3 has a critical role in regulating the immune system, especially in reducing inflammatory injury. The characteristic panel of altered immune clusters and markers provides novel insights leading to improved prediction and management of nephrolithiasis.

1. Introduction

Nephrolithiasis is a common urological disease with a nearly 50% recurrence rate within five years of the first occurrence. It has been reported that 80% of stones associated with the disease are composed of calcium, occurring as pure calcium

oxalate (CaOx) or mixed with calcium phosphate (CaP) [1]. The formation of nephrolithiasis starts with supersaturation and crystallization of CaOx in the renal tubular lumen [2]. The deposit of CaOx crystals adheres to injured and dead renal tubular epithelial cells, leading to further crystal aggregation [3]. Therefore, necrosis and apoptosis of renal tubular

epithelial cells are important in CaOx kidney stone formation.

Sirtuin 3 (SIRT3) is an NAD-dependent deacetylase that regulates acetylated substrate peptides, maintains energy homeostasis, and decreases ROS production and inflammation in proximal tubular epithelial cells [4]. Previous studies have shown that SIRT3 could prevent oxalate damage by promoting M2 polarization of macrophages and inhibiting cell death in renal tubular epithelial cells, indicating that SIRT3 has a protective role in the pathophysiology of nephrolithiasis [5].

Emerging data suggest that urinary CaOx could elicit a strong immunologic response. Kusmartsev et al. demonstrated that renal CaOx crystal deposits are usually surrounded, engulfed, and eventually disintegrated by tissue macrophages [6]. Furthermore, these activated macrophages release an array of cytokines and chemokines to attract circulating monocytes to the site of the injured tissue [7]. Similarly, Taguchi et al. recently demonstrated by renal papillary tip tissue biopsy that human CaOx stone formers have high amounts of tissue inflammatory markers [8]. However, macrophages may exhibit both proinflammatory and anti-inflammatory functions, depending on their phenotype and activation status.

Innovative single-cell technologies such as mass cytometry (CyTOF) can be used to comprehensively analyze the immune behavior in nephrolithiasis. In particular, CyTOF enables the simultaneous measurement of parameters previously presented at the single-cell level by combining metal isotope-labeled antibodies with mass spectrometry detection [9]. CyTOF has not been used in nephrolithiasis, which is associated with extensive immune alterations. In this study, we present a CyTOF-based atlas of the immune landscape in nephrolithiasis models. Unsupervised analysis strategies, such as SPADE and viSNE, are used to reveal the intrarenal resident immune components and the immune alterations caused by SIRT3 knockout and CaOx-induced renal injury.

2. Materials and Methods

2.1. Animal Models of Renal Injury. All animal experiments were performed in accordance with the Guidelines for the Care and Use of Laboratory Animals of the Laboratory Animal Ethics Committee of the Naval Medical University. SIRT3 knockout C57BL/6 mice were purchased from Shanghai Model Organisms Center, Inc. (Shanghai, China) and bred in an experimental animal room demonstrated to be specific-pathogen-free (SPF). For nephrolithiasis model establishment, mice received an intraperitoneal injection of 120 mg/kg glyoxylic acid (TCI Shanghai) for seven consecutive days, according to published protocols [10, 11]. Each mouse received 200 μ l of glyoxylic acid solution, which was made by dissolving 900 μ l of glyoxylic acid in 50 ml of 0.9% saline. Mouse kidneys were harvested 24 h after the last injection.

2.2. CyTOF Analysis of Immune Cells. All the kidney samples were processed in the same batch. CyTOF analysis was performed by PLTTech, Inc. (Hangzhou, China) according to a

published protocol [12]. The kidney tissue was dissociated into a single-cell suspension with a mixture of DNase I, collagenase IV, and hyaluronidase (Sigma-Aldrich). Immune cells were enriched using Percoll density gradient media (Sigma-Aldrich), and erythrocytes were fully removed using ACK Lysing Buffer (Sigma-Aldrich). Qualified samples were blocked and stained with a mixed panel of surface antibodies, followed by overnight fixation. After fixing with Fix & Perm Buffer (Fluidigm), the cells were incubated in an intracellular antibody mix. The signals of the stained cells were detected using a CyTOF system (Fluidigm). The types of immune cells were identified via nonlinear dimensionality reduction (t-SNE), followed by density clustering.

2.3. Statistical Analysis. The Mann–Whitney *U* test was used to compare the differences between the two test groups. One-way ANOVA was used to determine the differences among the three or four groups. Statistical significance was set at $P < 0.05$.

3. Results

3.1. Immunophenotyping of Nephrolithiasis Models Using Mass Cytometry. We performed a large-scale CyTOF analysis of immune cell abundance profiles in nephrolithiasis. Briefly, the immunophenotyping data were collected from four different mouse models, including SIRT3 wild-type or knockout, CaOx inducement, or noninducement (Supplementary Figure 1A). There were 5, 4, 5, and 5 mice, respectively, in SIRT3^{WT}/Ctrl, SIRT3^{WT}/CaOx, SIRT3^{KO}/Ctrl, and SIRT3^{KO}/CaOx groups. To confirm the efficiency of SIRT3 knockout and CaOx inducement, we performed von Kossa staining for calcium deposits and immunohistochemical staining for SIRT3, cleaved caspase-3, and BCL-2 in the kidney (Supplementary Figure 1B). Von Kossa staining revealed that SIRT3 knockout increased calcium deposits in the kidney, especially in the renal cortex. Consistently, immunohistochemical staining indicated that CaOx-induced renal injury was significantly enhanced by SIRT3 knockout. These results confirmed that high expression of SIRT3 was required to maintain renal homeostasis and protect against CaOx-induced cell death. We stained cells with a 42-antibody panel to identify different populations of naive, memory, effector, regulatory, and exhausted T cells, B cells, NK cells, monocytes, macrophages, DCs, and granulocytes (Figure 1(a)). A summary of the 42-antibody cocktail and output data from our mass cytometry experiments, including the total number and viability of cells collected for each sample, event counts detected by the instrument, and number of lives for analysis, is provided in Supplementary Figure 1C and 1D.

3.2. Overview Analysis of Immune Landscape in Nephrolithiasis Models. To partition the cells into distinct phenotypes, the PhenoGraph clustering algorithm was applied to illustrate the phenotypic adjacency of cells in a high-dimensional space. This analysis identified the main immune cell types (Figures 1(b) and 1(c)). Macrophages, T

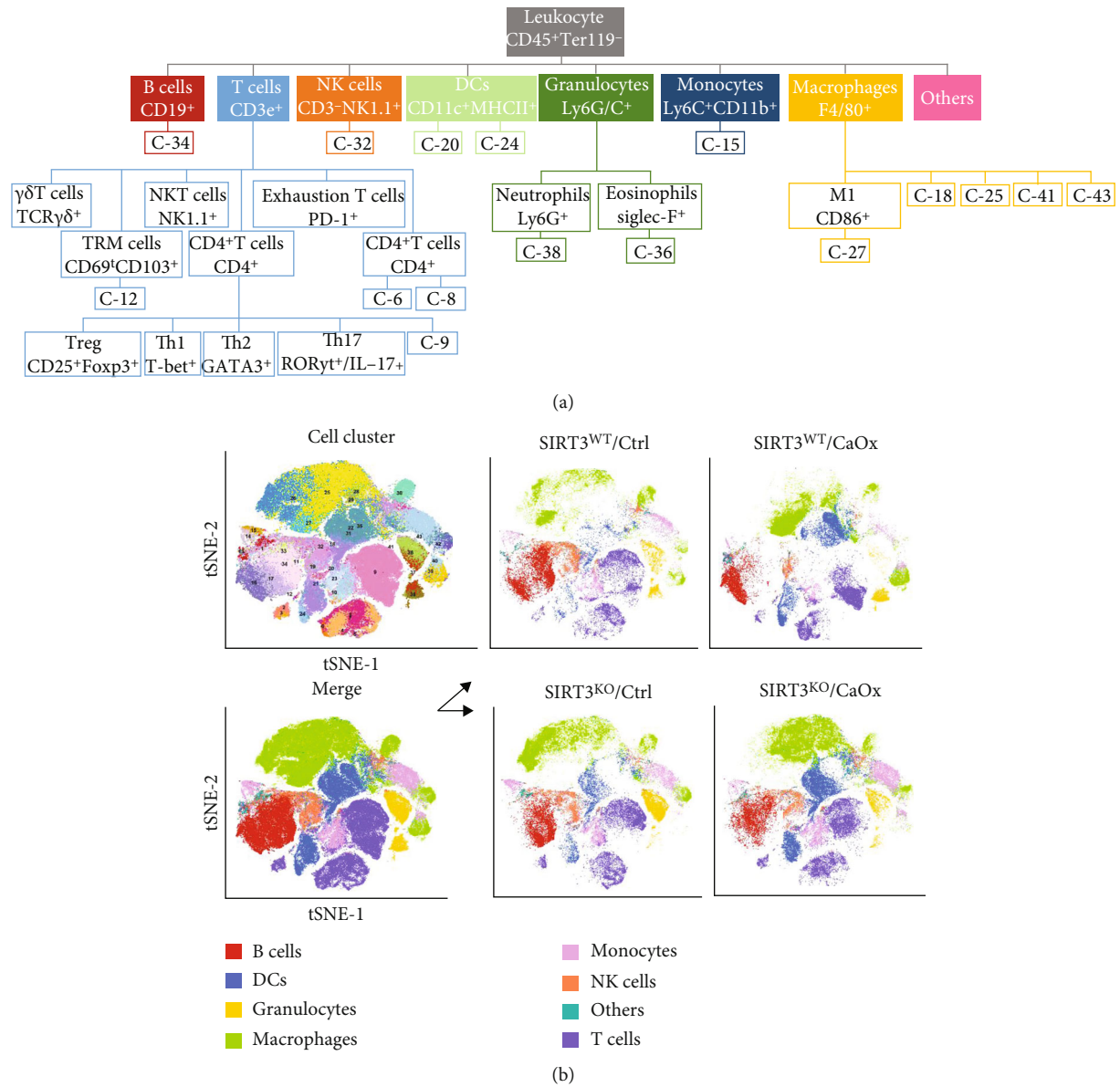


FIGURE 1: Continued.

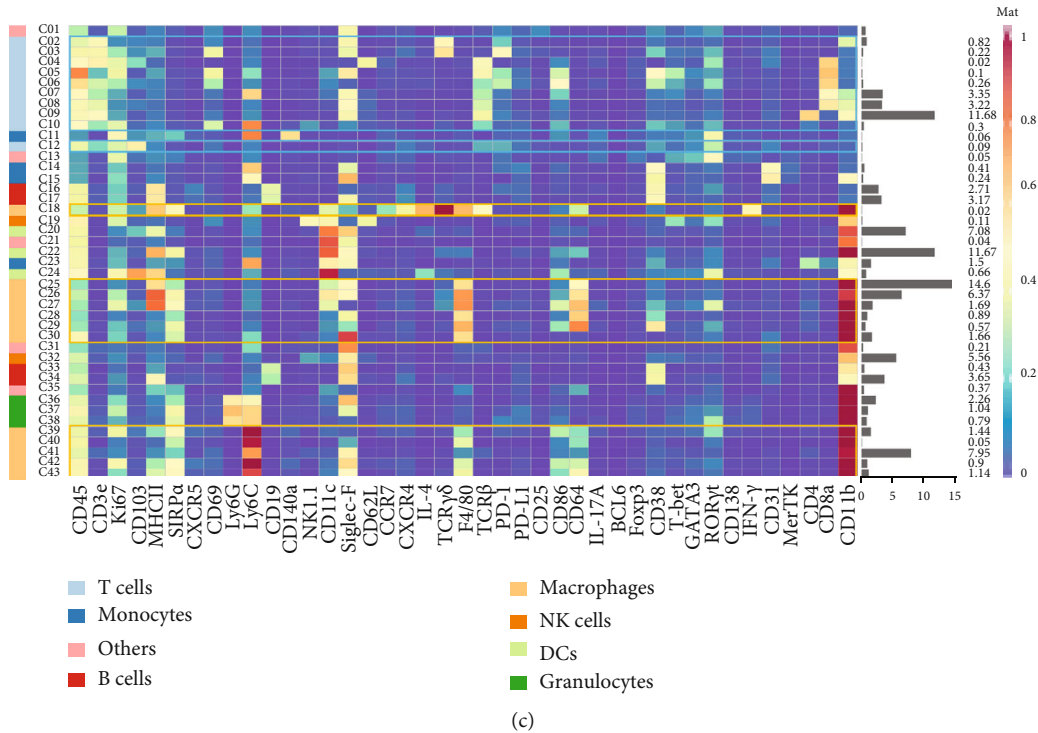


FIGURE 1: Characterization of immune cells in nephrolithiasis using mass cytometry. (a) Schematic showing how clusters are related to parent populations. (b) t-SNE maps displaying 9935 cells from the nephrolithiasis models analyzed with 42-antibody panel and colored by the main cell populations. (c) Heatmap showing normalized expression of the markers from 42-antibody panel for PhenoGraph clusters. Clusters are grouped by expression profiles, and cell types are indicated by color. The cluster IDs and relative frequencies are displayed as a bar graph on the left.

cells, and DCs accounted for the majority of the immune cell population in the nephrolithiasis models, respectively, with a mean of $27.7 \pm 6.7\%$, $21.8 \pm 4.4\%$, and $13.7 \pm 8.2\%$, respectively. The mean frequencies of B cells, monocytes, and NK cells were $12.8 \pm 5.7\%$, $9.7 \pm 2.9\%$, and $8.1 \pm 5.5\%$, respectively. Granulocytes constituted the minimum fraction in most samples ($4.8 \pm 3.4\%$).

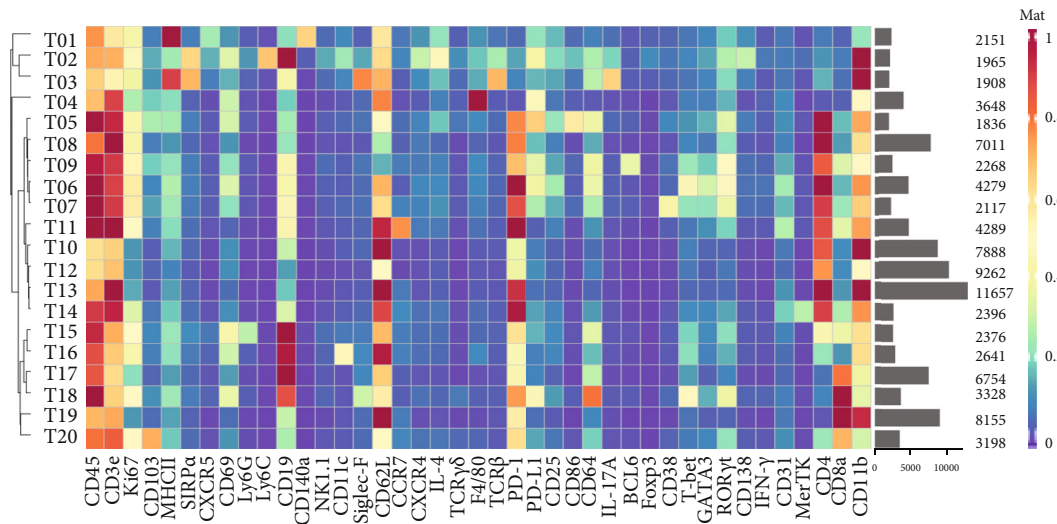
The CD19⁺ B cells were further classified into four subphenotypes (C-16, C-17, C-33, and C-34). The C-16 cluster was positive for MHC II, CD19, and CD38, while the C-17 cluster had the same expression pattern, except for the coexpression of Siglec-F. In addition, C-33 and C-34 cells also expressed moderate levels of CD11b. Among the CD3⁻ cells, two subphenotypes (C-19 and C-32) were defined as NK cells because of their positive NK1.1 status. The expression of other markers varied between them, as the C-19 cluster was positive for Ki67, CD11c, CD62L, and CD11b, while the C-32 cluster was positive for Siglec-F and CD11b. DCs characterized by CD11c⁺ MHCII⁺ were identified into three subphenotypes (C-20, C-22, and C-24). C-24 cells expressed high levels of Ki67 and CD103, whereas C-20 and C-22 cells were negative for these markers. For the Ly6G⁺/C⁺ granulocytes, three subphenotypes were defined as eosinophils (C-36 and C-37) and neutrophils (C-38) according to the expression status of Siglec-F. All three clusters were strongly positive for CD11b expression. Ly6C⁺CD11b⁺ monocytes also had four subphenotypes (C-11, C-14, C-15, and C-23). The C-11 and C-23 clusters characteristically expressed

CD140a and CD11c, respectively. Clusters C-14 and C-15 had the same expression pattern, including Siglec-F, CD38, and CD31, but with markers expressed at different levels.

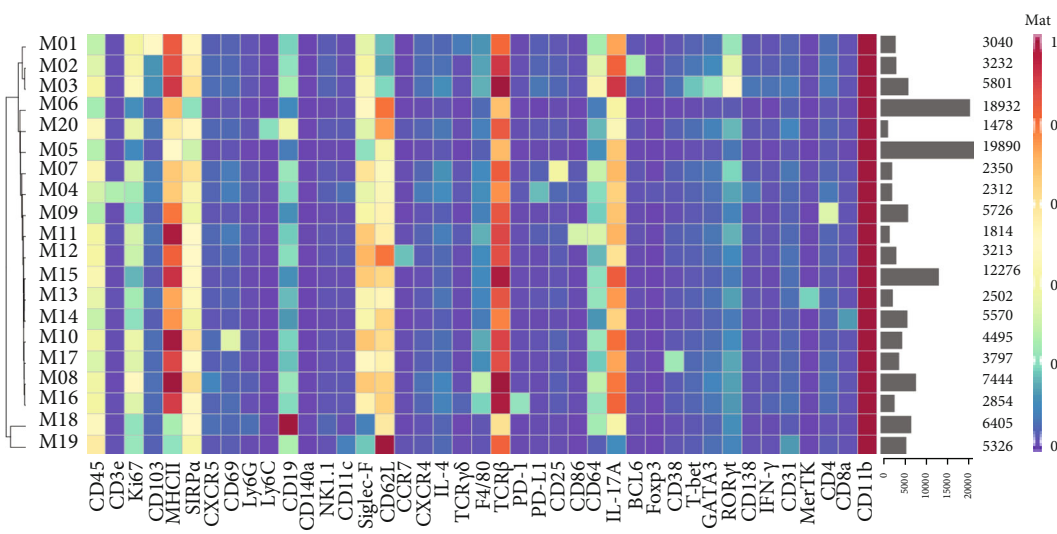
3.3. In-Depth Analysis of the Dominant Immune Phenotypes.

As the subsets of T cells, macrophages, and DCs are the dominant immune phenotypes, additional t-SNE and PhenoGraph analyses were performed to exhaustively map these cell phenotypes. These approaches identified the expression profiles of T cells as indicated in the following: 10 CD4⁺ phenotypes, four CD8⁺ phenotypes, one CD4/CD8 double-positive phenotype, and five double-negative phenotype (Figure 2(a) and Supplementary Figure 2A). We observed highly similar phenotypes among CD4⁺ and CD8⁺ subsets, including cells expressing Ki67, Ly6C, Siglec-F, and TCRβ. The subset of CD4⁺ helper T cells further consisted of clusters such as Treg (T07), Th1 (T06), Th2 (T05), and Th17 (T09). Five populations of CD3⁺ cells but CD4/CD8 double-negative cells were noted and were predominantly defined by the presence of Siglec-F and absence of TCRβ. However, some clusters also showed different features, such as the positive expression of PD-1, NK1.1, and TCRγδ, indicating exhaustion of T cells (T02), NKT cells (T16), and γδT cells (T04).

The identification of 20 macrophage phenotypes indicated that the macrophages had more subtle differences in marker expression than T cells (Figure 2(b) and Supplementary Figure 2B). The PhenoGraph analysis confirmed a



(a)



(b)

FIGURE 2: Continued.

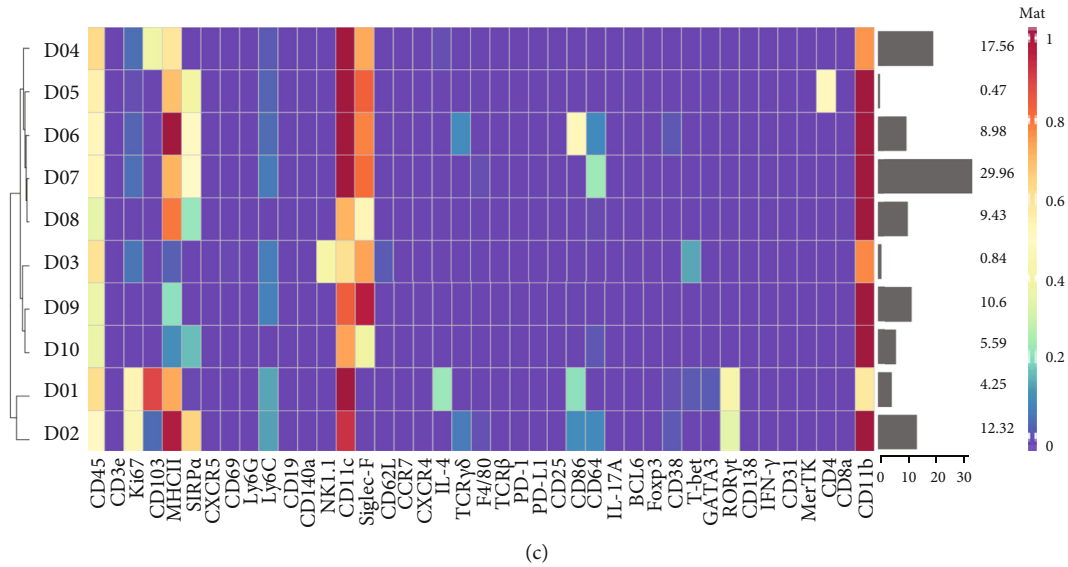


FIGURE 2: Identification of the dominant immune components in nephrolithiasis models. (a) Heatmap showing normalized expression of the 42-antibody panel markers for the 20 T cell clusters identified with PhenoGraph. (b) Heatmap showing normalized expression of the 42-antibody panel markers for the 20 macrophage clusters identified with PhenoGraph. (c) Heatmap showing normalized expression of the 42-antibody panel markers for the 10 DC clusters identified with PhenoGraph. Clusters are grouped by expression profile with the relative frequencies that are displayed as a bar graph on the right.

characteristic panel of markers with varied expression levels, including MHC II, SIRP α , CD11c, Siglec-F, F4/80, CD64, and CD11b. However, some macrophages may form a spectrum of phenotypically related cell subsets. For instance, M01, M02, and M03 were the only macrophage clusters with high levels of ROR γ t expression. Furthermore, M18 and M19 expressed relatively low levels of MHC II and CD11c compared to the other macrophage clusters. For subsets of DCs, a highly similar phenotype of Siglec-F expression was observed in addition to characteristic markers such as MHC II and CD11c (Figure 2(c) and Supplementary Figure 2C).

3.4. Correlation Analysis of Intrarenal Resident Immune Components. To systematically quantify the relationships between resident immune cell populations present in the kidney, we calculated the frequencies for each immune cell phenotype (Figure 3). Multiple robust relationships were first identified and presented in SIRT3 wild-type and CaOx-untreated models. Significant negative correlations were found between certain clusters (C07-09, C15, C20, C30-34, and C41) and the other clusters, indicating that they might be exposed to a similar milieu and tend to follow similar polarization schemes. In addition, the correlations between certain clusters (C02, C05, C17, C22, and C29) and the remaining clusters were reversed under CaOx inducement. However, the same correlation change induced by CaOx was not observed after SIRT3 knockout.

The influence of SIRT3 knockout and/or CaOx inducement on the frequency correlation of each expressed marker was also analyzed (Figure 4). Except for Siglec-F, CD11b, CD4, and CD8a, the majority of the 42 markers were positively correlated with each other in SIRT3 wild-type and

CaOx-untreated renal samples. Under CaOx inducement, the expression of CD4 and CD8a was positively correlated with that of most markers. In contrast, the expression of more markers such as CD31 and TCR β showed negative correlations with those of other markers after SIRT3 knockout combined with CaOx inducement.

3.5. Comparative Analysis of Immune Landscape between Nephrolithiasis Models. First, we applied viSNE to the immune landscape of four different groups, including SIRT3 wild-type or knockout, CaOx inducement, or noninducement (Figure 5(a)). The resulting t-SNE maps showed several differences in densities of particular localized regions, implying altered relative abundances of immune cell types and their subsets. The SIRT3^{KO}/CaOx and SIRT3^{WT}/CaOx groups exhibited global differences in the intrarenal immune landscape, whereas only small differences were observed between the SIRT3^{KO}/CaOx and SIRT3^{KO}/Ctrl groups. This indicates that in the CaOx-induced nephrolithiasis model, SIRT3 has a critical role in regulating the immune system, especially in reducing inflammatory injury. When the frequencies of immune lineages were further analyzed for each individual sample (Figure 5(b)), the SIRT3^{KO}/Ctrl group displayed the widest variability of immune cell population among samples, followed by the SIRT3^{WT}/Ctrl group. However, regardless of SIRT3 knockout, the CaOx-induced nephrolithiasis models had a small heterogeneity of immune cell types within its samples. This indicated that the influence of CaOx on the intrarenal immune components of each individual was consistent.

As shown in Figure 5(c), among the major immune lineages, the response of CD4⁺ T cells, NK cells, monocytes, M1, neutrophils, and eosinophils to CaOx inducement was

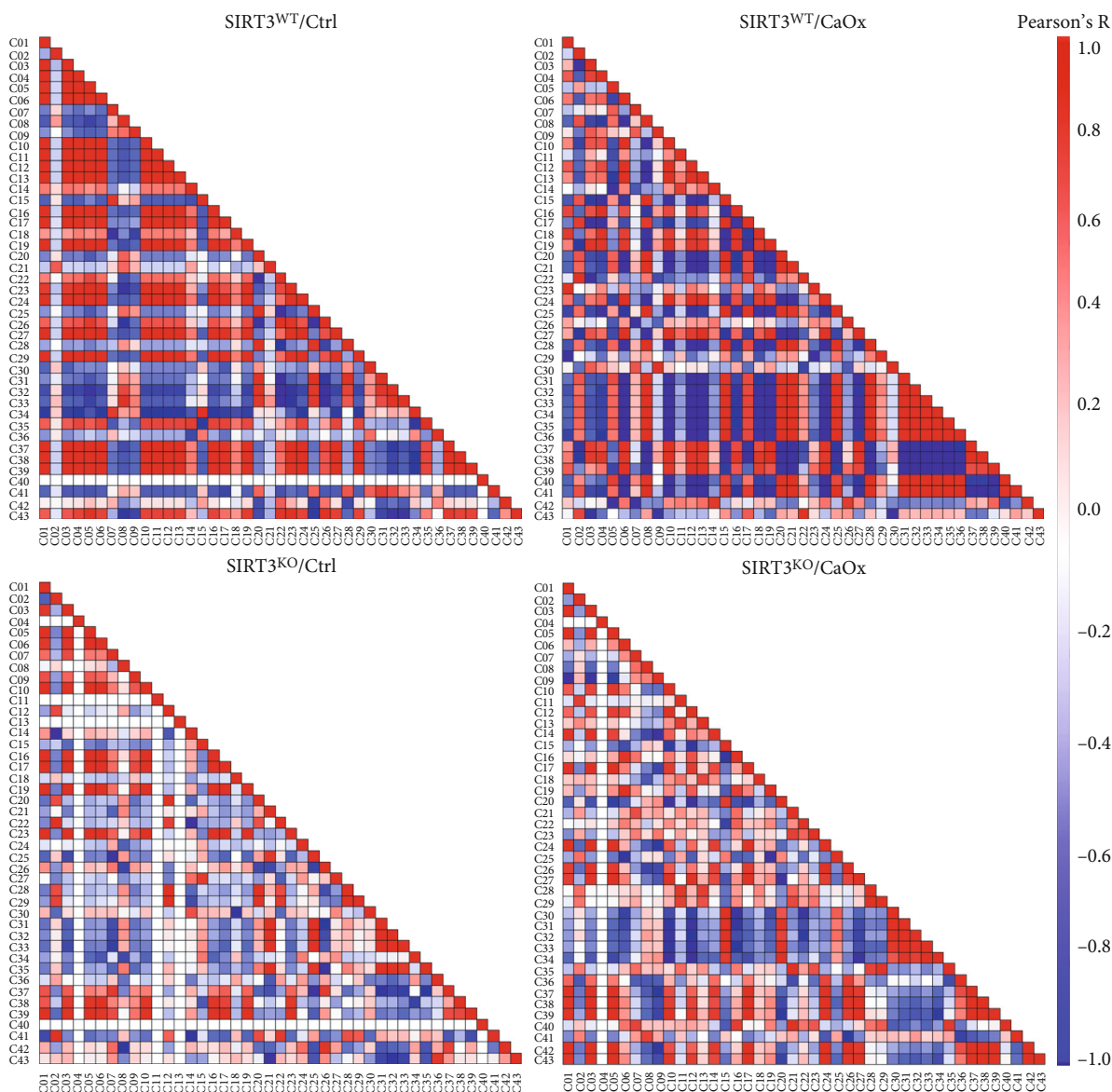


FIGURE 3: Heatmaps showing Pearson coefficients of correlation for relationships between immune cell phenotypes in four different models with SIRT3 wild-type or knockout and CaOx inducement or not.

regulated by SIRT3 expression. Furthermore, B cells and granulocytes with/without CaOx inducement were also altered by the SIRT3 genetic status. However, the response of B cells, DCs, and granulocytes to CaOx inducement was not influenced by SIRT3 expression, as the degree of expression changes was identical in SIRT3^{WT} and SIRT3^{KO} models. Interestingly, no significant changes in the cell abundance profile of CD8⁺ T cells and macrophages were detected after either CaOx inducement or SIRT3 knockout. As shown in Figure 6(a), a significantly higher abundance of both Th17 and Treg cells and a lower abundance of NKT cells were found in the SIRT3^{KO}/CaOx group. No statistically significant difference was found in frequency ratios of Th17 and Treg cells (1.43 ± 0.62 vs. 1.85 ± 0.18 vs. 1.43 ± 0.30 vs. 1.56 ± 0.46) among the four groups. However, upregulated abundance of $\gamma\delta$ T cells was seen

in both SIRT3^{KO}/CaOx and SIRT3^{WT}/CaOx groups. To further explore which subphenotypes were the dominantly affected, the cell abundances of the clusters identified by our markers were also analyzed (Figures 6(b)–6(d), Supplementary Figure 3). Among the four subtypes of T cells, three clusters (C09, C06, and C12) were found to be significantly lower in abundance in SIRT3^{KO}/CaOx relative to the SIRT3^{WT}/CaOx group, whereas the remaining one (C08) was more abundant in the SIRT3^{KO}/CaOx group (Figure 6(b)). Regarding the many subtypes of macrophages, there were three clusters (C25, C41, and C43) that were found to have significantly elevated abundance in SIRT3^{KO}/CaOx relative to the SIRT3^{WT}/CaOx group, whereas two clusters (C18 and C27), whose abundance changed in the opposite sense (Figure 6(c)). In addition, the expression difference could

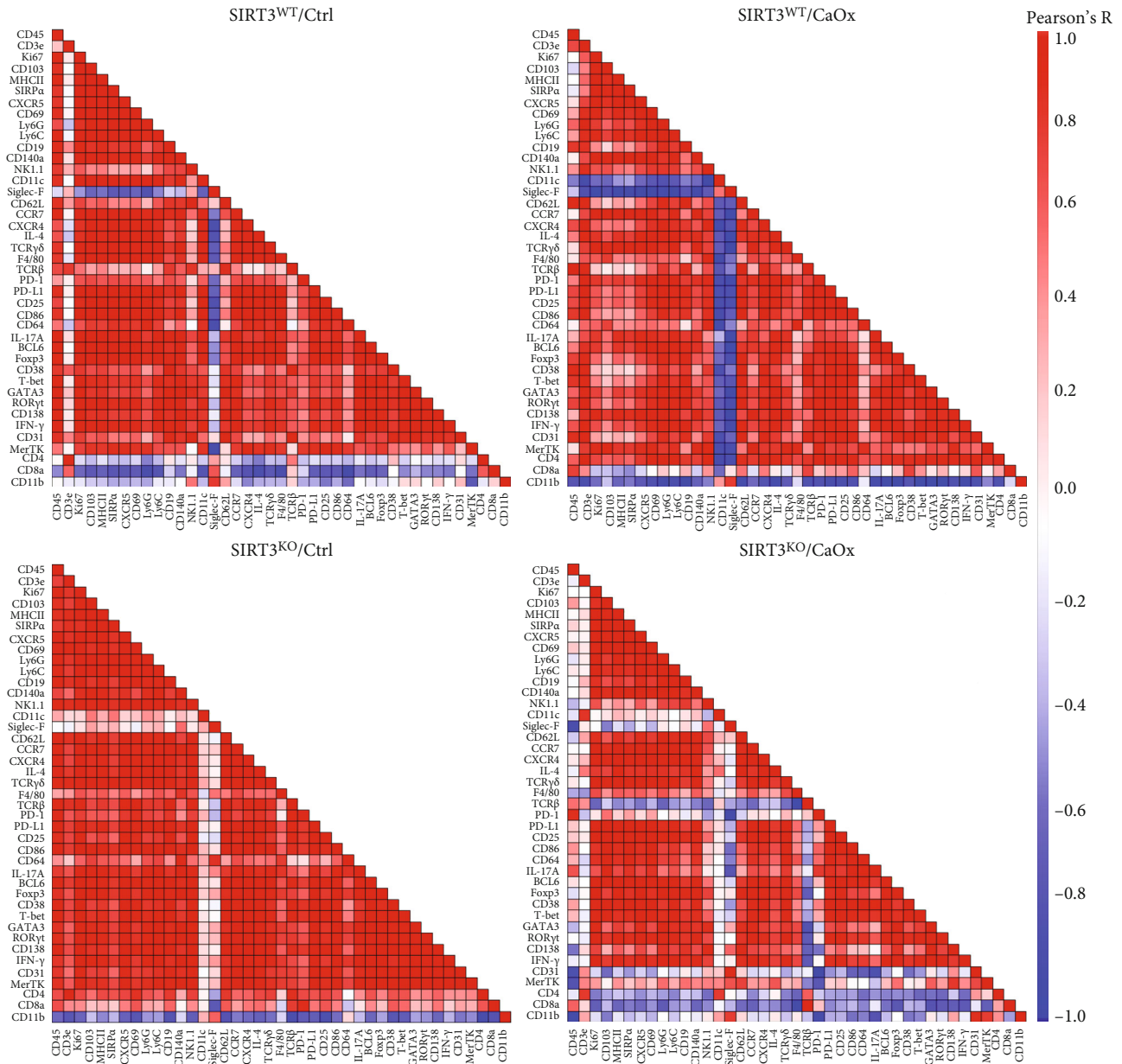


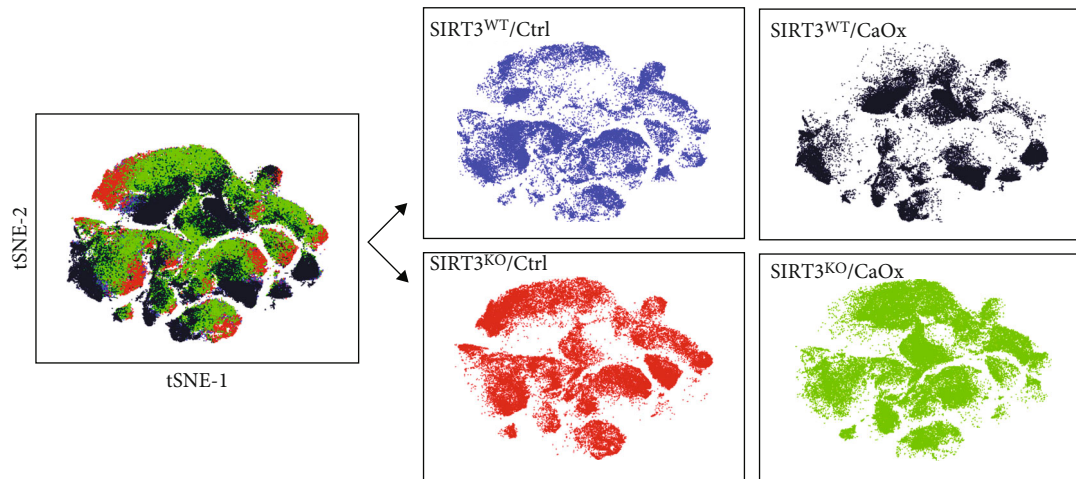
FIGURE 4: Heatmaps showing Pearson coefficients of correlation for relationships between expressed markers in four different models with SIRT3 wild-type or knockout and CaOx inducement or not.

also be significantly detected in subphenotypes of immune cells, including B cells (C34), DCs (C20, C24), and granulocytes (C36, C38) (Figure 6(d)).

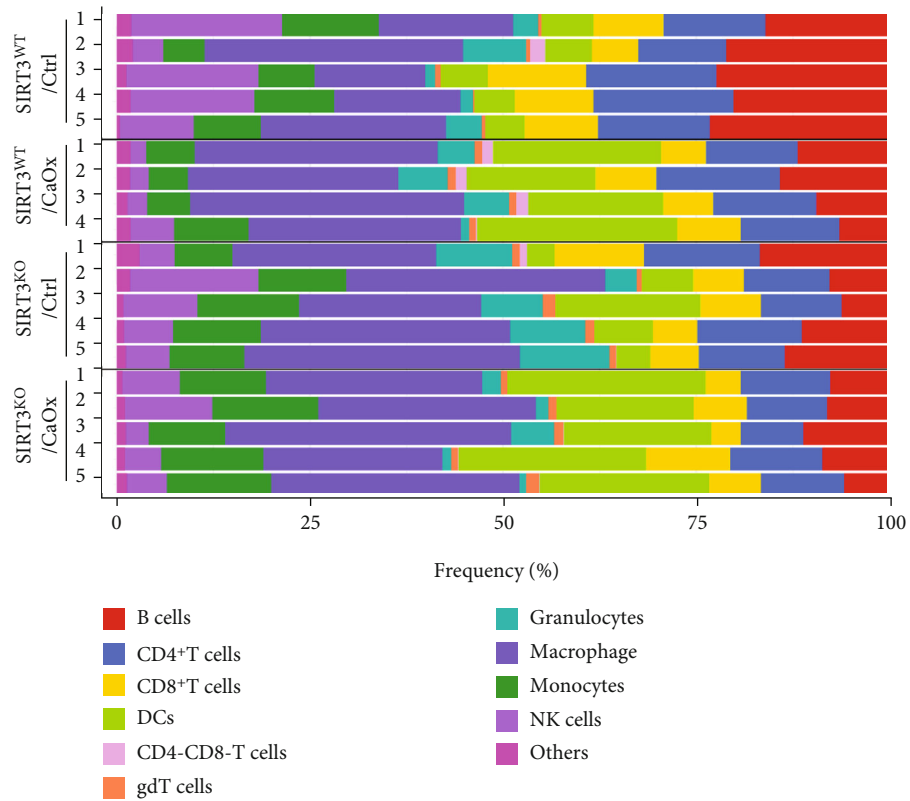
3.6. Expression Patterns of Immune Markers Associated with Nephrolithiasis Risk. Using CytoClusterR, the heterogeneity of the 42 detected marker signatures from four different groups, including SIRT3 wild-type or knockout, CaOx inducement, was clearly revealed on heatmaps (Figure 7(a)). Additionally, the normalized mean expression of the indicated markers was compared between the two groups (Figure 7(b)).

The comparison between SIRT3^{WT}/Ctrl and SIRT3^{KO}/Ctrl models indicated that SIRT3 knockout alone with-

out CaOx inducement had little effect on the expression levels of the markers from immune cells. In contrast, SIRT3 knockout upregulated Siglec-F and downregulated IL-17A, RORyt, and PD-1 levels in the CaOx inducement groups. Under the two situations with SIRT3 knockout or not, the panel of markers influenced by CaOx inducement varied to a great extent. In the SIRT3^{WT}/CaOx group, the expression of PD-1, IL-17A, RORyt, and CD103 was higher, while expression of CD19, Siglec-F, and CD62L was lower than that in the SIRT3^{WT}/Ctrl group (Supplementary Figure 5). However, in the SIRT3^{KO}/CaOx group, the expression of most markers such as Ly6G, CCR7, GATA3, and IFN-γ was lower than those in the SIRT3^{KO}/Ctrl group.



(a)



(b)

FIGURE 5: Continued.

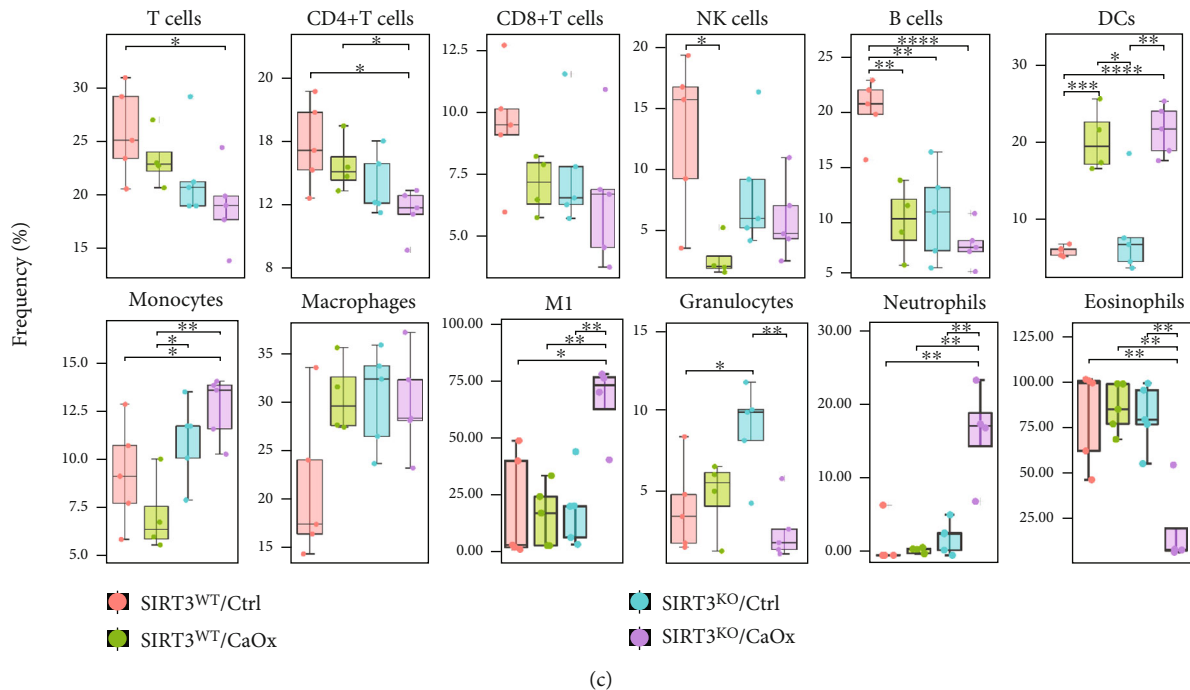


FIGURE 5: Immune cell population changes after SIRT3 knockout and CaOx inducement. (a) t-SNE maps displaying 9935 cells analyzed with 42-antibody panel and colored by different models. (b) Frequencies of 11 intrarenal immune cell populations for each nephrolithiasis sample. Cell types are indicated by color. (c) Boxplots showing the frequencies of indicated immune cell clusters among four different models with SIRT3 wild-type or knockout and CaOx inducement or not. * $P < 0.05$, ** $P < 0.01$, *** $P < 0.001$.

4. Discussion

As a cutting-edge, single-cell technology, CyTOF permits high multiparametric measurement of up to 50 metal isotope tags on a single cell simultaneously [13]. This innovation has been applied to understand the heterogeneity and complexity of cellular development [14], differentiation [15], and tumor immunology [16]. Our study is the first to identify distinct immune cell abundance profiles associated with nephrolithiasis through CyTOF-based immunophenotyping. A better understanding of the mechanisms relating the immune system and the underlying renal injury caused by SIRT3 knockout and CaOx inducement could provide novel insights leading to improved prediction and management of nephrolithiasis.

Several recent studies have reported the response of the immune system to CaOx crystals using cell culture and animal models. Dominguez et al. found that monocytes recognize CaOx crystals through a lipopolysaccharide-mediated mechanism, leading to their differentiation into inflammatory M1 macrophages [17]. However, Okada et al. indicated that monocyte-macrophage migration and phagocytosis play roles in the prevention of CaOx crystal formation in mouse kidneys [7]. In addition, two studies demonstrated that both androgen receptor knockout and SIRT3 overexpression could increase renal anti-inflammatory macrophage differentiation and decrease CaOx deposition in mouse models [5, 18]. Intrarenal macrophages participate in both inflammatory and anti-inflammatory processes by phagocytizing antigens in the microenvironment and undergoing phenotypic changes [19]. Overall, these results suggest

that the responses of the renal immune system to crystal formation are diverse and dynamic; consequently, the precise function of macrophages in kidney stone formation and elimination could not be determined. Therefore, a better understanding of which macrophages are proinflammatory or anti-inflammatory and the potential interaction mechanism between them will have more practical value.

In-depth immune profiling of this dominant immune phenotype using extensive antibody panels revealed the complexity of macrophage clusters and identified multiple disease-specific subsets. In our study, three of the four macrophage clusters positive for M1 markers CD86 (C27, C29, and C39) were found to be elevated by CaOx inducement, indicating that CaOx promoted M1 macrophage development. Furthermore, the other three clusters (C25, C28, and C41) were elevated by CaOx inducement only in SIRT3 knockout, suggesting that their inflammatory capabilities were suppressed by SIRT3. One cluster (C30) was regarded as a possible anti-inflammatory macrophage, because the abundance was downregulated after CaOx inducement. A genome-wide analysis of the CaOx nephrolithiasis model demonstrated in genetic level that immune reactivity through macrophage migration was involved in both calculi formation and elimination in mouse kidneys [20]. Further *in vivo* and *in vitro* studies have shown that M1 and anti-inflammatory M2 macrophages have opposing roles in nephrolithiasis [6]. In summary, these suggest the potential of immune-based therapies for urinary calculi.

Our study indicated that MHC II, SIRP α , CD11c, Siglec-F, F4/80, CD64, and CD11b were the characteristic panels of markers for interstitial macrophages. Other studies have also

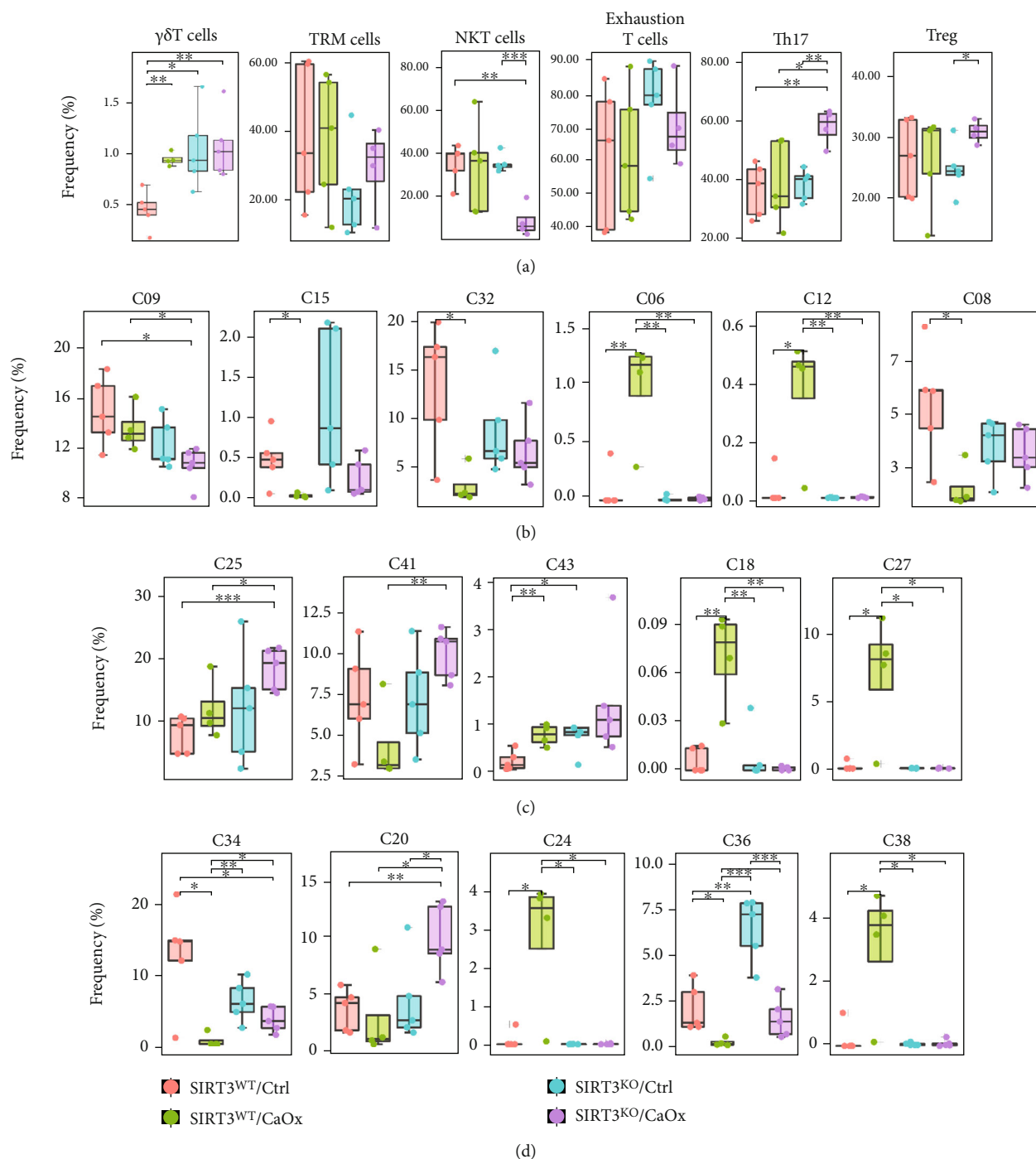


FIGURE 6: Subphenotypes of (a, b) T cells, (c) macrophages, and (d) other immune cell populations dominantly affected by SIRT3 knockout and CaOx inducement. **P* < 0.05, ***P* < 0.01, ****P* < 0.001.

reported changes in the expression level and potential biological capabilities of these immune molecules. During CaOx crystal formation, MHCII was immunohistochemically upregulated around crystal formation sites along with an increase in interstitial macrophages. Furthermore, the association analysis of the related gene expression by RT-PCR indicated a high association of CCL2, CD44, CSF-1, SPP-1, fibronectin 1, and TGF- β 1 with the amount of both renal crystals and F4/80, a mouse macrophage marker [7]. Inter-

estingly, the absolute number of renal interstitial macrophages did not increase constantly but fluctuated with the glyoxylate-induced crystal deposition process.

In the innate immune response, helper T cells play a prominent role by recognizing self-antigens, regulating cytokine production, and inducing humoral immunity [21]. As the two main subsets of helper T cells, Th1 and Th2 cells are regarded as inflammatory and anti-inflammatory helper T cells, respectively. Hsi et al. reported that Th1 cells drove

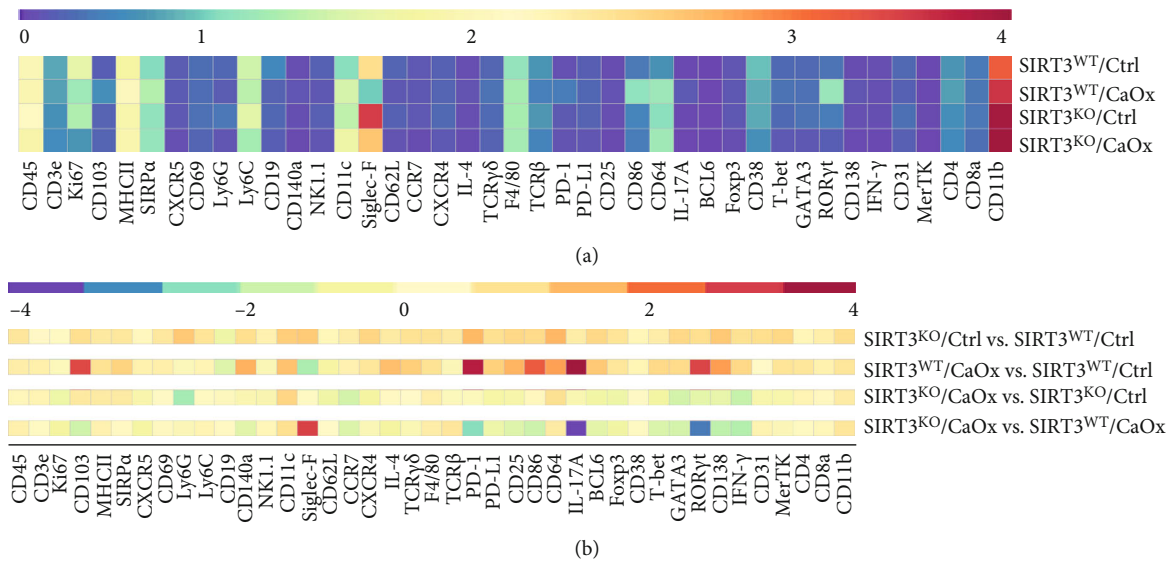


FIGURE 7: Expression patterns of immune markers associated with nephrolithiasis risk. (a) Heatmap showing the normalized median expression of indicated markers in immune cell populations of four different models with SIRT3 wild-type or knockout and CaOx inducement or not. (b) Heatmaps displaying the relative expression changes of indicated markers in immune cell populations between any two of the four different models.

the proinflammatory and Th2 anti-inflammatory responses in atherosclerosis, which have similar calcification lesions on vascular endothelial cells as urolithiasis [22]. In this study, we discovered that cluster T06, belonging to Th1, was more abundant in the CaOx inducement model than in the control model, although the difference was not statistically significant. RORγt⁺IL-17⁺ Th17 and FOXP3⁺CD25⁺ Treg cells are critical subsets of CD4⁺ T cells that are essential in immune homeostasis. The transcription factor FOXP3 is essential for Treg cell development and function (inhibition and suppression, self-tolerance), whereas transcription factor RORγt is also essential for Th17 cells (induction and propagation, tissue inflammation) [23]. The frequency intervention of Th17/Treg cells may provide new insights into the therapeutic targets of nephrolithiasis. In this study, we demonstrated that cluster T09 belonged to Th17, while cluster T07 belonged to Treg, and the ratio of T09/T07 was significantly increased after CaOx inducement.

In normal mouse kidneys, CD4/CD8 double-negative T cells were shown to comprise a higher percentage of the T cell population than those in other organs such as the liver and lungs [24]. Furthermore, CD4/CD8 double-negative T cells were discovered to have a pathogenic role in early renal injury after ischemia-reperfusion injury (IRI) [25]. γδT cells are a minor subset of T cells and are often thought to form a bridge between innate and adaptive immunity. Savransky et al. suggested that deficiency of γδT cells protected the kidney from IRI to a similar extent as deficiency of αβT cells [26]. In our study, the intrarenal γδT cell population was found to be increased in CaOx-induced nephrolithiasis compared to controls. Targeting this subphenotype with additional markers will be of interest in future research. NKT cells belong to a unique lymphocyte population expressing both NK receptors and TCRs and exert regulatory functions

by secreting cytokines such as IL-4, IL-10, IFN-γ, and NK1.1 [25]. However, NKT cells play conflicting roles in the process of renal injury. Li et al. showed that NKT cells contribute to the induction of early renal injury by mediating neutrophil IFN-γ production [27]. Another report by Yang et al. indicated that NKT cells, especially type II NKT cells, attenuated the severity of renal injury [28].

In this study, we discovered that the expression of Siglec-F and CD11b was negatively correlated with all the other markers in intrarenal resident immune cell populations. Siglec-F is conveniently used as a cell-specific marker of eosinophils. A recent study by Tateyama et al. showed that the expression of Siglec-F in bone marrow-derived macrophages could be stimulated by granulocyte-macrophage colony-stimulating factor (GM-CSF) first and then down-regulated upon prolonged GM-CSF stimulation. Furthermore, Siglec-F positively regulated the STAT6 signaling pathway as well as the expression of arginase-1 in IL-4-stimulated macrophages. These results suggested that Siglec-F was induced by GM-CSF and fine-tuned macrophage responses [29]. Alexander et al. suggested that knockout of CD11b on mononuclear cells could recruit more M1 macrophages and CD4⁺ T cells in glomerulonephritis, indicating that CD11b is instrumental in generating an anti-inflammatory response in the inflamed kidney [30]. Kitagawa et al. suggested that urinary CD11b might be a useful biomarker to estimate histopathological activity, particularly glomerular leukocyte accumulation, in lupus nephritis [31]. In addition, while renal tissue is not amenable to regular sampling, the peripheral immune system is easily accessible and well-suited for routine measurement. Therefore, the future of identifying high-risk populations with nephrolithiasis and predicting the recurrence possibility seems to rely on a panel of multiple urinary or peripheral immune markers.

The compelling evidence from our study and others demonstrates the role of the immune system in mediating renal CaOx calculi formation and pathogenesis. Thus, modulating the immune response, such as promoting M2 over M1 macrophages and inhibiting inflammation, might provide a means to prevent CaOx nucleation and renal injury. Investigating the relationship between the immune system and calculi disease may lead to a new era of nephrolithiasis [32]. Future studies on calculi formation and immune biology will identify immunotherapeutic targets for the treatment and prevention of nephrolithiasis [33].

With five individual samples (four in the SIRT3^{WT/-}-CaOx group) in each mouse model, our study was able to identify a number of immune cell subsets demonstrating altered abundance in CaOx inducement models relative to controls and in SIRT3 knockout models compared to wild-type models. However, the relatively small sample size could not eliminate the average variations that could hide high interindividual variations. Furthermore, the mechanism by which these altered immune cell types and their subsets are involved in the pathogenesis of SIRT3 knockout and CaOx-induced renal injury remains unclear. Lastly, further investigations are warranted to include a wider range of cell type-specific markers and more clinical samples to verify the novel biomarkers and immunotherapeutic targets for nephrolithiasis.

5. Conclusions

In summary, our research is the first to present a CyTOF-based atlas of the immune landscape in nephrolithiasis models to better understand how the immune system contributes to, and is affected by, the underlying renal injury caused by SIRT3 knockout and CaOx inducement. The data indicated that SIRT3 plays a critical role in regulating the immune system, especially in reducing inflammatory injury, in the CaOx-induced nephrolithiasis model. The characteristic panel of changed immune clusters and markers will provide novel insights leading to improved prediction and management of nephrolithiasis.

Data Availability

The authors can make data available on request through contacting the corresponding authors.

Disclosure

The funders had no role in study design, data collection and analysis, decision to publish, or preparation of the manuscript.

Conflicts of Interest

The authors declare that they have no competing interests.

Authors' Contributions

Xiaofeng Gao, Wei Zhang, Ling Li, Yonghan Peng, and Jianwen Zeng contributed to the conception and design.

Xiaofeng Gao, Yonghan Peng, and Jianwen Zeng contributed to the administrative support. Ti Zhang and Xiaomin Gao contributed to the provision of study materials or patients. Wei Zhang, Ling Li, Ti Zhang, Zeyu Wang, Shaoyong Ming, Baoyi Zhu, and Junhao Liao contributed to the collection and assembly of data. Wei Zhang, Ling Li, Ti Zhang, Yonghan Peng, Min Liu, and Hao Dong contributed to the data analysis and interpretation. All authors contributed to the manuscript writing. All authors contributed to the final approval of manuscript. Wei Zhang, Ling Li, and Ti Zhang have contributed equally to this work and share first authorship.

Acknowledgments

This work was sponsored by the National Natural Science Foundation of China (81670642, Xiaofeng Gao; 81974091, Xiaofeng Gao; 81500531, Yonghan Peng; 81802581, Wei Zhang), the National Key Research and Development Program of China (2017YFB1302804, Xiaofeng Gao), the Guangdong Provincial Science and Technology Plan Project (2017B030314108, Yonghan Peng), and the Naval Medical University Sailing Program (Wei Zhang).

Supplementary Materials

Supplementary 1. Supplementary Figure 1: (A) Experimental approach used in this study. (B) Von Kossa staining and immunohistochemical staining to confirm the efficiency of SIRT3 knockout and CaOx inducement. (C) Cell numbers and vitalities of single-cell suspension detected using a CyTOF system. (D) Markers used to characterize the immune cell phenotypes.

Supplementary 2. Supplementary Figure 2: (A) t-SNE map displaying 2096 cells from T cell clusters identified with PhenoGraph colored by cluster. (B) t-SNE map displaying 2792 cells from macrophage clusters identified with PhenoGraph colored by cluster. (C) t-SNE map displaying 1361 cells from DC clusters identified with PhenoGraph colored by cluster.

Supplementary 3. Supplementary Figure 3: complete presentation of immune cell subphenotype changes after SIRT3 knockout and CaOx inducement in all the intrarenal immune cells.

Supplementary 4. Supplementary Figure 4: complete presentation of immune cell subphenotype changes after SIRT3 knockout and CaOx inducement in (A) T cells, (B) macrophages, and (C) DCs.

Supplementary 5. Supplementary Figure 5: t-SNE maps displaying the most significant differentially expressed markers among four different models with SIRT3 wild-type or knockout and CaOx inducement or not.

References

- [1] E. M. Worcester and F. L. Coe, "Clinical practice. Calcium kidney stones," *The New England Journal of Medicine*, vol. 363, no. 10, pp. 954–963, 2010.

- [2] A. P. Evan, J. E. Lingeman, F. L. Coe et al., "Randall's plaque of patients with nephrolithiasis begins in basement membranes of thin loops of Henle," *The Journal of Clinical Investigation*, vol. 111, no. 5, pp. 607–616, 2003.
- [3] C. F. Verkoelen and A. Verhulst, "Proposed mechanisms in renal tubular crystal retention," *Kidney International*, vol. 72, no. 1, pp. 13–18, 2007.
- [4] M. D. Hirschey, T. Shimazu, E. Goetzman et al., "SIRT3 regulates mitochondrial fatty-acid oxidation by reversible enzyme deacetylation," *Nature*, vol. 464, no. 7285, pp. 121–125, 2010.
- [5] J. Xi, Y. Chen, J. Jing et al., "Sirtuin 3 suppresses the formation of renal calcium oxalate crystals through promoting M2 polarization of macrophages," *Journal of Cellular Physiology*, vol. 234, no. 7, pp. 11463–11473, 2019.
- [6] S. Kusmartsev, P. R. Dominguez-Gutierrez, B. K. Canales, V. G. Bird, J. Vieweg, and S. R. Khan, "Calcium oxalate stone fragment and crystal phagocytosis by human macrophages," *The Journal of Urology*, vol. 195, 4 Part 1, pp. 1143–1151, 2016.
- [7] A. Okada, T. Yasui, Y. Fujii et al., "Renal macrophage migration and crystal phagocytosis via inflammatory-related gene expression during kidney stone formation and elimination in mice: detection by association analysis of stone-related gene expression and microstructural observation," *Journal of Bone and Mineral Research*, vol. 25, no. 12, pp. 2701–2711, 2010.
- [8] K. Taguchi, S. Hamamoto, A. Okada et al., "Genome-wide gene expression profiling of Randall's plaques in calcium oxalate stone formers," *Journal of the American Society of Nephrology*, vol. 28, no. 1, pp. 333–347, 2017.
- [9] Y. Simoni, M. H. Y. Chng, S. Li, M. Fehlings, and E. W. Newell, "Mass cytometry: a powerful tool for dissecting the immune landscape," *Current Opinion in Immunology*, vol. 51, pp. 187–196, 2018.
- [10] A. Okada, S. Nomura, Y. Higashibata et al., "Successful formation of calcium oxalate crystal deposition in mouse kidney by intraabdominal glyoxylate injection," *Urological Research*, vol. 35, no. 2, pp. 89–99, 2007.
- [11] M. Hirose, K. Tozawa, A. Okada et al., "Glyoxylate induces renal tubular cell injury and microstructural changes in experimental mouse," *Urological Research*, vol. 36, no. 3–4, pp. 139–147, 2008.
- [12] G. Han, M. H. Spitzer, S. C. Bendall, W. J. Fantl, and G. P. Nolan, "Metal-isotope-tagged monoclonal antibodies for high-dimensional mass cytometry," *Nature Protocols*, vol. 13, no. 10, pp. 2121–2148, 2018.
- [13] S. C. Bendall, E. F. Simonds, P. Qiu et al., "Single-cell mass cytometry of differential immune and drug responses across a human hematopoietic continuum," *Science*, vol. 332, no. 6030, pp. 687–696, 2011.
- [14] S. C. Bendall, K. L. Davis, A. D. Amir el et al., "Single-cell trajectory detection uncovers progression and regulatory coordination in human B cell development," *Cell*, vol. 157, no. 3, pp. 714–725, 2014.
- [15] F. J. Hartmann, D. Mrdjen, E. McCaffrey et al., "Single-cell metabolic profiling of human cytotoxic T cells," *Nature Biotechnology*, vol. 39, no. 2, pp. 186–197, 2021.
- [16] E. Friebel, K. Kapolou, S. Unger et al., "Single-cell mapping of human brain cancer reveals tumor-specific instruction of tissue-invading leukocytes," *Cell*, vol. 181, no. 7, pp. 1626–1642.e20, 2020.
- [17] P. R. Dominguez-Gutierrez, S. Kusmartsev, B. K. Canales, and S. R. Khan, "Calcium oxalate differentiates human monocytes into inflammatory M1 macrophages," *Frontiers in Immunology*, vol. 9, p. 1863, 2018.
- [18] H. J. Anders, B. Suarez-Alvarez, M. Grigorescu et al., "The macrophage phenotype and inflammasome component NLRP3 contributes to nephrocalcinosis-related chronic kidney disease independent from IL-1-mediated tissue injury," *Kidney International*, vol. 93, no. 3, pp. 656–669, 2018.
- [19] P. J. Nelson, A. J. Rees, M. D. Griffin, J. Hughes, C. Kurts, and J. Duffield, "The renal mononuclear phagocytic system," *Journal of the American Society of Nephrology*, vol. 23, no. 2, pp. 194–203, 2012.
- [20] A. Okada, T. Yasui, S. Hamamoto et al., "Genome-wide analysis of genes related to kidney stone formation and elimination in the calcium oxalate nephrolithiasis model mouse: detection of stone-preventive factors and involvement of macrophage activity," *Journal of Bone and Mineral Research*, vol. 24, no. 5, pp. 908–924, 2009.
- [21] S. Guia and E. Narni-Mancinelli, "Helper-like innate lymphoid cells in humans and mice," *Trends in Immunology*, vol. 41, no. 5, pp. 436–452, 2020.
- [22] R. S. Hsi, A. J. Spieker, M. L. Stoller et al., "Coronary artery calcium score and association with recurrent nephrolithiasis: the multi-ethnic study of atherosclerosis," *The Journal of Urology*, vol. 195, 4 Part 1, pp. 971–976, 2016.
- [23] Z. Chen, F. Lin, Y. Gao et al., "FOXP3 and ROR γ t: transcriptional regulation of Treg and Th17," *International Immunopharmacology*, vol. 11, no. 5, pp. 536–542, 2011.
- [24] D. B. Ascon, M. Ascon, S. Satpute et al., "Normal mouse kidneys contain activated and CD3+CD4- CD8- double-negative T lymphocytes with a distinct TCR repertoire," *Journal of Leukocyte Biology*, vol. 84, no. 6, pp. 1400–1409, 2008.
- [25] H. R. Jang and H. Rabb, "Immune cells in experimental acute kidney injury," *Nature Reviews. Nephrology*, vol. 11, no. 2, pp. 88–101, 2015.
- [26] V. Savransky, R. R. Molls, M. Burne-Taney, C. C. Chien, L. Racusen, and H. Rabb, "Role of the T-cell receptor in kidney ischemia-reperfusion injury," *Kidney International*, vol. 69, no. 2, pp. 233–238, 2006.
- [27] L. Li, L. Huang, S. S. Sung et al., "NKT cell activation mediates neutrophil IFN-gamma production and renal ischemia-reperfusion injury," *Journal of Immunology*, vol. 178, no. 9, pp. 5899–5911, 2007.
- [28] S. H. Yang, J. P. Lee, H. R. Jang et al., "Sulfatide-reactive natural killer T cells abrogate ischemia-reperfusion injury," *Journal of the American Society of Nephrology*, vol. 22, no. 7, pp. 1305–1314, 2011.
- [29] H. Tateyama, Y. Murase, H. Higuchi et al., "Siglec-F is induced by granulocyte-macrophage colony-stimulating factor and enhances interleukin-4-induced expression of arginase-1 in mouse macrophages," *Immunology*, vol. 158, no. 4, pp. 340–352, 2019.
- [30] J. J. Alexander, L. D. Chaves, A. Chang, A. Jacob, M. Ritchie, and R. J. Quigg, "CD11b is protective in complement-mediated immune complex glomerulonephritis," *Kidney International*, vol. 87, no. 5, pp. 930–939, 2015.
- [31] A. Kitagawa, N. Tsuboi, Y. Yokoe et al., "Urinary levels of the leukocyte surface molecule CD11b associate with glomerular inflammation in lupus nephritis," *Kidney International*, vol. 95, no. 3, pp. 680–692, 2019.

- [32] B. Knudsen, "New frontiers in stone disease: immune cells," *The Journal of Urology*, vol. 195, 4 Part 1, pp. 825-826, 2016.
- [33] P. R. Dominguez-Gutierrez, E. P. Kwenda, S. R. Khan, and B. K. Canales, "Immunotherapy for stone disease," *Current Opinion in Urology*, vol. 30, no. 2, pp. 183-189, 2020.

Research Article

Perilipin 2 Impacts Acute Kidney Injury via Regulation of PPAR α

Sujuan Xu ^{1,2}, Edward Lee ¹, Zhaoxing Sun ¹, Xiaoyan Wang ¹, Ting Ren ¹,
Zhouping Zou ¹, Jifu Jin ^{1,3}, Jie Li ¹, Jian Zhang ^{1,4}, Yingxiang Li ¹, Qiang Yang ¹,
Yang Zhang ¹, Man Guo ¹, Yi Fang ^{1,5,6,7,8} and Xiaoqiang Ding ^{1,2,5,6,7,8}

¹Department of Nephrology, Zhongshan Hospital, Fudan University, Shanghai, China

²Human Phenome Institute, Fudan University, 825 Zhangheng Road, Shanghai, China

³Department of Cardiovascular Medicine, Shanghai East Hospital, Tongji University School of Medicine, Shanghai, China

⁴Institutes of Biomedical Sciences, Fudan University, Shanghai, China

⁵Shanghai Medical Center of Kidney Disease, China

⁶Kidney and Dialysis Institute of Shanghai, China

⁷Kidney and Blood Purification Key Laboratory of Shanghai, China

⁸Hemodialysis Quality Control Center of Shanghai, Shanghai, China

Correspondence should be addressed to Xiaoqiang Ding; 18111210033@fudan.edu.cn

Received 29 March 2021; Revised 5 July 2021; Accepted 17 August 2021; Published 9 September 2021

Academic Editor: Amar Singh

Copyright © 2021 Sujuan Xu et al. This is an open access article distributed under the Creative Commons Attribution License, which permits unrestricted use, distribution, and reproduction in any medium, provided the original work is properly cited.

Renal ischemia-reperfusion (I/R) can induce oxidative stress and injury via the generation of reactive oxygen species (ROS). Renal proximal tubular cells are susceptible to oxidative stress, and the dysregulation of renal proximal tubular cellular homeostasis can damage cells via apoptotic pathways. A recent study showed that the generation of ROS can increase perilipin 2 (Plin2) expression in HepG2 cells. Some evidence has also demonstrated the association between Plin2 expression and renal tumors. However, the underlying mechanism of Plin2 in I/R-induced acute kidney injury (AKI) remains elusive. Here, using a mouse model of I/R-induced AKI, we found that ROS generation was increased and the expression of Plin2 was significantly upregulated. An *in vitro* study further revealed that the expression of Plin2, and the generation of ROS were significantly upregulated in primary tubular cells treated with hydrogen peroxide. Accordingly, Plin2 knockdown decreased apoptosis in renal proximal tubular epithelial cells treated with hydrogen peroxide, which depended on the activation of peroxisome proliferator-activated receptor α (PPAR α). Overall, the present study demonstrated that Plin2 is involved in AKI; knockdown of this marker might limit apoptosis via the activation of PPAR α . Consequently, the downregulation of Plin2 could be a novel therapeutic strategy for AKI.

1. Introduction

Acute kidney injury (AKI) is a problem associated with rapid renal dysfunction and high mortality [1], which is often caused by renal ischemia-reperfusion (I/R) in clinics. Renal I/R injury (IRI) is characterized by the restriction of blood supply to the kidney followed by the restoration of blood flow. Currently, there are few therapies for IRI. I/R can induce oxidative stress and injure organs via the generation of reactive oxygen species (ROS). In IRI, the production of ROS remains high for 24h after reperfusion [2]. It was found that renal proximal tubular cells are susceptible

to this oxidative stress. The dysregulation of renal proximal tubular cellular homeostasis can damage cells via apoptotic pathways [3–5]. Therefore, managing ROS is an important target for the prevention and treatment of AKI.

The main cellular lipid droplet proteins are members of the perilipin family. There are five members of the perilipin family (Plin1–5), and these proteins have an amphipathic helical structure with large hydrophobic residues, which can bind tightly to the lipid droplet surface [6]. Each perilipin isoform has a different role, but few have been studied in the context of renal proximal tubular cells. Among them, perilipin 2 (Plin2) was the first lipid droplet surface protein

to be identified, and it has been considered the marker protein of lipid droplets. Plin2 interacts with many signaling pathways. It also affects the homeostasis of intracellular lipid metabolism and promotes the accumulation of intracellular lipids by regulating the PPAR α -RXRA and CREB-CREBBP pathways. The transcriptional coactivator CREB binding protein (CREBBP) is important for the function of CREB, and the overexpression of Plin2 increases CREBBP expression, which promotes CREB transcriptional activity, consequently enhancing CREB functions [7]. PPAR α is a free fatty acid receptor that plays an important role in maintaining the homeostasis of lipid metabolism. Plin2 activation can protect neutral lipids from hydrolysis by lipases, affecting the expression and activation of PPAR α [7, 8]. Plin2 also regulates lipophagy in the heart [9]. Furthermore, elevated levels of ROS increase Plin2 expression and promote lipid droplet formation in HepG2 cells [7]. Some evidence has also demonstrated an association between Plin2 expression and renal tumors [10–12]. However, the role of Plin2 in IRI has not been investigated to date.

In the present study, we found that the expression of Plin2 was upregulated in the kidneys of mice after I/R treatment. Furthermore, mitochondrial ROS generation and apoptosis were associated with I/R. In vitro, hydrogen peroxide treatment was found to increase the expression of Plin2 and the generation of ROS in primary tubular cells. Moreover, Plin2 knockdown decreased apoptosis after hydrogen peroxide treatment, which was dependent on the activation of PPAR α . Collectively, we suggest that a Plin2 inhibitor may be a promising treatment for IRI, functioning through the inhibition of oxidative stress.

2. Materials and Methods

2.1. AKI Animal Model Induced by I/R. The animal experiments were approved by the Animal Care and Use of Committee of Zhongshan Hospital and performed in accordance with the National Institutes of Health Guide for the Care and Use of Laboratory Animals. Male C57BL/6 mice (8–10 weeks old) were obtained from the Animal Center of Jiesijie company. The I/R procedure was performed with bilateral renal pedicles clamped for 30 min, and the animal body temperature was maintained at 36–37°C. The sham group underwent the same process except the pedicles were not clamped [13].

2.2. Chemicals and Reagents. The anti-Plin2 antibody (NB110-40877) anti-PPAR α antibody (NBP2-76958) were obtained from NOVUS. The anti-Bax (14796), anti-Bcl-2 (3498), anti-pro-Caspase-3 (9662), and anti-cleaved-Caspase-3 (9664) antibodies were obtained from Cell Signaling Technology. Plin2 overexpression adenoviruses (Ad-Plin2), green fluorescent protein- (GFP-) expressing control adenoviruses (Ad-GFP), Plin2 knockdown adenoviruses, and control adenoviruses were obtained from Heyuan Biotechnology. The terminal deoxynucleotidyl transferase dUTP nick-end labeling (TUNEL) assay kit was purchased from Beyotime Biotechnology.

2.3. Culture of Primary Mouse Proximal Tubular Cells. Male C57BL/6 mice (6–8 weeks) were euthanized via intraperitoneal injection of sodium pentobarbital. The kidneys were dissected and transferred to Hank's salt solution. The kidney capsule was removed, and the renal cortex dissected and transferred to Hank's salt solution and minced. The minced cortex tissue was then digested in enzyme solution (1 ml Hank's salt solution with 0.75 mg collagenase and 0.75 mg trypsin inhibitor) for 60 min at 37°C. The cells were then mechanically separated from the digested tissue by being forced through a 40 μ m mesh. The cells were centrifuged at 50 \times g for 2 min and washed with a culture medium. The cell suspension was transferred to a Percoll density gradient and centrifuged at 14,000 rpm for 1 h. The uppermost cells were the proximal tubular cells. Finally, the cells were seeded into six-well plates at a density of 5.0×10^5 cells per well. Cell viability was determined using the trypan blue exclusion method. Confocal immunofluorescence was performed to detect primary mouse proximal tubular cells marker AQP1 (Supplemental Figure 1).

2.4. Serum Creatinine Quantification. Creatinine levels were evaluated in 30 μ l of serum from each mouse using the QuantiChromTM Creatinine Assay Kit (Bio Assay Systems, Hayward, CA, USA) following the manufacturer's instructions.

2.5. TUNEL Assay. Cell apoptosis was detected in paraffin-embedded kidney tissue sections using the commercially available TUNEL assays kit according to the manufacturer's instructions. Nuclei were stained with 4',6-diamidino-2-phenylindole (DAPI). The number of TUNEL-positive cells in five random areas per slide was counted using an Olympus FV1000 confocal microscope. Apoptotic cells were identified as green fluorescent cells.

2.6. Flow Cytometry. The ratio of apoptotic cells to total cells was determined by flow cytometric analysis using an Annexin V-FITC/7-AAD kit (KGA1023-1026, Kaiji Biotechnology) according to the manufacturer's instructions.

2.7. Western Blot Analysis. Protein was extracted from primary proximal tubular cells or kidneys using a lysis buffer (RIPA P0013B, Beyotime Biotechnology) containing protease inhibitor phenylmethylsulfonyl fluoride (PMSF) and PPI. Aliquots of the protein samples (30 ~ 80 μ g) were mixed with 5 \times loading buffer, separated on 10% (wt/vol) SDS/PAGE gels, and transferred to nitrocellulose membranes. Then, the membranes were blocked with 10% (wt/vol) nonfat skim milk at room temperature for 1 h and incubated with primary antibodies at 4°C overnight. The primary antibodies used were rabbit anti-Plin2 (1:1000), rabbit anti-Bax (1:1000), rabbit anti-Bcl-2 (1:1000), rabbit anti-Caspase-3 (1:1000), rabbit anti-cleaved Caspase-3 (1:1000), rabbit anti-PPAR α (1:1000), and mouse anti- β -actin (1:1000). After three washes of 10 min each with Tris-buffered saline containing Tween 20 (TBS-T), the membranes were incubated for 1 h at room temperature with 1:10000 horseradish peroxidase- (HRP-) conjugated secondary antibodies. Detection of the bound antibody was

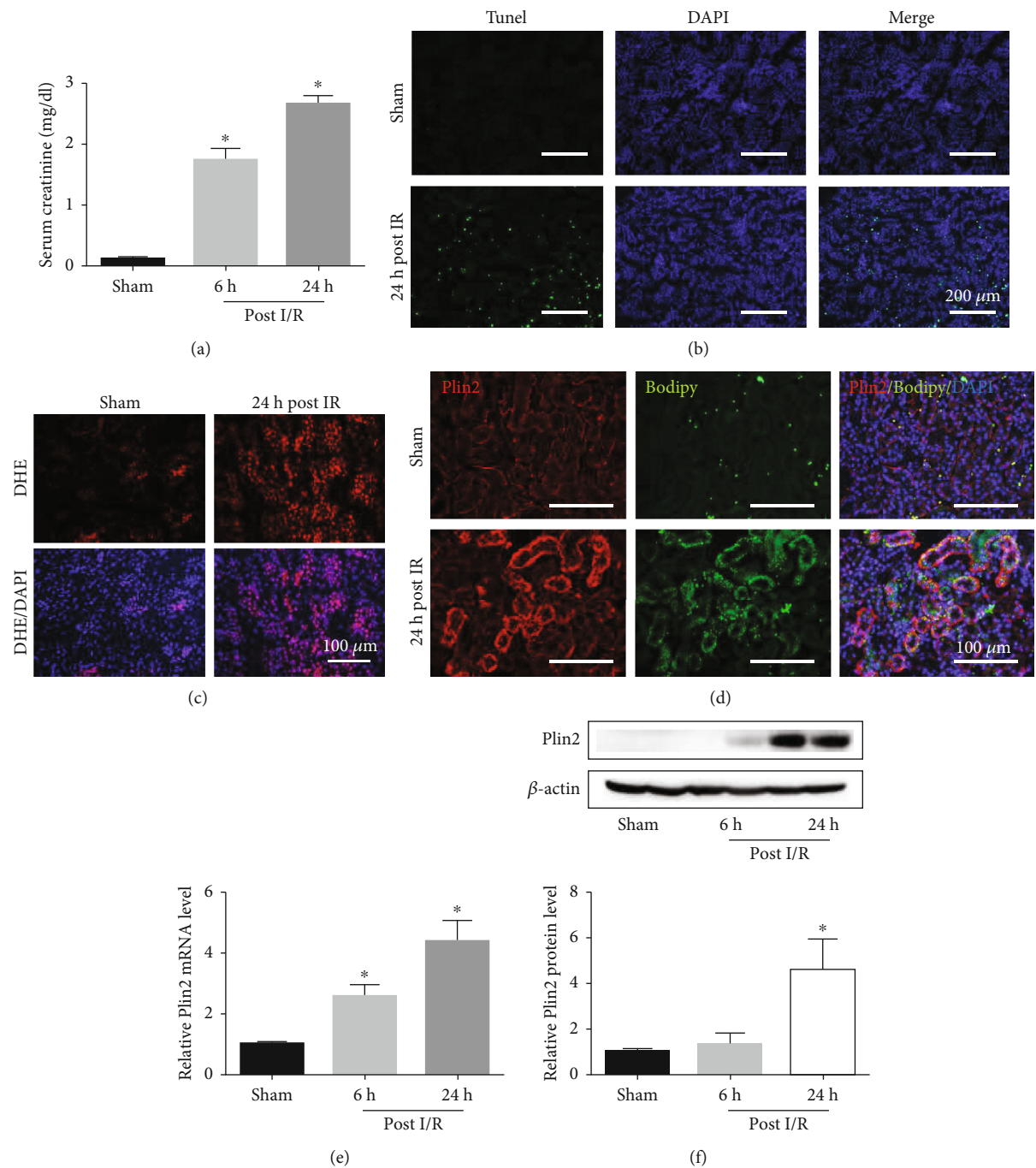


FIGURE 1: I/R-induced Plin2 upregulation and AKI. Eight-week-old C57/BL6 mice were treated with I/R and euthanized after 0, 6, and 24 h. (a) Serum creatinine (SCr) levels in the different groups of mice ($n = 4-5$). (b) Representative terminal deoxynucleotidyl transferase-mediated dUTP nick end-labeling (TUNEL) staining of kidney sections 24 h after renal IR ($n = 5$). (c) Representative images of dihydroethidium (DHE) staining of reactive oxygen species (ROS) generation of kidney sections 24 h after renal IR ($n = 5$). (d) Costaining for Plin2 and lipid droplet in kidney sections 24 h after renal IR ($n = 5$). (e) Quantitative RT-PCR analysis of Plin2 mRNA expression in the different groups of mice after renal IR ($n = 5$). (f) Western blot analysis of Plin2 expression in the different groups of mice after renal IR ($n = 3$). * $P < 0.05$ vs. sham mice. Data are presented as mean \pm SEM. h: hour; IR: ischemia reperfusion.

carried out using a chemiluminescence substrate. Protein expression levels were quantified using ImageJ software.

2.8. Real-Time PCR. Total RNA was extracted from mouse tissues or primary mouse proximal tubular epithelial cells using TRIzol reagent (Sigma-Aldrich, T9424-200 ml). The

RNA was reverse transcribed into complementary DNA (cDNA) using a PrimeScript RT Reagent Kit (TaKaRa, Japan) according to the manufacturer's instructions. Real-time PCR analysis was carried out using cDNA as template in the PCR reactions with SYBR Premix Ex Taq (TaKaRa). The PCR primer sequences are listed in Supplemental Table 1.

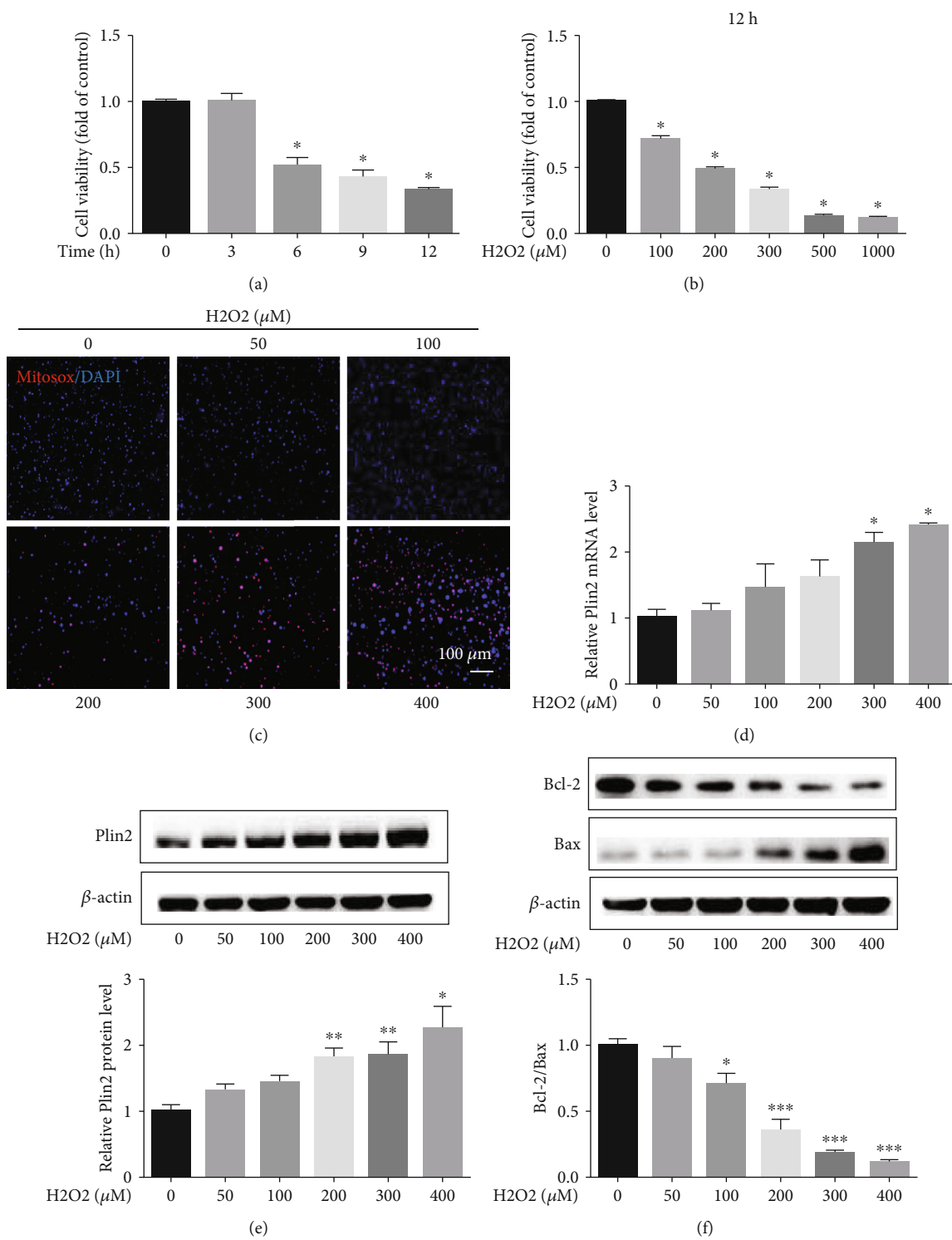


FIGURE 2: Continued.

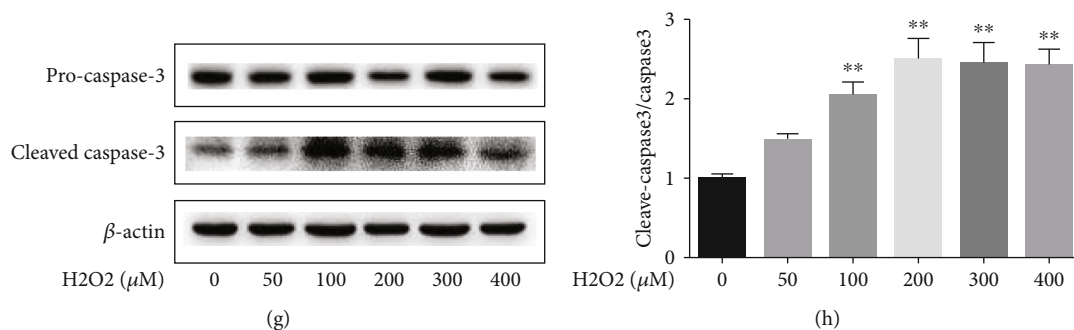


FIGURE 2: Plin2 levels increase after hydrogen peroxide treatment in primary renal proximal tubular cells. Primary renal proximal tubular cells were treated with hydrogen peroxide. (a, b) Cell viability measured using CCK-8 assays after hydrogen peroxide treatment ($n = 10$). $*P < 0.05$ vs. 0 h or 0 μM hydrogen peroxide. (c) Images of mitochondrial reactive oxygen species (ROS) generation after hydrogen peroxide treatment for 12 hours. (d) Quantitative RT-PCR analysis of Plin2 mRNA expression after hydrogen peroxide treatment for 12 hours ($n = 4$). $*P < 0.05$ vs. 0 μM hydrogen peroxide. (e–h) Western blot analysis of Plin2, BAX, Bcl-2, and cleaved caspase-3 expressions after hydrogen peroxide treatment for 12 hours ($n = 4$). $*P < 0.05$ vs. 0 μM hydrogen peroxide; $**P < 0.01$ vs. 0 μM hydrogen peroxide; and $***P < 0.001$ vs. 0 μM hydrogen peroxide. Data are presented as mean \pm SEM. H_2O_2 : hydrogen peroxide.

2.9. Cell Viability Assessment. Cell viability was determined using cell counting kit-8 (CCK-8) assays. Briefly, mouse tubular epithelial cells were grown to 70%–80% confluence in 96-well plates and then subjected to various treatments indicated. The CCK-8 reagent was added to the medium and incubated for 1–4 h in the dark. Absorbance was measured at 450 nm using a microplate reader, and the cell viability was calculated.

2.10. Immunofluorescence. Frozen kidney sections were fixed with cold acetone for 10 min. The sections were permeabilized with 0.2% Triton X-100 for 10 min and then blocked with 5% bovine serum albumin for 30 min. The prepared sections were incubated with primary antibody at 4°C overnight. The sections were washed and then incubated with secondary antibody (Dye Light488-conjugated, green) for 30 min at room temperature. Nuclei were stained with DAPI. Images were acquired using the Olympus FV1000 confocal microscope.

2.11. Mitochondrial ROS Assay. Primary proximal tubular cell mitochondrial ROS was detected using MitoSOX Red Mitochondrial Superoxide Indicator (Invitrogen) following the manufacturer's instructions. Renal tissue ROS was detected in frozen sections using dihydroethidium (DHE) staining following the manufacturer's instruction. Nuclei were stained with DAPI solution. Images were acquired with confocal microscopy, and the fluorescent signal was quantified using ImageJ software.

2.12. Statistical Analysis. All data are expressed as mean \pm S.E.M. and analyzed using the Prism software package (GraphPad Software). Unpaired two-sided Student's t -tests were used to differentiate the significance between two groups. Intergroup differences were analyzed using analysis of variance (ANOVA). A P value < 0.05 was considered statistically significant.

3. Results

3.1. Plin2 Is Upregulated in the Kidneys of Mice after I/R Treatment. To investigate changes in the context of I/R-induced AKI, mice treated with I/R were examined at different timepoints posttreatment (0, 6, and 24 h). Our results showed that I/R robustly induced serum creatinine levels, which were increased at 24 h (Figure 1(a)). Consistently, periodic acid–Schiff staining showed severe tubular and interstitial damage at 24 h (Supplemental Figure 2a). Furthermore, TUNEL staining demonstrated that the number of apoptotic cells increased significantly at 24 h after I/R (Figure 1(b)). In addition, mRNA expression of the proinflammatory mediators *IL-6* and *TNF α* increased after I/R treatment (Supplemental Figure 2b and 2c). Interestingly, the expression of *IL-6* increased significantly at 6 h, whereas the expression of *TNF α* increased significantly at 24 h.

It has been indicated that the production of ROS remains high for 24 h after renal IRI [14]. Therefore, we used DHE staining to assess the production of ROS after renal IRI and found higher production (Figure 1(c)). It has been demonstrated that the production of ROS increases Plin2 expression in HepG2 cells [7]. To assess Plin2 expression after renal IRI, we analyzed tissue from I/R-induced AKI mice sacrificed 0, 6, and 24 h after I/R injury. Costaining for lipid droplet surface protein Plin2 and renal proximal tubular marker LTL in the kidneys indicated that Plin2 is mainly located in renal proximal tubulars (Supplemental Figure 2d). Costaining for Plin2 and BODIPY in the kidneys further demonstrated the levels of lipid droplet surface protein Plin2 increased after I/R (Figure 1(d)). RT-PCR showed the level of mRNA expression of Plin2 was robustly increased at 24 h, and western blotting demonstrated the protein levels also increased at 24 h (Figures 1(e) and 1(f)). These results indicated that Plin2 was upregulated after I/R-induced AKI. We presumed that the production of ROS and expression of Plin2 in kidney injury were interrelated.

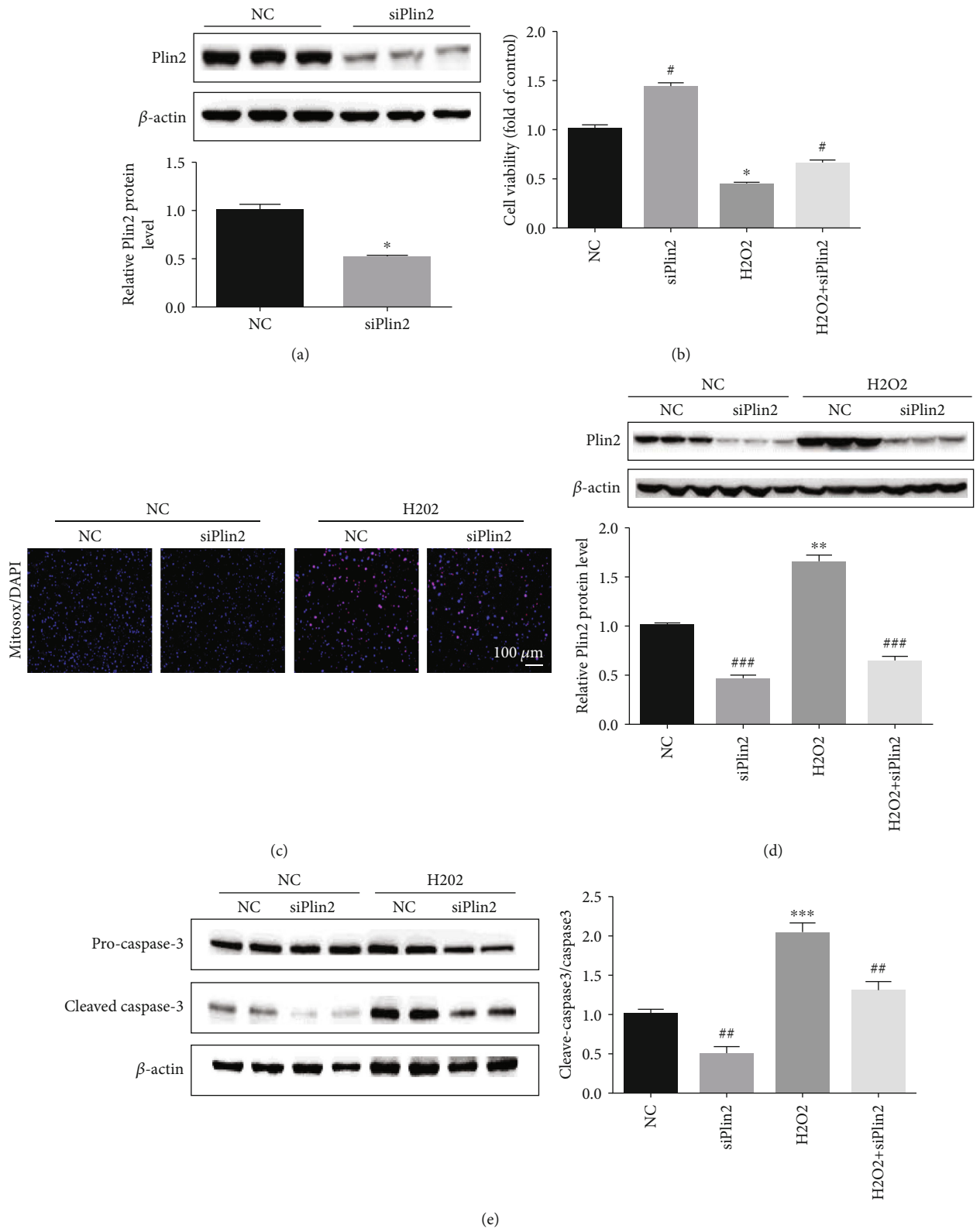


FIGURE 3: Continued.

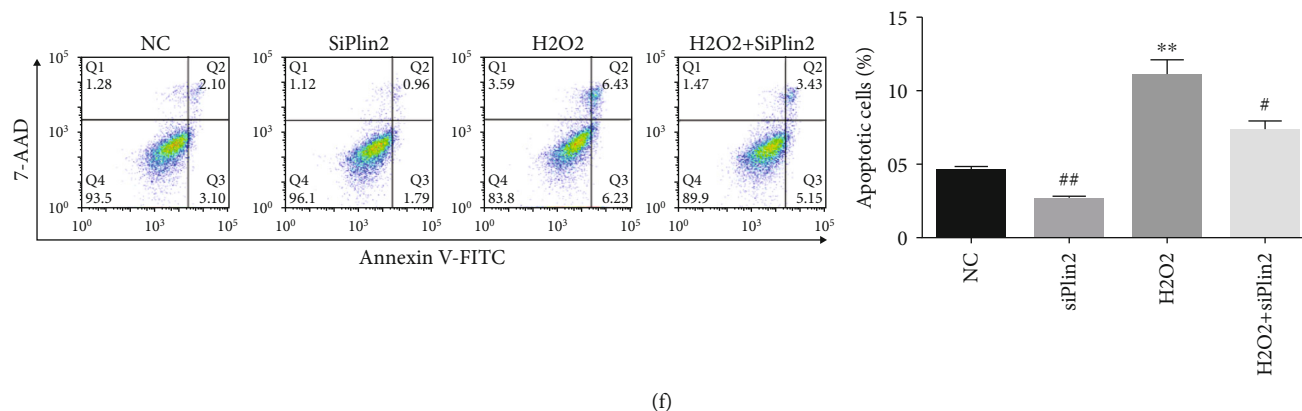


FIGURE 3: Knockdown of Plin2 attenuates apoptosis in primary renal proximal tubular cells. (a) Western blot analysis of Plin2 expression after Plin2 knockdown ($n = 3$). $*P < 0.05$ vs. the NC group. (b) Cell viability measured using CCK8 assays ($n = 15$). $*P < 0.05$ vs. the NC group, $^{\#}P < 0.05$ vs. the NC or H₂O₂ group. Data are presented as mean \pm SEM. (c) Images of mitochondrial reactive oxygen species (ROS) generation in PTECs transfected with Plin2 knockdown plasmid after hydrogen peroxide (300 μ M) treatment. (d, e) Western blot analysis of Plin2 ($n = 3$) and cleaved caspase-3 ($n = 4$) expression in primary renal proximal tubular cells transfected with Plin2 knockdown plasmid after hydrogen peroxide (300 μ M) treatment ($n = 4$). $*P < 0.05$ vs. the NC group, $***P < 0.001$ vs. the NC group, $^{\#}P < 0.05$ vs. the NC or H₂O₂ group, and $^{\#\#}P < 0.01$ vs. the NC or H₂O₂ group. (f) Cell apoptosis in hydrogen peroxide (300 μ M)-treated renal proximal tubular cells transfected with Plin2 knockdown plasmid or control plasmid. Annexin V-positive cells were considered apoptotic cells ($n = 4$). $**P < 0.05$ vs. the NC group, $^{\#}P < 0.05$ vs. the H₂O₂ group, and $^{\#\#}P < 0.01$ vs. the NC group. Data represent the mean \pm SEM. H₂O₂: hydrogen peroxide; NC: negative control.

3.2. Hydrogen Peroxide Treatment Increases Plin2 Expression in Primary Renal Proximal Tubular Cells. We first evaluate the effect of hydrogen peroxide treatment on the viability of primary renal proximal tubular cells. Our results showed that cell viability significantly decreased in a dose-dependent and time-dependent manner upon exposure to hydrogen peroxide (Figures 2(a) and 2(b)), Supplemental Figure 3a–3c). As expected, hydrogen peroxide treatment significantly increased mitochondrial ROS generation in primary renal proximal tubular cells (Figure 2(c)). Plin2 expression was increased in a dose-dependent manner upon exposure to hydrogen peroxide treatment (Figures 2(d) and 2(e)). Furthermore, hydrogen peroxide treatment significantly increased apoptosis of primary renal proximal tubular cells in a dose-dependent manner (Figures 2(f)–2(h)).

3.3. Plin2 Knockdown Attenuates Apoptosis in Primary Renal Proximal Tubular Cells. To further investigate the role of Plin2 in apoptosis, its expression was knocked down in primary renal proximal tubular cells (Figure 3(a)). Plin2 knockdown promoted cell viability and significantly decreased mitochondrial ROS generation upon exposure to hydrogen peroxide (Figures 3(b)–3(d)). In addition, this blocked the hydrogen peroxide-induced apoptosis in renal proximal tubular cells (Figures 3(e) and 3(f)). These results indicated that the knockdown of Plin2 could inhibit mitochondrial ROS generation and conferred protective effects against apoptosis in primary renal proximal tubular cells.

3.4. Plin2 Impacts Apoptosis via the Regulation of PPAR α . PPAR α is highly expressed in the proximal tubules and participates in the occurrence and development of kidney diseases [8–10]. It has been reported that PPAR α promotes

the repair of kidney injury induced by I/R. We found that PPAR α expression decreased in a dose-dependent manner in renal proximal tubular cells treated with hydrogen peroxide (Figures 4(a) and 4(b)). Plin2 downregulation was accompanied by an increase in PPAR α expression under hydrogen peroxide treatment conditions (Figure 4(c)). Consistently, CCK-8 assays confirmed that the inactivation of PPAR α reversed the effects of Plin2 on renal proximal tubular cells (Figures 4(d) and 4(e)). Moreover, PPAR α activation reversed the apoptosis induced by Plin2 overexpression upon hydrogen peroxide treatment (Figures 4(f)–4(h)). Taken together, our data indicated that Plin2 downregulation alleviates renal proximal tubular cell apoptosis via the upregulation of PPAR α .

4. Discussion

In the present study, we determined the relationship between Plin2 and PPAR α in the regulation of apoptosis in a model of AKI induced by I/R (Figure 5). Renal IRI resulted in the upregulation of Plin2, which inhibited PPAR α expression and increased mitochondrial ROS production, leading to cell apoptosis and AKI. Oxidative stress-induced injury is an important part of renal IRI [15]. The knockdown of Plin2 alleviated mitochondrial ROS-induced apoptosis in primary proximal renal tubular epithelial cells, which was mediated by the inhibition of PPAR α expression. Therefore, Plin2 knockdown may be targeted for the treatment of AKI induced by I/R.

Our results indicated that Plin2 was upregulated by ROS production in renal IRI. Perilipins are lipid droplet surface proteins that include five family members (Plin1–5) with different distributions and functions. Among them, Plin2 was the first identified and is highly expressed in adipose

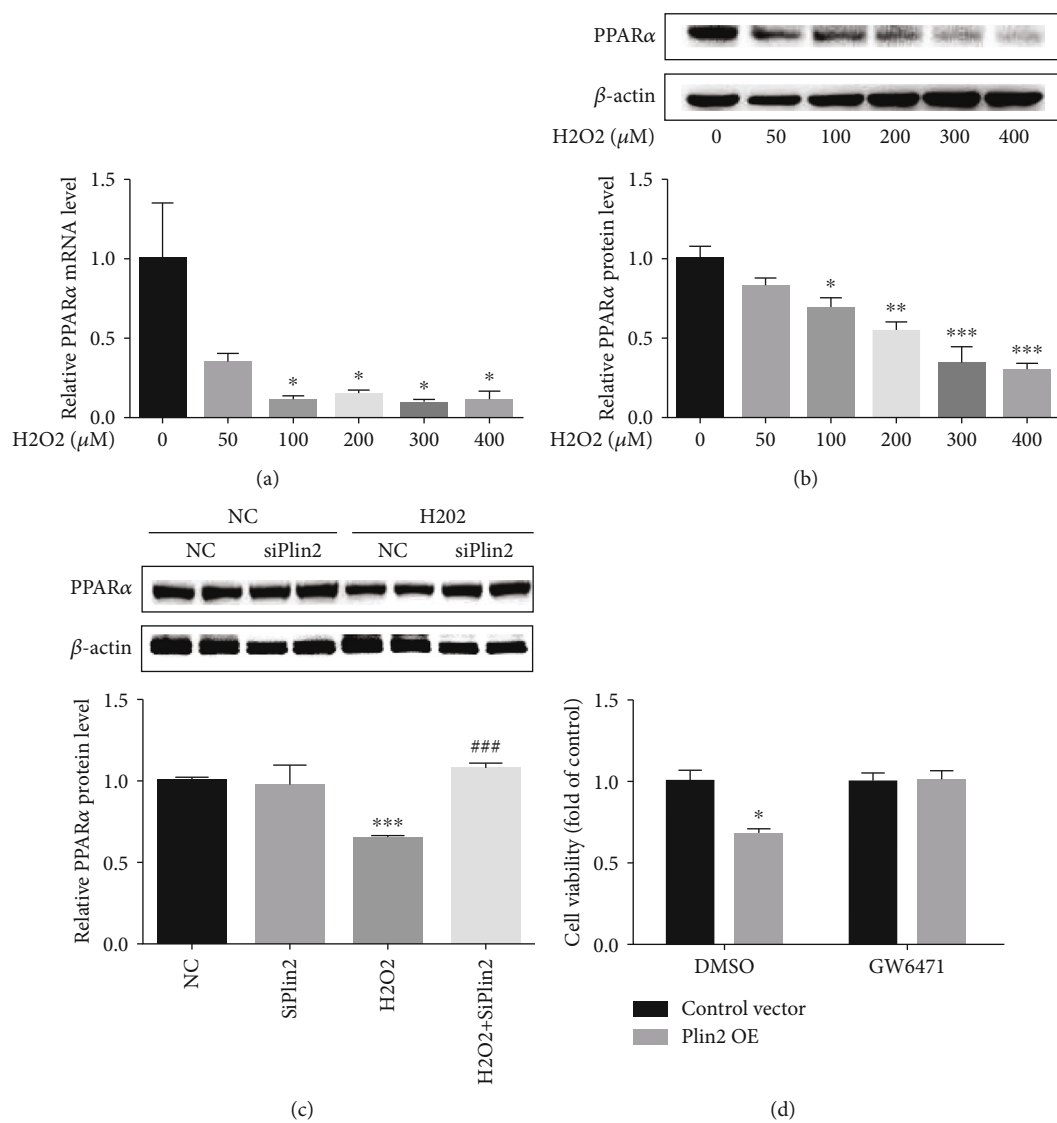


FIGURE 4: Continued.

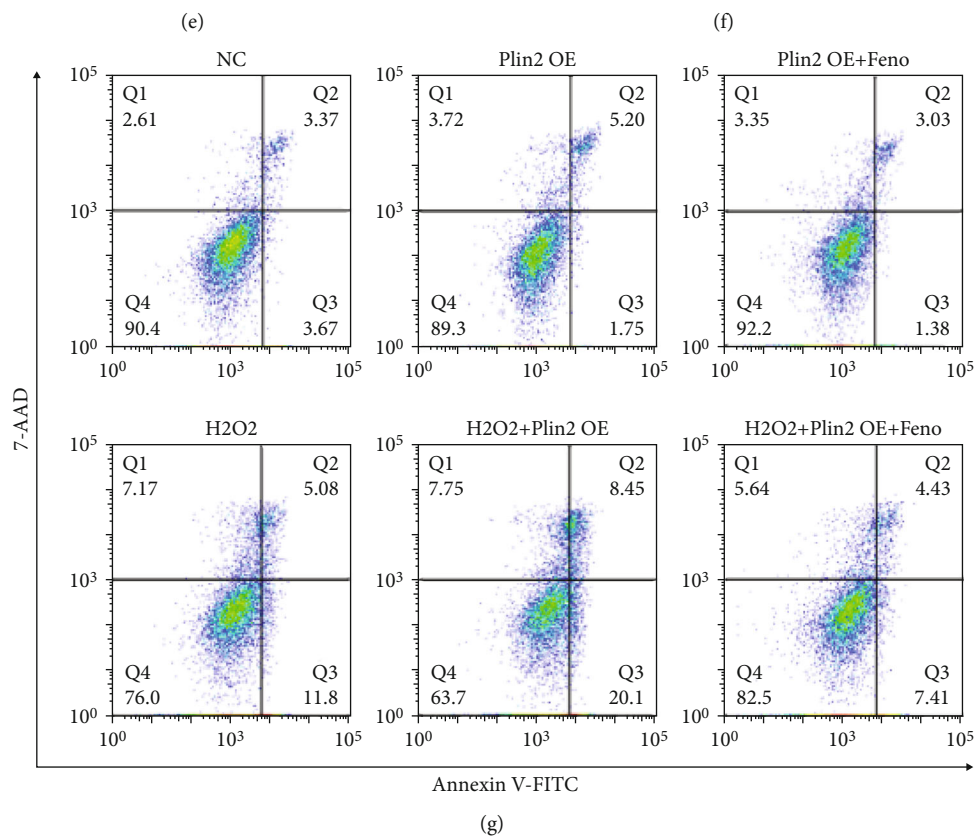
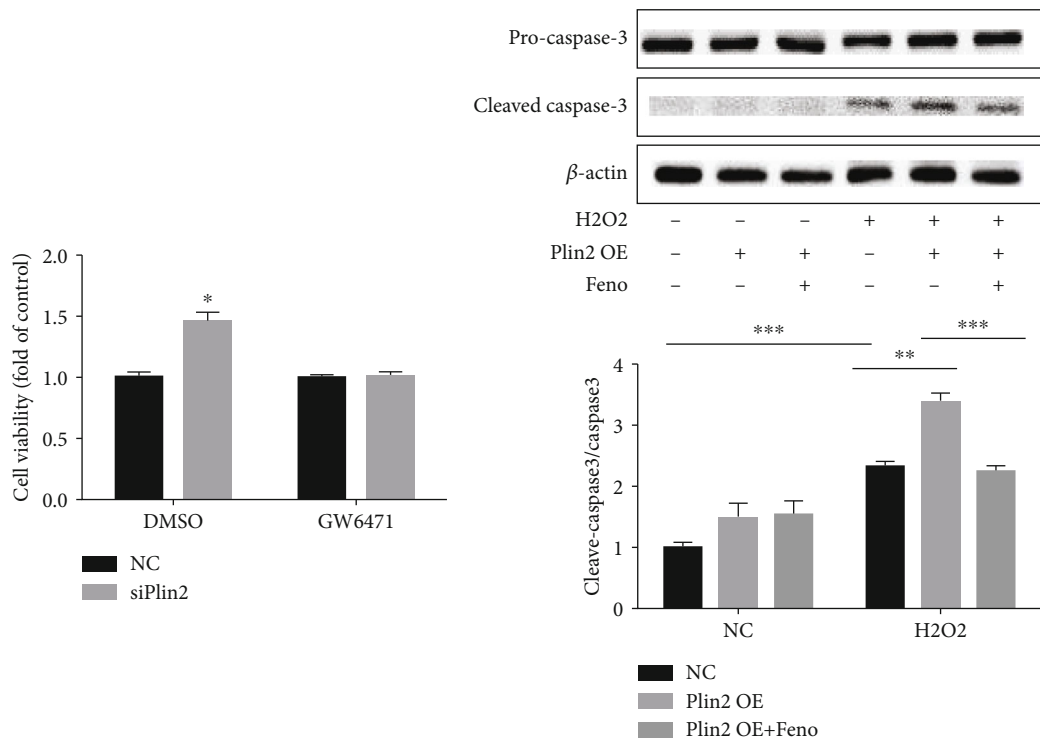


FIGURE 4: Continued.

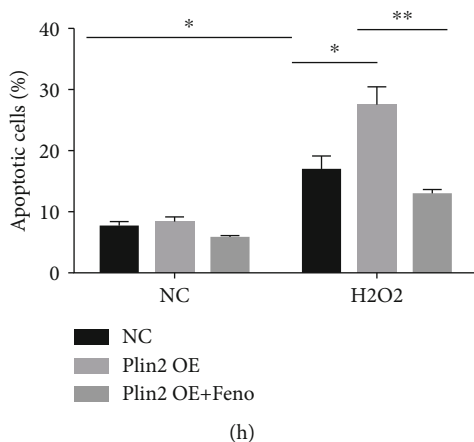


FIGURE 4: Plin2 impacts apoptosis via the regulation of PPAR α . (a, b) Expression of PPAR α after hydrogen peroxide treatment ($n = 4$). * $P < 0.05$ vs. $0 \mu\text{M}$ hydrogen peroxide; ** $P < 0.01$ vs. $0 \mu\text{M}$ hydrogen peroxide; and *** $P < 0.001$ vs. $0 \mu\text{M}$ hydrogen peroxide. (c) Western blot analysis of PPAR α in primary renal proximal tubular cells transfected with Plin2 knockdown plasmids after hydrogen peroxide treatment ($n = 4$). *** $P < 0.001$ vs. NC; ### $P < 0.001$ vs. hydrogen peroxide. (d, e) Cell viability of Plin2 knockdown or overexpression in primary renal proximal tubular cells after hydrogen peroxide treatment ($n = 4$). * $P < 0.05$ vs. DMSO NC. (f) Western blot analysis of cleaved caspase-3 expression in primary renal proximal tubular cells transfected with Plin2 overexpression plasmid with or without fenofibrate after hydrogen peroxide ($300 \mu\text{M}$) treatment ($n = 4$). ** $P < 0.01$, *** $P < 0.001$. (g, h) Cell apoptosis in hydrogen peroxide ($300 \mu\text{M}$)-treated renal proximal tubular cells transfected with Plin2 knockdown plasmid or control plasmid with or without fenofibrate. Annexin V-positive cells were considered apoptotic cells ($n = 3$), * $P < 0.05$, ** $P < 0.01$. Data represent mean \pm SEM. H₂O₂: hydrogen peroxide; NC: negative control; OE: overexpression.

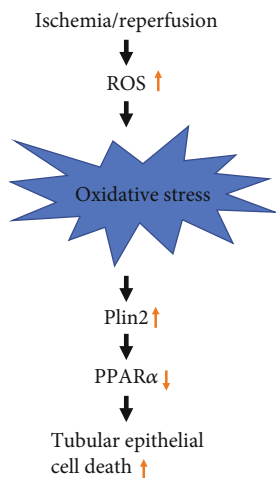


FIGURE 5: Proposed schema of the pathway for I/R-induced AKI, involving the promotion of mitochondrial reactive oxygen species (ROS) generation, upregulation of Plin2, and downregulation of PPAR α , resulting in cell apoptosis.

tissue and skeletal muscle of rodents and humans [16]. Plin2 is involved in the differentiation and lipolysis of adipose tissue, but its role in skeletal muscle is not yet clear. It plays an important role in the formation of lipid droplets in HepG2 cells, and Plin2 knockdown significantly reduces the size and number of lipid droplets [17]. However, its function and expression in the kidney was previously not well known. In the current study, we found that Plin2 was expressed in the normal kidney, mainly in the renal tubules. A previous study demonstrated that Plin2 is upregulated by ROS in HepG2 cells [7]. In the present

study, we found that Plin2 was upregulated by hydrogen peroxide in primary proximal tubular epithelial cells, while Plin2 knockdown could reduce the production of ROS in tubular cells.

It is noteworthy that Plin2 is a lipid droplet surface protein and its protein structure and subcellular localization are highly conserved among different species, which is essential for the formation and morphological stability of lipid droplets [18]. Whether ROS affects the formation of lipid droplets in renal tubular cells was not explored in this study. A recent study also indicated that ROS affects not only the expression of Plin2 but also the formation of lipid droplets in hepatocytes [7]. Further studies are needed to verify the effect of ROS on Plin2 expression and the formation of lipid droplets in renal tubular cells. Whether Plin2 affects the formation of lipid droplets in the presence of ROS also needs to be addressed.

It has been demonstrated that Plin2 affects the PPAR α -RXRA and CREB-CREBBP pathways [7]. PPAR α is a member of the nuclear receptor superfamily, which is highly expressed in the heart, liver, kidney, muscle, and other tissues with abundant mitochondria and fatty acid betaoxidation [19, 20]. It plays an important role in maintaining the homeostasis of lipid metabolism. In the kidney, PPAR α is highly expressed in the proximal tubules and the ascending branch of the medullary loop, suggesting that it might be involved in the occurrence and development of a several kidney diseases, including cystic kidney disease 8 [21], alcoholic kidney injury [22], and diabetic kidney disease [23]. In addition, some evidence suggests that PPAR α promotes repair of the injured kidney induced by I/R [24, 25]. In our study, we found that the PPAR α expression

patterns were opposite to those of Plin2 upon I/R or in primary proximal tubular epithelial cells treated with hydrogen peroxide. Plin2 thus has the potential to negatively regulate the expression of PPAR α , thereby regulating the production of ROS induced by I/R or hydrogen peroxide and affecting the apoptosis of renal tubular cells. In our study, we used the PPAR α agonist pioglitazone to pretreat primary renal tubular epithelial cells with Plin2 overexpression before hydrogen peroxide treatment. Pretreatment with pioglitazone abolished the apoptosis induced by Plin2 overexpression.

In addition, under hydrogen peroxide treatment conditions, pretreatment with the PPAR α agonist fenofibrate alleviated the decrease in cell viability induced by Plin2 overexpression, whereas the PPAR α inhibitor GW6471 inhibited the increase in cell viability induced by Plin2 knockdown. Collectively, our results provide insights suggesting that Plin2 increases apoptosis of renal tubular epithelial cells by inhibiting PPAR α expression and ROS produced upon renal I/R or hydrogen peroxide exposure.

Evidence indicates that Plin2 is an important player in renal tumors [10–12, 26]. Based on our experiments, we speculate that the expression of Plin2 is upregulated, whereas the expression of PPAR α is downregulated, in patients with AKI. Whether Plin2 participates in the development of AKI requires further investigation in the future.

In general, we illustrated that ROS production and the expression of Plin2 were significantly upregulated after renal I/R. The expression of Plin2 was also significantly increased after hydrogen peroxide treatment in vitro. The overexpression of Plin2 markedly increased apoptosis of proximal tubular epithelial cells after hydrogen peroxide treatment by inhibiting the expression of PPAR α . These results indicate, for the first time, that the targeted inhibition of Plin2 has a protective effect on ROS, which implies this is a potential target for the treatment of AKI.

Data Availability

The figures and table used to support the findings of this study are included within the article and the supplementary information file.

Conflicts of Interest

The authors declare no disclosures of interests.

Authors' Contributions

Sujuan Xu and Edward Lee contributed equally to this work. S.J.X. and X.Q.D. designed the study. S.J.X., Edward Lee, Z.X.S., X.Y.W., T.R., Z.P.Z., and J.F.J. carried out experiments. J.Z. and S.J.X. analyzed the data. Y.F., S.J.X., Q.Y., and Y.Z. made the figures. S.J.X., M.G., J.L., Y.X.L., and X.Q.D. drafted and revised the paper. All authors approved the final version of the manuscript.

Acknowledgments

This work was supported by the Science and Technology Commission of Shanghai Municipality (14DZ2260200, the project of Shanghai Key Laboratory of Kidney and Blood Purification) and the National Natural Science Foundation of China (81670614 to Xiaoqiang Ding).

Supplementary Materials

Supplemental Figure 1: confocal immunofluorescence was performed to detect primary mouse proximal tubular cells marker AQP1. Supplemental Figure 2: I/R-induced AKI and inflammation. Supplemental Figure 3: cell viability decreases after hydrogen peroxide treatment in primary renal proximal tubular cells. Supplemental Table 1: primers used for amplifying mouse genes. (*Supplementary Materials*)

References

- [1] R. BELLOMO, J. A. KELLUM, and C. RONCO, "Acute kidney injury," *Lancet*, vol. 380, no. 9843, pp. 756–766, 2012.
- [2] H. L. Liang, G. Hilton, J. Mortensen, K. Regner, C. P. Johnson, and V. Nilakantan, "MnTMPyP, a cell-permeant SOD mimetic, reduces oxidative stress and apoptosis following renal ischemia-reperfusion," *American Journal of Physiology. Renal Physiology*, vol. 296, no. 2, pp. F266–F276, 2009.
- [3] W. Zhang, M. Wang, H. Y. Xie et al., "Role of reactive oxygen species in mediating hepatic ischemia-reperfusion injury and its therapeutic applications in liver transplantation," *Transplantation Proceedings*, vol. 39, no. 5, pp. 1332–1337, 2007.
- [4] P. K. Chatterjee, S. Cuzzocrea, P. A. J. Brown et al., "Tempol, a membrane-permeable radical scavenger, reduces oxidant stress-mediated renal dysfunction and injury in the rat," *Kidney International*, vol. 58, no. 2, pp. 658–673, 2000.
- [5] M. Hüttemann, S. Helling, T. H. Sanderson et al., "Regulation of mitochondrial respiration and apoptosis through cell signaling: Cytochrome *c* oxidase and cytochrome *c* in ischemia/reperfusion injury and inflammation," *Biochimica et Biophysica Acta*, vol. 1817, no. 4, pp. 598–609, 2012.
- [6] A. Čopič, S. Antoine-Bally, M. Giménez-Andrés et al., "A giant amphipathic helix from a perilipin that is adapted for coating lipid droplets," *Nature Communications*, vol. 9, no. 1, p. 1332, 2018.
- [7] Y. Jin, Y. Tan, L. Chen, Y. Liu, and Z. Ren, "Reactive oxygen species induces lipid droplet accumulation in HepG2 cells by increasing perilipin 2 expression," *International Journal of Molecular Sciences*, vol. 19, no. 11, p. 3445, 2018.
- [8] N. Graffmann, S. Ring, M.-A. Kawala et al., "Modeling nonalcoholic fatty liver disease with human pluripotent stem cell-derived immature hepatocyte-like cells reveals activation of PLIN2 and confirms regulatory functions of peroxisome proliferator-activated receptor alpha," *Stem Cells and Development*, vol. 25, no. 15, pp. 1119–1133, 2016.
- [9] I. Mardani, K. T. Dalen, C. Drevinge et al., "Plin2-deficiency reduces lipophagy and results in increased lipid accumulation in the heart," *Scientific Reports*, vol. 9, no. 1, p. 6909, 2019.
- [10] J. J. Morrissey, V. M. Mellnick, J. Luo et al., "evaluation of urine aquaporin-1 and perilipin-2 concentrations as biomarkers to screen for renal cell carcinoma: a prospective

- cohort study," *JAMA Oncology*, vol. 1, no. 2, pp. 204–212, 2015.
- [11] B. Qiu, D. Ackerman, D. J. Sanchez et al., "HIF2 α -dependent lipid storage promotes endoplasmic reticulum homeostasis in clear-cell renal cell carcinoma," *Cancer Discovery*, vol. 5, no. 6, pp. 652–667, 2015.
- [12] J. J. Morrissey, J. Mobley, R. S. Figenschau, J. Vetter, S. Bhayani, and E. D. Kharasch, "Urine aquaporin 1 and perilipin 2 differentiate renal carcinomas from other imaged renal masses and bladder and prostate cancer," *Mayo Clinic Proceedings*, vol. 90, no. 1, pp. 35–42, 2015.
- [13] P. Jia, J. Teng, J. Zou et al., "miR-21 contributes to xenon-conferred amelioration of renal ischemia-reperfusion injury in mice," *Anesthesiology*, vol. 119, no. 3, pp. 621–630, 2013.
- [14] P. Jia, X. Wu, T. Pan, S. Xu, J. Hu, and X. Ding, "Uncoupling protein 1 inhibits mitochondrial reactive oxygen species generation and alleviates acute kidney injury," *EBioMedicine*, vol. 49, pp. 331–340, 2019.
- [15] E. Noiri, A. Nakao, K. Uchida et al., "Oxidative and nitrosative stress in acute renal ischemia," *American Journal of Physiology. Renal Physiology*, vol. 281, no. 5, pp. F948–F957, 2001.
- [16] R. Minnaard, P. Schrauwen, G. Schaart et al., "Adipocyte differentiation-related protein and OXPAT in rat and human skeletal muscle: involvement in lipid accumulation and type 2 diabetes mellitus," *The Journal of Clinical Endocrinology and Metabolism*, vol. 94, no. 10, pp. 4077–4085, 2009.
- [17] F. L. Chen, Z. H. Yang, X. C. Wang et al., "Adipophilin affects the expression of TNF- α , MCP-1, and IL-6 in THP-1 macrophages," *Molecular and Cellular Biochemistry*, vol. 337, no. 1–2, pp. 193–199, 2010.
- [18] M. Bosma, M. K. C. Hesselink, L. M. Sparks et al., "Perilipin 2 improves insulin sensitivity in skeletal muscle despite elevated intramuscular lipid levels," *Diabetes*, vol. 61, no. 11, pp. 2679–2690, 2012.
- [19] R. Mukherjee, L. Jow, D. Noonan, and D. P. McDonnell, "Human and rat peroxisome proliferator activated receptors (PPARs) demonstrate similar tissue distribution but different responsiveness to PPAR activators," *The Journal of Steroid Biochemistry and Molecular Biology*, vol. 51, no. 3–4, pp. 157–166, 1994.
- [20] A. L. Bookout, Y. Jeong, M. Downes, R. T. Yu, R. M. Evans, and D. J. Mangelsdorf, "Anatomical profiling of nuclear receptor expression reveals a hierarchical transcriptional network," *Cell*, vol. 126, no. 4, pp. 789–799, 2006.
- [21] R. Lakhia, M. Yheskel, A. Flaten, E. B. Quittner-Strom, W. L. Holland, and V. Patel, "PPAR α agonist fenofibrate enhances fatty acid β -oxidation and attenuates polycystic kidney and liver disease in mice," *American Journal of Physiology. Renal Physiology*, vol. 314, no. 1, pp. F122–F131, 2018.
- [22] J.-T. Yu, X.-W. Hu, H.-Y. Chen et al., "DNA methylation of FTO promotes renal inflammation by enhancing m (6) A of PPAR-alpha in alcohol-induced kidney injury," *Pharmacological Research*, vol. 163, 2021.
- [23] A. C. Calkin, S. Giunti, K. A. Jandeleit-Dahm, T. J. Allen, M. E. Cooper, and M. C. Thomas, "PPAR- α and - γ agonists attenuate diabetic kidney disease in the apolipoprotein E knockout mouse," *Nephrology, Dialysis, Transplantation*, vol. 21, no. 9, pp. 2399–2405, 2006.
- [24] S. Li, K. K. Nagothu, V. Desai et al., "Transgenic expression of proximal tubule peroxisome proliferator-activated receptor- α in mice confers protection during acute kidney injury," *Kidney International*, vol. 76, no. 10, pp. 1049–1062, 2009.
- [25] C.-F. Cheng, W.-S. Lian, S.-H. Chen et al., "Protective effects of adiponectin against renal ischemia-reperfusion injury via prostacyclin-PPAR α -Heme oxygenase-1 signaling pathway," *Journal of Cellular Physiology*, vol. 227, no. 1, pp. 239–249, 2012.
- [26] Q. Cao, H. Ruan, K. Wang et al., "Overexpression of PLIN2 is a prognostic marker and attenuates tumor progression in clear cell renal cell carcinoma," *International Journal of Oncology*, vol. 53, no. 1, pp. 137–147, 2018.

Review Article

Uterine Sensitization-Associated Gene-1 in the Progression of Kidney Diseases

Xiaohu Li , Wenlong Yue , Guiwen Feng , and Jinfeng Li 

Department of Kidney Transplantation, The First Affiliated Hospital of Zhengzhou University, Zhengzhou 450052, China

Correspondence should be addressed to Guiwen Feng; feng_guiwen123@163.com and Jinfeng Li; jinfenglis512@126.com

Received 26 May 2021; Accepted 23 July 2021; Published 9 August 2021

Academic Editor: Cheng Yang

Copyright © 2021 Xiaohu Li et al. This is an open access article distributed under the Creative Commons Attribution License, which permits unrestricted use, distribution, and reproduction in any medium, provided the original work is properly cited.

Uterine sensitization-associated gene-1 (USAG-1), originally identified as a secretory protein preferentially expressed in the sensitized rat endometrium, has been determined to modulate bone morphogenetic protein (BMP) and Wnt expression to play important roles in kidney disease. USAG-1 affects the progression of acute and chronic kidney damage and the recovery of allograft kidney function by regulating the BMP and Wnt signaling pathways. Moreover, USAG-1 has been found to be involved in the process of T cell immune response, and its ability to inhibit germinal center activity and reduce humoral immunity is of great significance for the treatment of autoimmune nephropathy and antibody-mediated rejection (AMR) after renal transplantation. This article summarizes the many advances made regarding the roles of USAG-1 in the progression of kidney disease and outlines potential treatments.

1. Introduction

Acute kidney injury (AKI) is a clinical syndrome involving acute renal dysfunction caused by ischemia-reperfusion, drug toxicity, and sepsis [1]. If AKI is not treated in a timely manner, it may further develop into chronic kidney disease (CKD) or even end-stage renal disease (ESRD), during which renal tubular epithelial cells (TECs) and the endothelium are damaged more severely, leading to renal tubular damage with severe interstitial fibrosis [2]. Unfortunately, there is currently no effective treatment for reversing ESRD [3]. Kidney transplantation has gradually become the best treatment option for patients with ESRD. However, the survival of the transplanted kidney is restricted by antibody-mediated rejection (AMR) after kidney transplantation. Tubule atrophy and interstitial fibrosis are also risk factors for progressive graft dysfunction [4]. Uterine sensitization-associated gene-1 (USAG-1) is a newly discovered important cell signaling regulator that has been reported to play a key role in kidney injury, tooth development, hair growth, limb morphology, and trigeminal ganglion formation [5–8]. USAG-1, as a regulator of the bone morphogenetic protein (BMP) and Wnt signaling pathways, is abundantly expressed in the kidney

and expected to repair renal tubular damage and reverse the process of interstitial fibrosis [5, 9, 10]. Furthermore, recent studies have shown that USAG-1 participates in the germinal center (GC) reaction and inhibits humoral immunity. These findings may provide new directions for the future development of treatments for AMR after kidney transplantation, as well as vaccines and therapies for autoimmune kidney diseases [11].

2. USAG-1 in Kidney Disease

2.1. Discovery and Identification of USAG-1. USAG-1 (also known as WISE, *sostdc1*, and *ectodin*) is a secreted protein with a molecular weight of 28–30 kDa that contains a C-terminal cysteine knot-like domain. Laurikkala and colleagues first discovered this gene, which they named *ectodin*, while studying enamel junctions [12]. Simmons and Kennedy identified USAG-1 as a novel gene expressed in the endometrium of rats during maximum sensitization/uterine receptivity [13]. In addition, USAG-1 has been reported to be downregulated in renal tumors as a tumor suppressor gene, while it is highly expressed in normal kidneys [14]. Some studies have shown that USAG-1 is abundant in renal tubules and teeth at the later

stage of embryonic development. In adult tissues, USAG-1 is most highly expressed in the kidney and is mainly concentrated in distal collecting duct epithelial cells, while its expression is relatively low in other tissues and organs (Figure 1) [15–17]. Yanagita et al. found that USAG-1 is a novel BMP antagonist that is highly expressed in the kidney and acts synergistically with BMP7 in developing and adult kidneys [18]. In addition, USAG-1 has been reported to act as a Wnt regulator, modulating the balance of Wnt signaling through Wnt coreceptor complex integration inputs [19].

2.2. USAG-1: A Novel BMP7 Antagonist Expressed in the Kidney, Accelerates Tubular Injury. BMP is a developmentally conserved signaling molecule that has been proven to belong to the transforming growth factor- β -1 (TGF- β) superfamily [1]. It was originally named for its ability to induce the formation of bone, cartilage, and multiple ectopic bones. It was found to play an important regulatory role in proliferation, differentiation, apoptosis, embryonic development, and organ formation in most cells [20]. Bone morphogenetic protein 7 (BMP7) is a 35 kDa homodimeric protein, also known as osteogenic protein-1 (OP-1) [21, 22]. Dudley et al. found that kidney development is severely delayed in BMP7-deficient mice and that these mice generally die within a short period of time after birth [23]. Subsequently, in several other animal models, such as models of acute ischemic injury, diabetic nephropathy, and chronic kidney injury, BMP7 expression was shown to be downregulated and then to gradually increase with further development of disease [24–26]. Thus, BMP7 may play an indispensable role in the normal development of the kidney. Multiple reports have demonstrated that BMP7 alleviates acute and chronic kidney injury, including by reducing apoptosis and necrosis of renal TECs, inhibiting the expression of inflammatory cytokines, reducing inflammatory cell infiltration, and reversing the progression of renal fibrosis [1, 24, 27]. Unfortunately, due to the widespread distribution of BMP receptors, exogenous administration of BMP may cause additional damage in other tissues. However, the activity of BMP has been found to be regulated by BMP antagonists, which have targeted effects by directly binding to BMP and inhibiting its binding to the corresponding receptor. Thus, USAG-1 may be a new target for the treatment of kidney disease [28].

Yanagita et al. compared the expression of USAG-1 and other BMP antagonists in the adult kidney by modified real-time PCR and in situ hybridization and found that USAG-1 is the most abundant BMP antagonist in the adult kidney [29]. Recombinant USAG-1 protein can directly bind to BMP and inhibit BMP-mediated alkaline phosphatase (ALP) activity in C2C12 and MC3T3-E1 cells in a dose-dependent manner [28]. USAG-1 knockout mouse models of AKI caused by cisplatin and chronic kidney injury caused by unilateral ureteral obstruction (UUO) were found to have significantly longer survival times and more complete renal function preservation than wild-type mouse models of these conditions. Moreover, the application of an anti-BMP7 neutralizing antibody can eliminate the renal protective effect of USAG-1 deficiency, suggesting that USAG-1 can block the repair of renal injury by antagonizing BMP7 [29]. Subse-

quent reports have proven that USAG-1 always colocalizes with BMP7 in the developing glomerulus and that its expression decreases during renal tubular injury and increases during renal tubular regeneration [5]. In addition to being a possible therapeutic target for kidney disease, USAG-1 may also be used as a biomarker of renal prognosis—the expression of USAG-1 in a renal biopsy specimen from a mouse model of CKD is related to the prognosis of renal function [5, 28]. Tanaka et al. found that USAG-1 may enhance the expression of MMP-12 in the glomerulus by inhibiting the inhibitory effect of BMP7 and aggravate the progression of glomerular disease in Alport syndrome, while the genetic ablation effect of USAG-1 greatly reduces disease progression in Col4a3 $^{-/-}$ mice (a model of human Alport syndrome) and preserves kidney function [30]. Xia et al. found that febuxostat alleviates renal dysfunction and tubulointerstitial fibrosis in rats with UUO by inhibiting USAG-1 expression and activating the BMP7-SMAD1/5/8 pathway [31, 32]. In subsequent studies, it was demonstrated that USAG-1 expression is downregulated in vitro in a Madin-Darby canine kidney (MDCK) cell model, which helped reverse TGF- β 1-induced epithelial-mesenchymal transformation (EMT) [9]. Smad1/5/8 is a key intracellular protein for transducing BMP7 signals, and phosphorylation of Smad1/5/8 is also the central downstream event in the BMP signal transduction pathway [5, 9, 33]. As a specific antagonist of BMP7, USAG-1 is also an antagonist of TGF- β family ligands, which are involved in promoting EMT by at least partially inhibiting the activity of the Smad1/5/8 signaling pathway (Figure 1) [9, 34]. This finding is consistent with the working model proposed by Yanagita et al., in which USAG-1 and BMP7 play a role in EMT [29]. Interestingly, similar to the perspective above, the loss of USAG-1 promotes the expansion and differentiation of mesenchymal cells (MSCs) during fracture repair, thereby accelerating the healing of fractures [35].

2.3. USAG-1: Activator and Inhibitor of Wnt Signaling. The Wnt signaling pathway is a developmental signaling pathway that can promote embryonic development of the kidney, repair kidney damage, and regulate the formation of various structures in the kidney [36–38]. USAG-1 has been reported to activate and inhibit Wnt signaling in a context-dependent manner. USAG-1 not only interacts with the Wnt coreceptor lipoprotein receptor-related protein 6 (LRP6) but also competes with Wnt8 by binding with LRP6 [19]. According to Qian et al., USAG-1 inhibits endogenous Wnt-induced β -catenin-dependent transcriptional activity in a dose-dependent fashion and directly affects the expression of E-cadherin and α -smooth muscle actin (α -SMA) in renal epithelial cells and mesenchymal fibroblasts [39]. USAG-1 can enhance Wnt3A signal transduction and inhibit Wnt1 and Wnt10b to a certain extent in in vitro cell experiments, which is consistent with previously published data showing that USAG-1 activity depends on the type of Wnt [6, 19, 39].

Chronic allograft injury (CAD) is a disease characterized by renal tubule atrophy, interstitial fibrosis, and glomerular lesions, and it seriously affects the survival of renal transplant recipients [40]. Wnt signaling is known to regulate various morphogenetic pathways, such as cell migration, cell

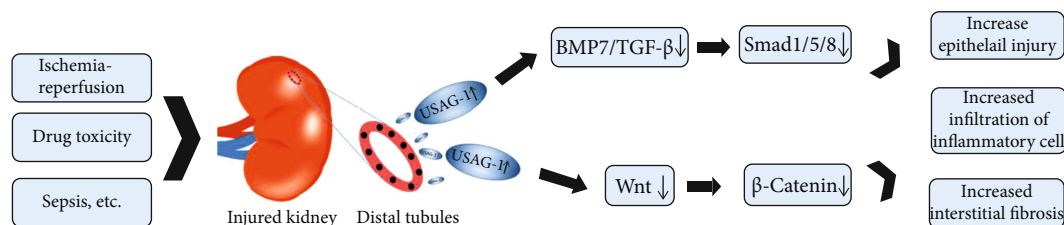


FIGURE 1: Theoretical effects of USAG-1 in renal diseases. The secretion of USAG-1 in the distal tubule increases when the kidney is damaged by ischemia reperfusion, drug toxicity, sepsis, or other factors. It aggravates tubule damage, inflammatory cell infiltration, and interstitial fibrosis by affecting the activity of the BMP7/TGF- β and Wnt/ β -catenin signaling pathways.

proliferation, and cell fate determination, and the dysregulation of these pathways is closely related to the occurrence of CAD. Therefore, increasing normal Wnt signaling and minimizing abnormal Wnt signaling may be potential strategies for therapeutic interventions in CAD and other progressive kidney diseases [41–43]. Seifert et al. found that the Wnt signaling pathway was associated with microvascular injury and renal allograft failure in a residual clinical biopsy conducted 10 years ago, and further mechanistic studies may identify the Wnt signaling pathway as a new target for the diagnosis and treatment of CAD [44]. In a rat kidney transplantation model, allogeneic transplanted kidneys were found to have Wnt signaling components, and the administration of an anti-USAG-1 antibody can significantly improve the recipient's transplanted kidney function. This may be related to the increase in total β -catenin expression induced by the anti-USAG-1 antibody. In addition, long-term prophylactic treatment with a rat anti-USAG-1 antibody can reduce CD68⁺ macrophage and CD8⁺ T cell infiltration, alleviate renal tubular damage and interstitial fibrosis, and reduce the degradation of graft structure [39]. Briefly, USAG-1 expressed in the kidney can cause renal allograft dysfunction by promoting renal tubular atrophy and interstitial fibrosis. Anti-USAG-1 antibodies have certain clinical significance for the treatment of CAD. However, the specific mechanism is still unclear, although we speculate that it may be related to regulation of the Wnt signaling pathway by USAG-1 (Figure 1) [39, 44].

2.4. USAG-1 and T Cell Immune Response. Loss of immune tolerance to autoantigen typifies most autoimmune kidney diseases, and the production of autoantibodies and infiltration of peripheral immune cells are typical pathological features of these autoimmune nephropathies. As crucial drivers of autoimmunity and associated organ injury, T cells play a central role in the regulation of immune responses. An enhanced understanding of the biochemistry and molecular biology of T cells in patients with autoimmune kidney disease will provide a unique opportunity for the identification of therapeutic targets for autoimmune kidney disease. Interestingly, USAG-1 has been found to be closely associated with the T cell immune response in recent studies.

In addition to its being involved in the progression of acute chronic kidney injury, USAG-1 is also associated with the development of several diseases, such as colorectal cancer, non-small-cell lung cancer, thyroid cancer, breast cancer, and gastric cancer [45–49]. In view of the important influ-

ence of USAG-1 on organ development and tumor formation, some researchers have speculated that USAG-1 may be involved in the T cell immune response. T follicle helper (TFH) cells are CD4⁺ T cells that are well known for their ability to assist in the production of B cell antibodies in the GC of lymphatic organs and enhance the B cell memory response [50]. USAG-1 has been reported to be expressed in both TFH cells and reticular fibroblast subsets [51]. The expression of USAG-1 in TFH cells is upregulated 7 days after immunization with sheep red blood cells (SRBCs) [52]. It was demonstrated in a mouse model of acute lymphocytic choroidal meningitis virus (LCMV) infection that USAG-1 is selectively expressed in TFH cells, but the authors found that the presence of USAG-1 is not essential for the differentiation or effector function of TFH cells during acute viral infection [15]. A recent report identified a distinct subpopulation of TFH cells characterized by USAG-1 expression. USAG-1-producing TFH cells can promote the differentiation and maturation of T follicular regulatory (TFR) cells [11]. In contrast to TFH cells, which trigger the GC response, TFR cells, which are newly discovered regulatory T cells (Tregs) that express Foxp3, can inhibit the GC response and humoral immunity [53]. Therefore, unlike USAG-1⁻ TFH cells, USAG-1⁺ TFH cells cannot help B cells produce antibodies. This is mainly because USAG-1 inhibits the transcriptome controlled by β -catenin, thereby preventing the differentiation and maturation of TFR cells [11]. In addition, the Wnt- β -catenin signaling pathway has been shown to be involved in the occurrence and development of a variety of autoimmune kidney diseases [54, 55]. Blocking Wnt stimulation with exogenous USAG-1 to promote commitment to the fate of TFR cells may be a new therapeutic direction for autoimmune kidney diseases.

AMR after kidney transplantation has become a major obstacle affecting the long-term survival of transplanted kidneys [56, 57]. When AMR occurs, B cells and TFH cells in lymphoid tissues are activated by the alloantigen. The persistent immunological damage caused by the production of donor-specific antibodies (DSAs) by GC B cells through mediating the secretion of IL-21 is the main cause of renal graft function deterioration and even renal graft loss [58–61]. Tregs are potent inhibitors of immune function, playing a unique role in alleviating long-term inflammation and maintaining immunological self-tolerance [62]. Classical Wnt signaling can inhibit the function of Treg cells [63], while USAG-1 can inhibit the canonical Wnt- β -catenin pathway [6, 19]. In consideration of the above findings and

the inhibitory effect of USAG-1⁺ THF cells on the GC reaction and humoral immunity, we speculate that further mechanistic studies will identify potential approaches for the prevention and treatment of AMR in renal transplantation.

Furthermore, NK cells, as innate lymphocytes, play an important role in eliminating viral infections and cancer cells. Millan et al. found that USAG-1 expressed by T cells and stromal cells can affect NK cell maturation and cytotoxicity by regulating Wnt signaling in NK cells [16].

3. Summary

As a modulator of the BMP and Wnt signaling pathways, USAG-1 is involved in the development and progression of kidney disease. We summarized the theoretical effects of USAG-1 in renal disease (Figure 1). BMP7 plays a vital role in the development and regeneration of the kidney [64]. USAG-1 can inhibit the interaction of BMP and its receptor by directly binding BMP ligands, thereby limiting the activity of BMP [18]. USAG-1 is a kidney-specific gene. Compared with exogenous administration of BMP7, which may cause extrarenal side effects, therapeutic option targeting USAG-1 enables more specific targeting and minimize adverse effects [65]. Wnt signaling is closely related to the occurrence and development of natural and transplanted CKD [44]. Wnt signaling also plays an important role in regulating microangiogenesis and damage repair and reducing immune cell infiltration [66–68]. More significantly, as the role of USAG-1 in the T cell immune response has been gradually confirmed, targeted regulation of the USAG-1-Wnt signaling pathway may be a potential approach for treating autoimmune kidney disease and preventing the occurrence of AMR. Of course, the existing small animal models and cell experiments are far from sufficient, and more evidence and further mechanistic exploration are needed to provide a theoretical basis for the use of treatments targeting this protein.

Conflicts of Interest

The authors declare that there is no conflict of interest regarding the publication of this paper.

Acknowledgments

This work was supported by the National Natural Science Foundation of China (No. 82070771) and Foundation of Henan Provincial Health Bureau (SBGJ2018022).

References

- [1] L. Gao, X. Zhong, J. Jin, J. Li, and X. M. Meng, “Potential targeted therapy and diagnosis based on novel insight into growth factors, receptors, and downstream effectors in acute kidney injury and acute kidney injury-chronic kidney disease progression,” *Signal transduction and targeted therapy*, vol. 5, no. 1, p. 9, 2020.
- [2] C. Y. Hsu, “Yes, AKI truly leads to CKD,” *Journal of the American Society of Nephrology*, vol. 23, no. 6, pp. 967–969, 2012.
- [3] C. Ronco, R. Bellomo, and J. A. Kellum, “Acute kidney injury,” *Lancet*, vol. 394, no. 10212, pp. 1949–1964, 2019.
- [4] J. Sellarés, D. G. de Freitas, M. Mengel et al., “Understanding the causes of kidney transplant failure: the dominant role of antibody-mediated rejection and nonadherence,” *American Journal of Transplantation*, vol. 12, no. 2, pp. 388–399, 2012.
- [5] M. Tanaka, S. Endo, T. Okuda et al., “Expression of BMP-7 and USAG-1 (a BMP antagonist) in kidney development and injury,” *Kidney International*, vol. 73, no. 2, pp. 181–191, 2008.
- [6] Y. Ahn, B. W. Sanderson, O. D. Klein, and R. Krumlauf, “Inhibition of Wnt signaling by Wise (Sostdc1) and negative feedback from Shh controls tooth number and patterning,” *Development*, vol. 137, no. 19, pp. 3221–3231, 2010.
- [7] K. Närhi, M. Tummers, L. Ahtiainen, N. Itoh, I. Thesleff, and M. L. Mikkola, “Sostdc1 defines the size and number of skin appendage placodes,” *Developmental Biology*, vol. 364, no. 2, pp. 149–161, 2012.
- [8] Y. Shigetani, S. Howard, S. Guidato, K. Furushima, T. Abe, and N. Itasaki, “Wise promotes coalescence of cells of neural crest and placode origins in the trigeminal region during head development,” *Developmental Biology*, vol. 319, no. 2, pp. 346–358, 2008.
- [9] L. Lu, J. Zhu, Y. Zhang, Y. Wang, S. Zhang, and A. Xia, “Febuxostat inhibits TGF- β 1-induced epithelial-mesenchymal transition via downregulation of USAG-1 expression in Madin-Darby canine kidney cells in vitro,” *Molecular Medicine Reports*, vol. 19, no. 3, pp. 1694–1704, 2019.
- [10] I. I. Badshah, S. Brown, L. Weibel et al., “Differential expression of secreted factors SOSTDC1 and ADAMTS8 cause profibrotic changes in linear morphoea fibroblasts,” *The British Journal of Dermatology*, vol. 180, no. 5, pp. 1135–1149, 2019.
- [11] X. Wu, Y. Wang, R. Huang et al., “SOSTDC1-producing follicular helper T cells promote regulatory follicular T cell differentiation,” *Science*, vol. 369, no. 6506, pp. 984–988, 2020.
- [12] J. Laurikkala, Y. Kassai, L. Pakkasjärvi, I. Thesleff, and N. Itoh, “Identification of a secreted BMP antagonist, ectodin, integrating BMP, FGF, and SHH signals from the tooth enamel knot,” *Developmental Biology*, vol. 264, no. 1, pp. 91–105, 2003.
- [13] D. G. Simmons and T. G. Kennedy, “Uterine sensitization-associated gene-1: a novel gene induced within the rat endometrium at the time of uterine receptivity/sensitization for the decidual cell reaction,” *Biology of Reproduction*, vol. 67, no. 5, pp. 1638–1645, 2002.
- [14] K. R. Blish, W. Wang, M. C. Willingham et al., “A human bone morphogenetic protein antagonist is down-regulated in renal cancer,” *Molecular Biology of the Cell*, vol. 19, no. 2, pp. 457–464, 2008.
- [15] J. Hu, J. Wu, Y. Li et al., “Sclerostin domain-containing protein 1 is dispensable for the differentiation of follicular helper and follicular regulatory T cells during acute viral infection,” *American Journal of Translational Research*, vol. 11, no. 6, pp. 3722–3736, 2019.
- [16] A. J. Millan, S. R. Elizaldi, E. M. Lee et al., “Sostdc1 regulates NK cell maturation and cytotoxicity,” *Journal of Immunology*, vol. 202, no. 8, pp. 2296–2306, 2019.
- [17] B. Chicana, C. Donham, A. J. Millan, and J. O. Manilay, “Wnt antagonists in hematopoietic and immune cell fate: implications for osteoporosis therapies,” *Current Osteoporosis Reports*, vol. 17, no. 2, pp. 49–58, 2019.
- [18] M. Yanagita, M. Oka, T. Watabe et al., “USAG-1: a bone morphogenetic protein antagonist abundantly expressed in the kidney,” *Biochemical and Biophysical Research Communications*, vol. 316, no. 2, pp. 490–500, 2004.

- [19] N. Itasaki, C. M. Jones, S. Mercurio et al., "Wise, a context-dependent activator and inhibitor of Wnt signalling," *Development*, vol. 130, no. 18, pp. 4295–4305, 2003.
- [20] T. Katagiri and T. Watabe, "Bone morphogenetic proteins," *Cold Spring Harbor Perspectives in Biology*, vol. 8, no. 6, article a021899, 2016.
- [21] E. Özkaynak, P. N. Schnegelsberg, and H. Oppermann, "Murine osteogenic protein (OP-1): high levels of mRNA in kidney," *Biochemical and Biophysical Research Communications*, vol. 179, no. 1, pp. 116–123, 1991.
- [22] V. S. Salazar, L. W. Gamer, and V. Rosen, "BMP signalling in skeletal development, disease and repair," *Nature Reviews Endocrinology*, vol. 12, no. 4, pp. 203–221, 2016.
- [23] A. T. Dudley, K. M. Lyons, and E. J. Robertson, "A requirement for bone morphogenetic protein-7 during development of the mammalian kidney and eye," *Genes & Development*, vol. 9, no. 22, pp. 2795–2807, 1995.
- [24] S. Vukicevic, V. Basic, D. Rogic et al., "Osteogenic protein-1 (bone morphogenetic protein-7) reduces severity of injury after ischemic acute renal failure in rat," *Journal of Clinical Investigation*, vol. 102, no. 1, pp. 202–214, 1998.
- [25] S. N. Wang, J. Lapage, and R. Hirschberg, "Loss of tubular bone morphogenetic protein-7 in diabetic nephropathy," *Journal of the American Society of Nephrology*, vol. 12, no. 11, pp. 2392–2399, 2001.
- [26] M. Zeisberg, J. Hanai, H. Sugimoto et al., "BMP-7 counteracts TGF- β 1-induced epithelial-to-mesenchymal transition and reverses chronic renal injury," *Nature Medicine*, vol. 9, no. 7, pp. 964–968, 2003.
- [27] E. Vigolo, L. Markó, C. Hinze, D. N. Müller, R. Schmidt-Ullrich, and K. M. Schmidt-Ott, "Canonical BMP signaling in tubular cells mediates recovery after acute kidney injury," *Kidney International*, vol. 95, no. 1, pp. 108–122, 2019.
- [28] J. Nakamura and M. Yanagita, "Bmp modulators in kidney disease," *Discovery Medicine*, vol. 13, no. 68, pp. 57–63, 2012.
- [29] M. Yanagita, T. Okuda, S. Endo et al., "Uterine sensitization-associated gene-1 (USAG-1), a novel BMP antagonist expressed in the kidney, accelerates tubular injury," *Journal of Clinical Investigation*, vol. 116, no. 1, pp. 70–79, 2006.
- [30] M. Tanaka, M. Asada, A. Y. Higashi et al., "Loss of the BMP antagonist USAG-1 ameliorates disease in a mouse model of the progressive hereditary kidney disease Alport syndrome," *Journal of Clinical Investigation*, vol. 120, no. 3, pp. 768–777, 2010.
- [31] J. Cao, Y. Li, Y. Peng et al., "Febuxostat prevents renal interstitial fibrosis by the activation of BMP-7 signaling and inhibition of USAG-1 expression in rats," *American Journal of Nephrology*, vol. 42, no. 5, pp. 369–378, 2015.
- [32] J. Cao, W. Wang, Y. Li et al., "Artesunate attenuates unilateral ureteral obstruction-induced renal fibrosis by regulating the expressions of bone morphogenetic protein-7 and uterine sensitization-associated gene-1 in rats," *International Urology and Nephrology*, vol. 48, no. 4, pp. 619–629, 2016.
- [33] S. R. Manson, R. A. Niederhoff, K. A. Hruska, and P. F. Austin, "The BMP-7-Smad1/5/8 pathway promotes kidney repair after obstruction induced renal injury," *The Journal of Urology*, vol. 185, no. 6S, pp. 2523–2530, 2011.
- [34] C. Chang, "Agonists and antagonists of TGF- β family ligands," *Cold Spring Harbor perspectives in biology*, vol. 8, no. 8, article a021923, 2016.
- [35] N. M. Collette, C. S. Yee, N. R. Hum et al., "*Sostdc1* deficiency accelerates fracture healing by promoting the expansion of periosteal mesenchymal stem cells," *Bone*, vol. 88, pp. 20–30, 2016.
- [36] L. Xiao, D. Zhou, R. J. Tan et al., "Sustained activation of Wnt/ β -catenin signaling drives AKI to CKD progression," *Journal of the American Society of Nephrology*, vol. 27, no. 6, pp. 1727–1740, 2016.
- [37] T. Kawakami, S. Ren, and J. S. Duffield, "Wnt signalling in kidney diseases: dual roles in renal injury and repair," *Journal of Pathology*, vol. 229, no. 2, pp. 221–231, 2013.
- [38] K. Pulkkinen, S. Murugan, and S. Vainio, "Wnt signaling in kidney development and disease," *Organogenesis*, vol. 4, no. 2, pp. 55–59, 2008.
- [39] X. Qian, X. Yuan, S. Vonderfecht et al., "Inhibition of WISE preserves renal allograft function," *Journal of the American Society of Nephrology*, vol. 24, no. 1, pp. 66–76, 2013.
- [40] L. V. Riella, A. Djamali, and J. Pascual, "Chronic allograft injury: mechanisms and potential treatment targets," *Transplantation Reviews (Orlando, Fla.)*, vol. 31, no. 1, pp. 1–9, 2017.
- [41] C. von Toerne, C. Schmidt, J. Adams et al., "Wnt pathway regulation in chronic renal allograft damage," *American Journal of Transplantation*, vol. 9, no. 10, pp. 2223–2239, 2009.
- [42] J. Luo, J. Chen, Z. L. Deng et al., "Wnt signaling and human diseases: what are the therapeutic implications?," *Laboratory Investigation*, vol. 87, no. 2, pp. 97–103, 2007.
- [43] W. He, C. Dai, Y. Li, G. Zeng, S. P. Monga, and Y. Liu, "Wnt/beta-catenin signaling promotes renal interstitial fibrosis," *Journal of the American Society of Nephrology*, vol. 20, no. 4, pp. 765–776, 2009.
- [44] M. E. Seifert, J. P. Gaut, B. Guo et al., "WNT pathway signaling is associated with microvascular injury and predicts kidney transplant failure," *American Journal of Transplantation*, vol. 19, no. 10, pp. 2833–2845, 2019.
- [45] R. A. Bartolomé, L. Pintado-Berninches, M. Jaén, V. de Los Ríos, J. I. Imbaud, and J. I. Casal, "SOSTDC1 promotes invasion and liver metastasis in colorectal cancer via interaction with ALCAM/CD166," *Oncogene*, vol. 39, no. 38, pp. 6085–6098, 2020.
- [46] L. Liu, S. Wu, Y. Yang et al., "SOSTDC1 is down-regulated in non-small cell lung cancer and contributes to cancer cell proliferation," *Cell and Bioscience*, vol. 6, no. 1, p. 24, 2016.
- [47] Q. Zhou, J. Chen, J. Feng, Y. Xu, W. Zheng, and J. Wang, "SOSTDC1 inhibits follicular thyroid cancer cell proliferation, migration, and EMT via suppressing PI3K/Akt and MAPK/Erk signaling pathways," *Molecular and Cellular Biochemistry*, vol. 435, no. 1–2, article 3059, pp. 87–95, 2017.
- [48] K. A. Clausen, K. R. Blish, C. E. Birse et al., "SOSTDC1 differentially modulates Smad and beta-catenin activation and is down-regulated in breast cancer," *Breast Cancer Research and Treatment*, vol. 129, no. 3, pp. 737–746, 2011.
- [49] T. Rajkumar, N. Vijayalakshmi, G. Gopal et al., "Identification and validation of genes involved in gastric tumorigenesis," *Cancer Cell International*, vol. 10, no. 1, p. 45, 2010.
- [50] S. Crotty, "T follicular helper cell biology: a decade of discovery and diseases," *Immunity*, vol. 50, no. 5, pp. 1132–1148, 2019.
- [51] L. Xu, Y. Cao, Z. Xie et al., "The transcription factor TCF-1 initiates the differentiation of T_{FH} cells during acute viral infection," *Nature Immunology*, vol. 16, no. 9, pp. 991–999, 2015.
- [52] M. A. Linterman, W. Pierson, S. K. Lee et al., "Foxp3⁺ follicular regulatory T cells control the germinal center response," *Nature Medicine*, vol. 17, no. 8, pp. 975–982, 2011.

- [53] C. G. Vinuesa, M. A. Linterman, D. Yu, and I. C. MacLennan, "Follicular helper T cells," *Annual Review of Immunology*, vol. 34, no. 1, pp. 335–368, 2016.
- [54] J. van Loosdregt, V. Fleskens, M. M. Tiemessen et al., "Canonical Wnt signaling negatively modulates regulatory T cell function," *Immunity*, vol. 39, no. 2, pp. 298–310, 2013.
- [55] S. Keerthivasan, K. Aghajani, M. Dose et al., " β -Catenin promotes colitis and colon cancer through imprinting of proinflammatory properties in T cells," *Science Translational Medicine*, vol. 6, no. 225, pp. 225ra28–225228r, 2014.
- [56] A. S. Chong, D. M. Rothstein, K. Safa, and L. V. Riella, "Outstanding questions in transplantation: B cells, alloantibodies, and humoral rejection," *American Journal of Transplantation*, vol. 19, no. 8, pp. 2155–2163, 2019.
- [57] J. Li, Y. Luo, X. Wang, and G. Feng, "Regulatory B cells and advances in transplantation," *Journal of Leukocyte Biology*, vol. 105, no. 4, pp. 657–668, 2019.
- [58] M. I. Cascalho, B. J. Chen, M. Kain, and J. L. Platt, "The paradoxical functions of B cells and antibodies in transplantation," *Journal of Immunology*, vol. 190, no. 3, pp. 875–879, 2013.
- [59] L. Liu, Z. G. Wang, X. L. Pang et al., "Bortezomib ameliorates acute allograft rejection after renal transplant by inhibiting Tfh cell proliferation and differentiation via miR-15b/IRF4 axis," *International Immunopharmacology*, vol. 75, article 105758, 2019.
- [60] G. M. la Muraglia II, M. E. Wagener, M. L. Ford, and I. R. Badell, "Circulating T follicular helper cells are a biomarker of humoral alloreactivity and predict donor-specific antibody formation after transplantation," *American Journal of Transplantation*, vol. 20, no. 1, pp. 75–87, 2020.
- [61] S. Zhou, Z. Liu, H. Yuan et al., "Autoreactive B cell differentiation in diffuse ectopic lymphoid-like structures of inflamed pemphigus lesions," *Journal of Investigative Dermatology*, vol. 140, no. 2, pp. 309–318.e8, 2020.
- [62] S. Sakaguchi, M. Ono, R. Setoguchi et al., "Foxp3⁺ CD25⁺ CD4⁺ natural regulatory T cells in dominant self-tolerance and autoimmune disease," *Immunological Reviews*, vol. 212, no. 1, pp. 8–27, 2006.
- [63] T. Sumida, M. R. Lincoln, C. M. Ukeje et al., "Activated β -catenin in Foxp3⁺ regulatory T cells links inflammatory environments to autoimmunity," *Nature Immunology*, vol. 19, no. 12, pp. 1391–1402, 2018.
- [64] T. Tsujimura, M. Idei, M. Yoshikawa, O. Takase, and K. Hishikawa, "Roles and regulation of bone morphogenetic protein-7 in kidney development and diseases," *World journal of stem cells*, vol. 8, no. 9, pp. 288–296, 2016.
- [65] Y. Sato and M. Yanagita, "Functional heterogeneity of resident fibroblasts in the kidney," *Proceedings of the Japan Academy. Series B, Physical and Biological Sciences*, vol. 95, no. 8, pp. 468–478, 2019.
- [66] E. Dejana, "The role of wnt signaling in physiological and pathological angiogenesis," *Circulation Research*, vol. 107, no. 8, pp. 943–952, 2010.
- [67] J. L. Whyte, A. A. Smith, and J. A. Helms, "Wnt signaling and injury repair," *Cold Spring Harbor Perspectives in Biology*, vol. 4, no. 8, article a8078, 2012.
- [68] J. E. Lengfeld, S. E. Lutz, J. R. Smith et al., "Endothelial Wnt/ β -catenin signaling reduces immune cell infiltration in multiple sclerosis," *Proceedings of the National Academy of Sciences of the United States of America*, vol. 114, no. 7, pp. E1168–E1177, 2017.

Review Article

A Novel Insight into the Role of PLA2R and THSD7A in Membranous Nephropathy

Pingna Zhang ^{1,2}, Weijun Huang,² Qiyang Zheng,^{1,2} Jingyi Tang,^{1,2} Zhaocheng Dong ^{1,2},
Yuhua Jiang,^{1,2} Yuning Liu ^{1,2} and Weijing Liu ^{1,2,3}

¹Renal Research Institution of Beijing University of Chinese Medicine, Beijing, China

²Key Laboratory of Chinese Internal Medicine of Ministry of Education and Beijing, Dongzhimen Hospital Affiliated to Beijing University of Chinese Medicine, Beijing, China

³Institute of Nephrology, and Zhanjiang Key Laboratory of Prevention and Management of Chronic Kidney Disease, Guangdong Medical University, Zhanjiang, China

Correspondence should be addressed to Yuning Liu; liuyn2021@126.com and Weijing Liu; liuweijing-1977@hotmail.com

Received 8 May 2021; Revised 20 June 2021; Accepted 3 July 2021; Published 15 July 2021

Academic Editor: Cheng Yang

Copyright © 2021 Pingna Zhang et al. This is an open access article distributed under the Creative Commons Attribution License, which permits unrestricted use, distribution, and reproduction in any medium, provided the original work is properly cited.

Membranous nephropathy (MN) is an organ-restricted autoimmune disease mainly caused by circulating autoantibodies against podocyte antigens, including the M-type phospholipase A2 receptor (PLA2R) and thrombospondin domain-containing 7A (THSD7A). Antibodies against PLA2R are present in 70%–80% and against THSD7A in 2% of adult patients, which provides a paradigm shift in molecular diagnosis and management monitoring. Both antigens share some similar characteristics: they are expressed by podocytes and have wide tissue distributions; they are bound by autoantibodies only under nonreducing conditions, and the subtype of most autoantibodies is IgG4. However, the factors triggering autoantibody production as well as the association among air pollution, malignancy, and the pathogenesis of MN remain unclear. In this review, we discuss the similarity between the pathological mechanisms triggered by disparate antigens and their associated diseases. Furthermore, we demonstrated the possibility that PM2.5, malignancy, and gene expression specifically induce exposure of these antigens through conformational changes, molecular mimicry, or increased expression eliciting autoimmune responses. Thus, this review provides novel insights into the pathological mechanism of MN.

1. Introduction

Membranous nephropathy (MN) is a common autoimmune glomerular lesion, accounting for approximately 20%–30% of nephrotic syndrome cases in adults, with poor kidney prognosis [1, 2]. MN is caused by the deposition of immune complexes on the outer aspect of the glomerular basement membrane (GBM), which results in the thickening of the glomerular capillary wall, with expansion of the matrix material leading to the formation of spikes. The discovery of the M-type phospholipase A2 receptor (PLA2R) in 2009 [3] and thrombospondin domain-containing 7A (THSD7A) in 2014 [4] as two major autoantigens in idiopathic MN (iMN) has considerably advanced the understanding of the

molecular pathogenesis. These major breakthroughs have been quickly translated to clinical diagnosis and treatment monitoring, with anti-PLA2R [5] and anti-THSD7A antibodies being detected in 70%–80% and only 2% [4] of adult patients with iMN, respectively. Anti-PLA2R and anti-THSD7A antibody titers are key biomarkers that reflect disease activity [6], predict prognosis [7–10], and indicate treatment efficacy [11–13].

In recent years, more research has focused on the role of the lung as a potential contributor to autoimmune diseases [14]. The interesting phenomenon that long-term exposure to PM2.5 is closely related to the gradual increase in the morbidity of MN should be considered [15]. Furthermore, approximately 20% of patients with THSD7A-associated

MN are diagnosed with malignancy within a median time of 3 months since the diagnosis of MN, indicating that THSD7A-associated MN is related to an increased risk of malignancy. However, many aspects related to the initiation of autoantibody production and the association among air pollution, malignancy, and the pathogenesis of MN remain unclear. In this review, we highlight the similar characteristics between the two autoantigens and their associated diseases, discuss the possible mechanisms of initiation of antibody formation, and offer a novel view of the pathobiology of MN.

2. A Model Marker of iMN: PLA2R

2.1. The M-Type PLA2R. The landmark discovery of the PLA2R antigen revolutionized our understanding of MN, and research on its structural characteristics paved the way for revealing the molecular pathogenetic mechanisms of MN. In 2009, Beck et al. [3] identified a 185 kD protein in glomerular extracts in approximately 70% of samples from patients with iMN in nonreducing conditions. This protein was identified as PLA2R, a transmembrane glycoprotein that is largely confined to glomerular podocytes rather than other human glomerular cell types in the human kidneys. In addition, the endogenous glomerular expression of PLA2R is not detected in rodent or rabbit glomerular extracts. In the presence of reducing agents, reactivity is lost, suggesting that the antigenic epitope in PLA2R is a conformation and requires specific disulfide bonds. PLA2R is a type I transmembrane receptor and one of the four members of the mannose receptor family in mammals [16, 17]. Similar to the characteristics of the other members of this family, the extracellular portion of PLA2R contains an N-terminal cysteine-rich (CysR or ricin B) domain, a single fibronectin type 2 (FnII) domain, and eight C-type lectin-like domains (CTLDS). In addition, the short cytoplasmic domain of PLA2R contains motifs that allow constitutive endocytic recycling through clathrin-coated pits [18]. PLA2R undergoes endocytic recycling, which may provide a constant supply of accessible PLA2R for the formation of immune complexes at the podocyte membrane. Dong et al. [19] have made great progress in the determination of the structure of human M-type PLA2R by low-temperature electron microscopy. The ectodomain has high internal flexibility and adopts a compact dual-ring-shaped conformation at an acidic pH and an extended conformation at a basic pH. Owing to the expansion of the PLA2R structure at a basic pH, several major epitopes located in the CysR, CTLD1, and CTLD7 domains may be more accessible for the production of different antibodies [20–22]. However, whether this pH-dependent conformation is related to disease severity remains unknown. In a recent study, a transgenic mouse line expressing mouse PLA2R1 in podocytes was developed, which may open new avenues to address this problem [23].

2.2. PLA2R Epitopes and Spreading. Over the last decade, the measurement of the levels of circulating PLA2R antibodies has been broadly implemented in clinical practice worldwide for the diagnosis and monitoring of patients with iMN. In

addition to the total levels of circulating autoantibodies, a clear picture of major PLA2R epitopes is a prerequisite for understanding the pathogenic mechanism of anti-PLA2R autoantibody binding-induced iMN. Interestingly, two research groups identified B cell epitope-containing domains in the N-terminus of PLA2R with different conclusions because of the stability or folding of the truncated domains of PLA2R in their experimental protocols. Kao et al. [22] showed that the smallest immunodominant epitope in PLA2R containing CysR–FnII–CTLD1. Fresquet et al. [21] narrowed the region to CysR, where the 31 mer peptide blocked most of the autoantibody binding, possibly localizing the humoral epitope to this region. A subsequent study indicated that in addition to CysR, reactive epitopes were present in the CTLD1 and CTLD7 domains. CysR appeared as an immunodominant epitope and was recognized in all patients with circulating anti-PLA2R antibodies (Figure 1) [20].

With further research on autoimmune diseases, PLA2R epitope spreading has been recently identified as a prognostic biomarker to predict outcomes in MN. Epitope spreading, a phenomenon of diversity of epitopes recognized by T and B cells, begins with the outermost epitope of the target antigen (CysR for PLA2R), and then, other dominant immune epitopes (CTLD1 and/or CTLD7 for PLA2R) within the molecule or on neighboring molecules are exposed as the disease progresses, contributing to the expansion of the immune response [24]. As a result, the diversity of antibody repertoire is increased and the overall immune response is enhanced. Experimental evidence indicating that intramolecular epitope spreading might affect the severity of MN in humans has been previously established in Heymann nephritis [25]. Few weeks after the primary immune response, the serum of rats showed reactivity with ligand-binding domain fragments, indicating B cell epitope spreading; furthermore, proteinuria occurred as the epitope spread to further regions in the molecule. In a study, 69 patients with MN whose autoantibody repertoire was confined only to anti-CysR were younger and generally had mild disease activity [20], whereas those with antibodies against all three epitopes tended to be resistant to therapy and had poor renal prognosis. These observations showed that the immune response to PLA2R is an ordered process with prognostic relevance. Of note, the author hypothesized that a second immune hit induces intramolecular epitope spreading. In general, epitope spreading produces a more robust immune response and is more resistant to immunosuppressive treatment [26]. In a prospective cohort of 55 patients treated with rituximab [27], it was necessary to administer higher doses of rituximab to patients with epitope spreading to eliminate the autoantibodies and induce remission. Interestingly, spreaders tended to have higher anti-PLA2R autoantibody titers [28]. Therefore, until clinical testing of anti-PLA2R epitope spreading is routinely available, it seems appropriate that the total titer of anti-PLA2R autoantibodies serves as a surrogate for epitope spreading [29]. Identification of the epitopes will give rise to the development of novel and individualized therapies. Therefore, it is worth exploring the factors initiating epitope spreading.

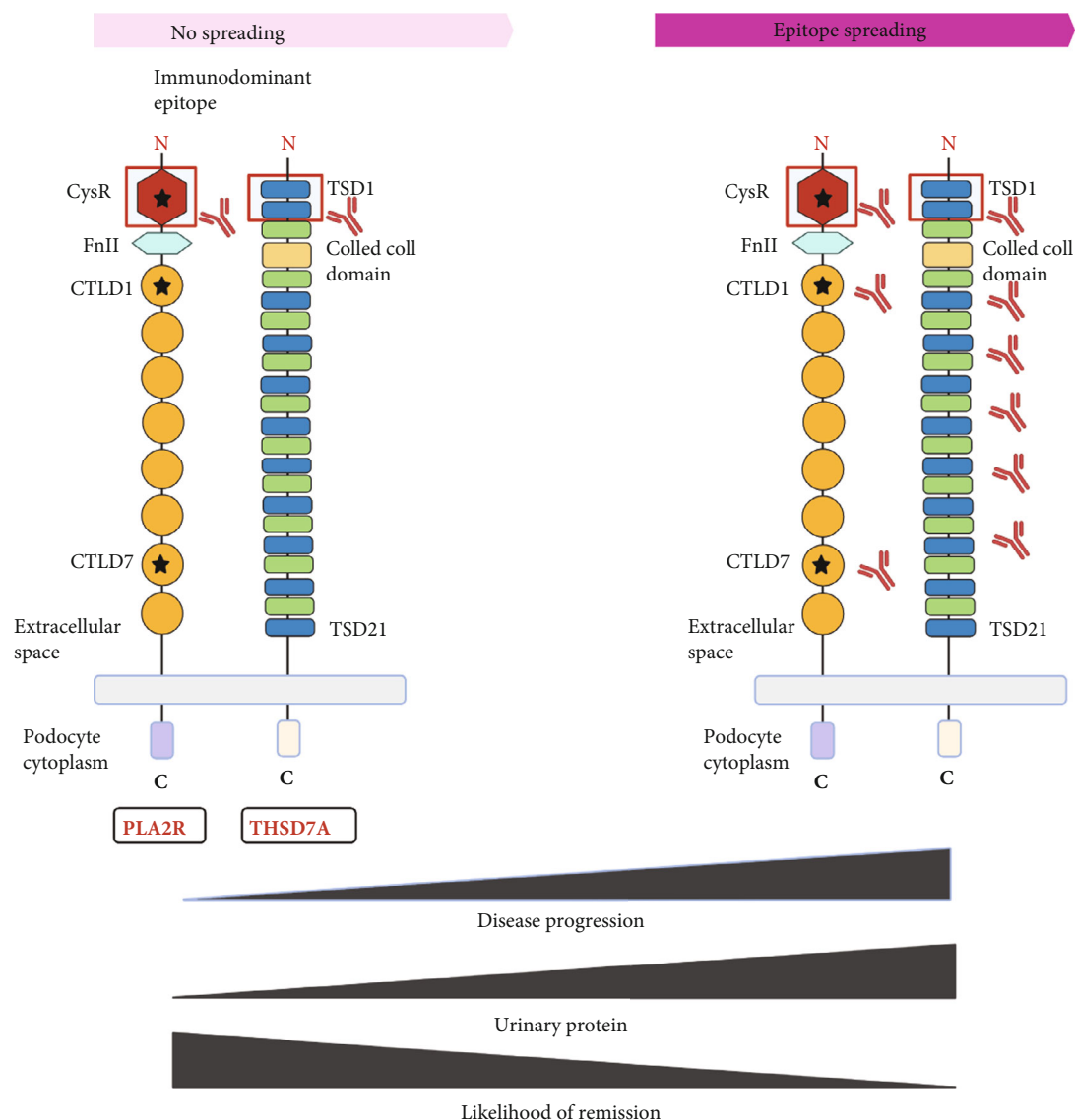


FIGURE 1: Schematic and epitope spreading of phospholipase A2 receptor (PLA2R) and of thrombospondin type 1 domain-containing 7A (THSD7A). The extracellular part of PLA2R contains an N-terminal cysteine-rich (CysR, or ricin B) domain, a single fibronectin type 2 (FnII) domain, and eight C-type lectin-like domains (CTLDs). The major epitopes are located in the CysR, CTLD1, and CTLD7 domains. THSD7A is a type 1 transmembrane protein with a large extracellular N-terminal region comprising 21 thrombospondin type 1 domains (TSDs) and a coiled coil domain in the extracellular. The predominant target of autoimmunity existed in the N-terminal region. Epitope spreading begins with the outermost epitope of the target antigen, and then, other dominant immune epitopes within the molecule or on neighboring molecules are exposed as the disease progresses, which are accompanied by the increase of proteinuria and the decrease of remission.

3. The Secondary Marker of iMN: THSD7A

3.1. Characteristics of THSD7A and Its Epitopes. The structural characteristics and epitopes of THSD7A have been gradually revealed. In 2014, after PLA2R, Tomas et al. [4] used a combination of glycoproteins purified from glomerular extracts, followed by Western blotting of the extracts under nonreducing conditions to detect antibodies that were reactive with a 250- kD protein in 2.5%–5% of samples from patients with iMN. This protein was identified by mass spectrometry as THSD7A, which is a type 1 transmembrane protein with a large extracellular N-terminal region comprising

21 thrombospondin type 1 (TSP-1) domains, a coiled coil domain, a single-pass transmembrane domain, and a short intracellular C-terminal tail (Figure 1). Seifert et al. [30] and Stoddard et al. [31] showed that these TSP-1 domains are included by alternating TSP-1-like and F-spondin-like domains, both of which consist of three antiparallel peptide strands tightly connected by three disulfide bridges between cysteine residues. Similar to PLA2R, THSD7A is expressed on the basal aspect of foot processes, and the subtype of most anti-THSD7A autoantibodies is IgG4. In addition, the nonreduced form of THSD7A can be exclusively recognized by autoantibodies, suggesting that disulfide bonds determine

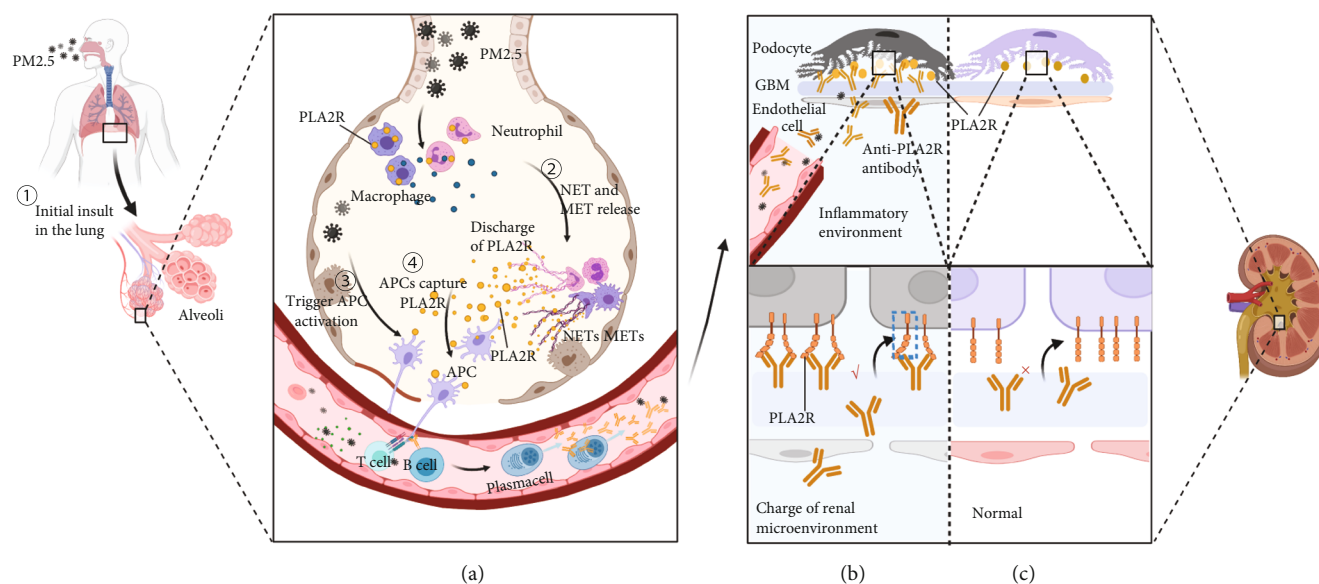


FIGURE 2: The hypothetical pathogenesis model of the relationship between the tumor and thrombospondin domain-containing 7A- (THSD7A-) associated membranous nephropathy (MN). (a) In theory, THSD7A acts as a potential tumor-associated antigen that is overexpressed by cancerous tissue allowing regional exposure of pathogenic epitopes of the autoantigen, which contributes to the production of anti-THSD7A antibodies. The extrarenal anti-THSD7A antibodies circulate into the glomerular capillaries and bind to THSD7A antigens located on podocytes. Besides, the tumor may alter the renal microenvironment that induces antigen conformational changes that allow binding of anti-THSD7A antibodies. (b) Pathogenicity of anti-THSD7A antibodies causing podocyte injury and proteinuria. The binding of anti-THSD7A antibodies to THSD7A on podocytes disrupts the slit diaphragm that allows albumin excretion into the urine, collapse of the actin cytoskeleton, and reduction of detachment from GBM. (c) The normal structure of podocyte foot processes. THSD7A that is present in foot processes closest to the slit diaphragm is involved in the stabilization of the slit diaphragm of mature podocytes, which forms the final barrier to albumin permeation. Abbreviations: APC: antigen-presenting cell; TCR: T cell receptor; MHC: major histocompatibility complex; GBM: glomerular basement membrane.

the antigenic epitope conformation. Compared with PLA2R, the identification of antigenic epitopes in THSD7A is less well defined. THSD7A is predicted to contain multiple epitopes in 18 domains (domains 1–17 and 19) by homology modeling [31], which corresponded well to the domains identified by Seifert et al. [30], except for domains 4 and 5. Additional epitope mapping revealed that the dominant epitope in THSD7A-associated MN is located within the N-terminal TSR1 domain, recognized by autoantibodies in 87% of patient serum samples. Although we have a general understanding of the epitopes in THSD7A, whether epitope spreading could also be a relevant biomarker of disease activity and clinical outcome remains to be determined.

3.2. Pathogenicity of Anti-THSD7A Antibodies. The possibility that antipodocyte antibodies alter podocyte function or induce podocyte injury in the absence of detectable complement activation is illustrated by THSD7A studies. In 2016, Tomas et al. [32] first isolated anti-THSD7A antibodies from patients and administered them to mice. They found that binding of autoantibodies to THSD7A on mouse podocytes resulted in the onset of proteinuria and a histopathological pattern that is typical of MN. Unlike previous findings that the activation of the complement system was responsible for podocyte damage, they detected that C3 and C5b-9 deposits were absent in these mice, whereas the histopathologic pattern of MN was initiated with induction of proteinuria at 3 days. In a subsequent study, they also could not

detect membrane attack complex in mice with podocyte injury after the injection of rabbit anti-THSD7A antibodies [33]. Further *in vitro* experiments showed that the anti-THSD7A antibody directly induced cytoskeleton rearrangement in THSD7A-expressing glomerular epithelial cells and activated focal adhesion-mediated signaling. These findings strengthen the preceding conclusion that complement activation is not vital in the initiation of podocyte injury and that anti-THSD7A antibodies can directly affect podocyte integrity *in vitro*, causing cell damage and proteinuria. Remarkably, knockdown of *thsd7aa*—the THSD7A ortholog—in zebrafish larvae interfered with podocyte differentiation and impaired glomerular filtration barrier integrity, suggesting an important role of THSD7A in normal podocyte function [33]. In a recent study, Herwig et al. [34] investigated the temporal expression, spatial expression, and biological function of THSD7A in podocytes to provide insights into the effect of THSD7A antibody in MN. THSD7A was found to be present in foot processes (FPs) closest to the slit diaphragm that connects interdigitating podocytes and prevents most proteins from entering the urinary space; its expression begun with glomerular vascularization during the capillary loop stage [35] (Figure 2(c)). In addition, they found that phenotypically, THSD7A was expressed in distinct membrane domains, such as TAPs, resulting in augmented podocyte adhesion and stabilization of podocyte cell dynamics. Addition of anti-THSD7A antibodies *in situ* disrupted the flexible nonclogging barrier to proteins by mechanical

alteration of the slit diaphragm, which is specific to the three-layered glomerular filter. Adhesion of the podocyte foot process to the glomerular filtration membrane was reduced by perturbation of the biological function of THSD7A. Both could destabilize the dynamics of FP and slit diaphragms, resulting in FP effacement and proteinuria, which are hallmarks of MN (Figure 2(b)).

4. Extrarenal Autoantigen Exposure

The location of autoantigens initially exposed to the immune system and how the immune response initiates the production of autoantibodies against podocytes and causes damage to podocytes remain controversial. Under normal circumstances, antigen-presenting cells or circulating T cells cannot directly contact autoantigens expressed in podocytes [36]. Notably, both PLA2R and THSD7A have a wide tissue distribution, including the kidneys. The extrarenal expression of antigens provides a basis for extrarenal autoantibody production. We hypothesize that primary exposure to autoantigens may occur in human organs other than the kidneys. PM2.5, gene expression, and tumors significantly facilitate the exposure of extrarenal antigens to the immune system and might account for the onset of MN.

4.1. Discharge of PLA2R: The Consequence of PM2.5 in iMN. Given that people who are exposed to high levels of PM2.5 in the province in China for a long time have an increased risk of MN, the effect of PM2.5 on glomerulopathy should be considered [15]. Although PLA2R is highly expressed in the kidney, it is also present in neutrophils [37], alveolar macrophages [38], airway epithelial cells, and submucosal epithelial cells in humans [39]. The lung, which has a large surface area, is vulnerable to environmental factors. Inhalation of PM2.5 can cause lung inflammation that results in the accumulation of inflammatory corpuscles in the airway or alveoli. Activated neutrophils and macrophages release neutrophil extracellular traps and macrophage extracellular traps, and PLA2R can also be discharged into the systemic circulation, initiating an autoimmune response [40] (Figure 3).

In addition, we hypothesize that PM2.5 exposure contributes to aberrant immune processing by activating antigen presentation and augmenting autoimmune responses. Experimental studies have shown that air pollution exposure and oxidative stress induce antigen-presenting cell (APC) maturation [41–45] and then equip them with antigen peptide MHC molecular complex required for the activation of T cell receptors. Interestingly, most of the cells involved in inflammation can also present antigens [46]. Of special relevance here is the observation that air pollutants (especially fine particulates) stimulated the production of cytokines, immunoglobulins, and immune complexes and led to immune dysfunction, which is related to the pathogenesis of some glomerular diseases [47–49]. In addition, PM2.5 can be considered a foreign body that induces activation of cellular immunity in the lungs. Thus, it is plausible that PM2.5-induced exposure of PLA2R outside the kidneys could increase the incidence of MN.

4.2. Facilitating Antigen Presentation: Genetic Susceptibility in MN. Genetic analysis has opened new ways to investigate the link between PLA2R-associated MN and T cell epitopes [50]. It is necessary to reveal the initial step of MN by understanding the interaction between the HLA-D and PLA2R1 loci in PLA2R-related MN. In 1979, iMN was already reported to be strongly associated with HLA-DR3 [51] and this was confirmed in subsequent studies. Owing to the development of genome-wide association studies for the identification of PLA2R, considerable progress has been made in the understanding of the molecular genotypes, which refined the locus to two series of alleles, HLA-DQAI and PLA2R1 [52]. The most significant locus was on chromosome 6, centered on HLA-DQAI, and homozygosity for the lead risk alleles increased the odds ratio (OR) for MN by 20-fold. The other strong signal came from PLA2R1, in which homozygosity increased the OR for MN by 4-fold. Meanwhile, because of the interaction between the two loci, homozygosity in both risk alleles increased the OR by 80-fold. Although the risk allele in PLA2R1 is intronic, it is unlikely to change the autoreactivity of PLA2R. A follow-up study by sequencing the coding sequence and splice sites of PLA2R1 in 95 patients with iMN identified no amino acid variations that were structurally specific to MN [53]. Because genetic variations in the amino acid sequence are common, it is hypothesized that the genetic susceptibility for iMN is conferred by single-nucleotide polymorphisms that might influence the expression levels or site of PLA2R in the presence of risk HLA alleles [54].

Based on these initial studies, several studies have confirmed the presence of risk alleles in or near HLA-DQAI [55–58] and found an association between the specific HLA – DQAI*0501 allele and the presence of circulating anti-PLA2R antibodies [56, 57, 59]. However, the situation is more complex; the degree of linkage disequilibrium of the HLA locus is high and several studies found that a risk signal could lie in the HLA-DRB locus. Cui et al. [60] identified independent risk alleles in DRB1 * 1501 and DRB1 * 0301, suggesting certain amino acid positions in the major histocompatibility complex (MHC) DRβ1 chain facilitate interactions with T cell epitopes of PLA2R. HLA class II genetic restriction controls specific peptides of PLA2R presenting to T cells to drive active B cells for high-affinity autoantibody production (Figure 4, ⊙). Another study by Le et al. [61] not only identified the most significant risk allele in DRB1 * 1501 but also revealed another independent significant risk allele in DRB3 * 0202. Of note, one of these two HLA haplotypes was also found in 44% of healthy controls, demonstrating that the presence of high-risk alleles may be necessary but not sufficient for the development of PLA2R-related MN. In addition to MN, HLA-DQAI risk alleles are significantly associated with lupus nephritis, type 1 diabetes, and focal segmental glomerulosclerosis in a German population [55].

In summary, the particular podocyte antigens targeted by autoantibodies may be involved in the genetic make-up. Genetic variants may change the molecular conformation of the antigens to expose new conformational epitopes or cryptic sites to enable processing to linear T cell peptides that facilitate the recognition of antigens by the immune system.

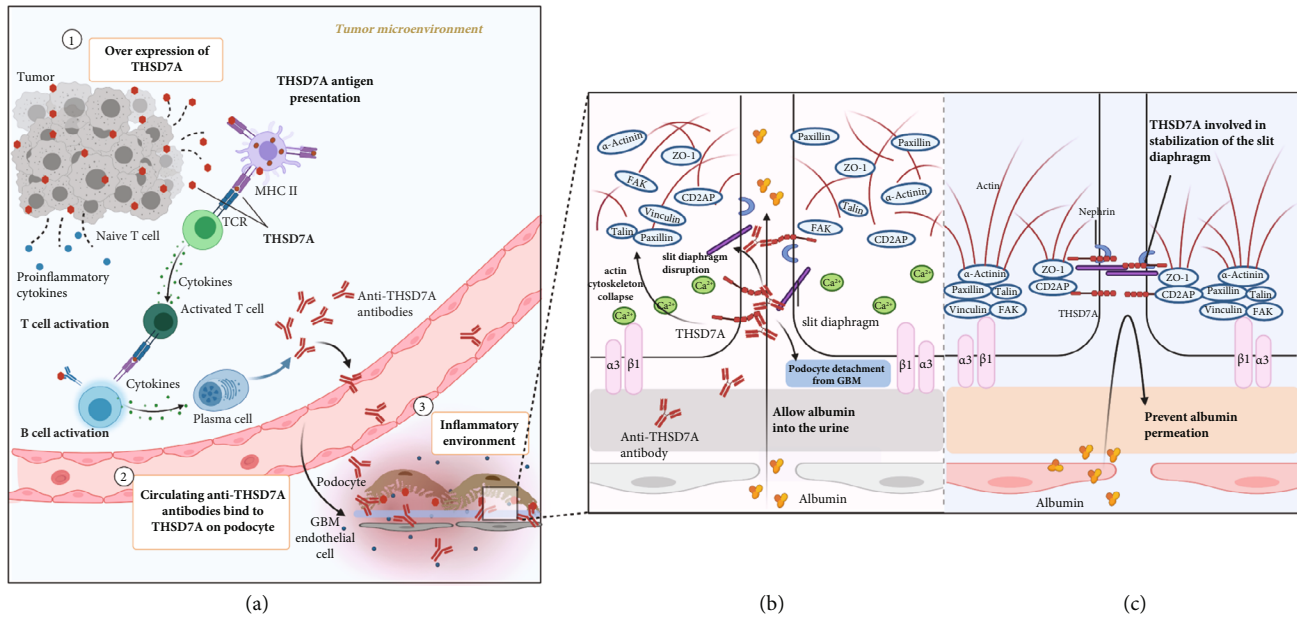


FIGURE 3: The hypothetical pathogenesis model of PM2.5-associated idiopathic membranous nephropathy (iMN). (a) PM2.5 induces extrarenal anti-PLA2R antibody production. Inhalation of PM2.5 results in the accumulation and activation of alveoli macrophages and neutrophils. PLA2R that is presented on these cells can be discharged into the inflammatory space, when neutrophil extracellular traps (NETs) and macrophage extracellular traps (METs) are released. Inflammation enhances the immunogenicity of the autoantigen and affects the antigen processing capacity of antigen-presenting cells (APCs), which contributes to the autoimmune response. We hypothesize that the PLA2R antigen may be captured by mature APCs, which become accessible producing anti-PLA2R antibodies. (b) The in situ immune complexes are initiated by binding of extrarenal anti-PLA2R antibodies to endogenous PLA2R in the glomeruli. PM2.5 can also cause renal injury and alter renal microenvironment, which may affect the molecular conformation of PLA2R antigen on the podocytes that is necessary for anti-PLA2R antibodies to bind. Abbreviations: GBM: glomerular basement membrane.

However, variants in the coding regions and HLA class II genes are common and gene expression alone is not enough to explain why some individuals develop MN, whereas others do not or some develop late onset disease [62]. Alternatively, we propose that the genetic susceptibility to iMN may not depend on the concurrence of PLA2R1 risk alleles but on the concurrence of HLA-D and other external triggers. Therefore, further studies are needed to identify other potential mechanisms affecting antigen conformation, and aberrant immune processing could lead to the production of anti-PLA2R antibodies in genetically predisposed patients with HLA and/or PLA2R1 risk variants.

4.3. Overexpression of THSD7A: The Role of Tumor in iMN.

The association between MN and cancer has been controversial, unlike PLA2R, which has been suggested to be a tumor suppressor [63], and patients with THSD7A-associated MN have a significantly increased risk of malignancy. Hoxha et al. [64] and Hanset et al. [65] found that 20% and 50% of patients with THSD7A-associated MN were diagnosed with malignancy on further work-up, respectively. In addition, two typical cases, one with metastases of endometrial carcinoma and the other with gallbladder tumor, further explain the potential molecular mechanism of disease induction in this setting [64, 66]. In both cases, THSD7A was found to be expressed in follicular dendritic cells of lymph nodes with metastatic infiltration. Assessment of the cancerous tissues showed increased THSD7A mRNA levels and elevated THSD7A protein expression, suggesting that THSD7A was

actively synthesized by cancer cells. In addition, several studies found that anti-THSD7A antibodies were correlated with malignancy, benign tumors, and neurological disease [66–68], which increases the possibility of extrarenal anti-THSD7A immunization. It is worth noting that upon tumor remission, even without the use of immunosuppressive agents, kidney disease can also be alleviated. Stahl et al. [69] reported that THSD7A, as a new tumor antigen, plays a potential role in human cancer. The finding that the expression of THSD7A differed according to the clinical stage and differentiation degree of various cancers suggests that THSD7A is involved in vascular invasion, cancer progression, metastasis, and angiogenesis mechanisms that support tumor growth.

Tumor growth requires an increased intratumoral blood supply that promotes angiogenesis, in which THSD7A, a tumor-associated antigen, is overexpressed, allowing regional exposure of the autoantigen to the immune system (Figure 2(a)). If this hypothesis is confirmed, it is necessary to reconsider the concept of primary versus secondary MN.

5. Antigen Conformational or Expression Changes

In the inflammatory state, the production and accumulation of reactive oxygen species (ROS) exceeds the ability of cells to clear oxides, and the imbalance between the oxidation and antioxidant systems leads to the development of oxidative stress. Under conditions of intense oxidative stress, disulfide

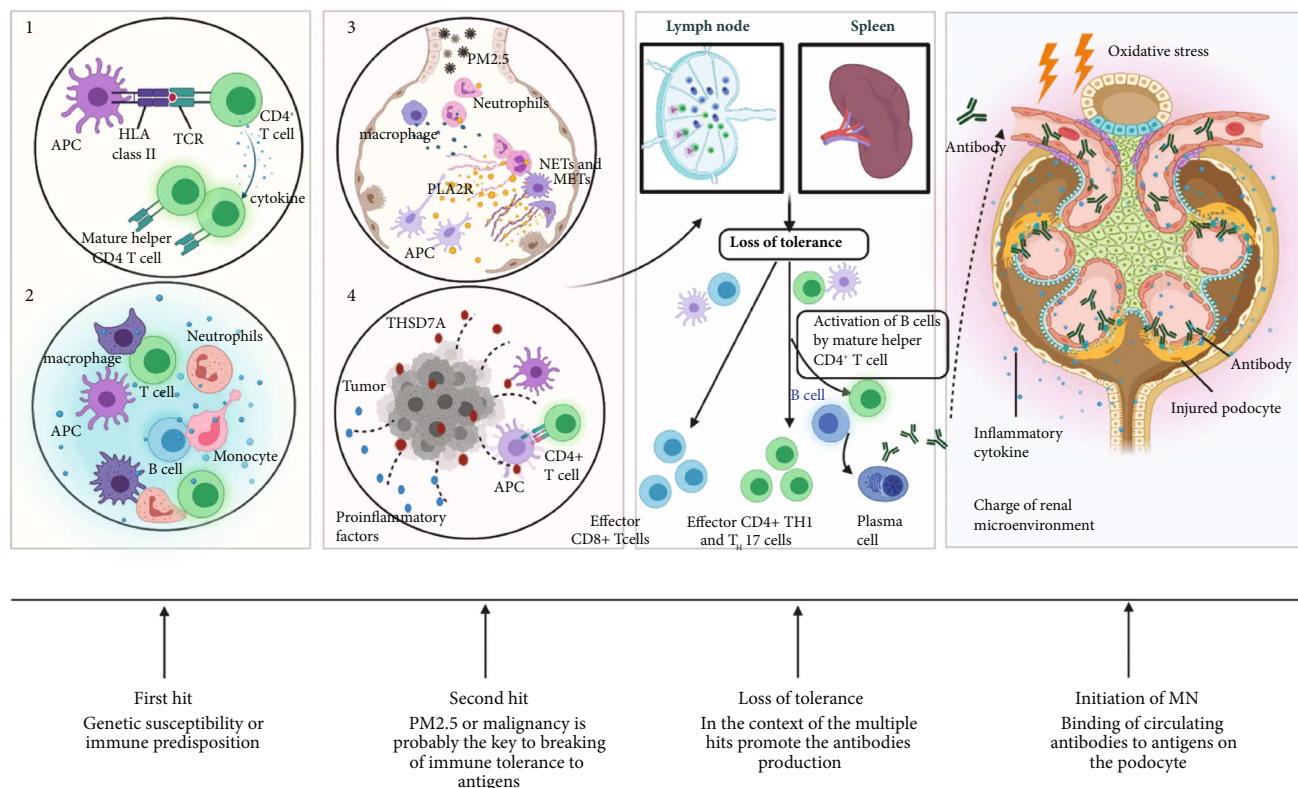


FIGURE 4: A multihit mechanism for the development of membranous nephropathy (MN). Genetic susceptibility or immune predisposition is thought to be involved in the ‘first hit’ that probably drives the initial development of MN. Furthermore, PM2.5 or malignancy probably emerges as “second hit” that exerts an additive effect on the activation of the immune response. In the context of multihit that causes loss of immune tolerance, T helper 1 (T_H1) and 17 (T_H17) cells are essential for autoantibody production. Once such an autoimmune response is established, proinflammatory cytokines would act to exacerbate the ongoing response. Besides, inflammation or pathogenic factors alter renal microenvironment, injure podocytes, and enhance the immunogenicity of autoantigens, which contribute to the development of MN. During the development of MN, circulating antibodies binding to the podocyte may be a perfect storm, rather than a straight forward conformeropathy. ① Risk allele associated with MN. ② Immune predisposition. ③ PM2.5 induces extrarenal phospholipase A2receptor (PLA2R) exposure to immune cells. ④ Malignancy induces thrombospondin domain-containing 7A (THSD7A) overexpression. Abbreviations: APC: antigen-presenting cell; HLA: human leukocyte antigen; TCR: T cell receptor; NETs: neutrophil extracellular traps; METs: macrophage extracellular traps.

bonds are formed; however, most proteins do not form disulfide bonds in a reducing environment [70]. It is worth noting that epitopes in both PLA2R and THSD7A require intact disulfide bonds to maintain their spatial structure and bioactivity [3, 4]. Thus, the antigenicity of PLA2R and THSD7A requires additional conditions. If oxidative stress is able to influence the development of disulfide bonds, a synergistic effect of exposure to these antigens or overexpression under pathological conditions can be expected.

5.1. Change in Conformation of Intrarenal Antigens. Because the lungs are directly exposed to the external world, pulmonary inflammation and airway injury caused by PM2.5 are highly prevalent [71]. PM2.5 is the carrier of toxic substances, and polycyclic aromatic hydrocarbons and transition metals adsorbed in it can also directly produce ROS, exacerbating inflammation [72]. Moreover, it has been reported that levels of superoxide radicals, H_2O_2 , and malondialdehyde increased and superoxide dismutase decreased in tissues and cells, suggesting that PM2.5 upregulated oxidative stress [73]. Under this strongly oxidizing environment, disul-

fide bonds can be formed in cytoplasmic proteins [74]. Therefore, when the lungs are exposed to PM2.5, the stability of PLA2R epitopes may facilitate selection of B cells for generation of captured antigens on MHC molecules to present to T cells, which is an important step in the initiation of the autoimmune mechanism in MN. Then, activated B cells differentiate into plasma cells with the assistance of Th cells and produce antibodies against the different epitopes of the PLA2R antigen [21]. In addition, PLA2R, following a pH-dependent configuration change, may adopt an extended configuration in the extracellular domain when the microenvironment is altered. Thus, the three main epitopes located in the CysR, CTLD1, and CTLD7 domains may be more accessible in the extended conformation of PLA2R that would otherwise not be recognized by the immune system, triggering epitope spreading.

Inflammation is one of the pathways activated because of environmental stimuli as well as cancer, which is linked to the pathogenesis of MN. Recent studies have demonstrated that cancer initiation and progression are linked to inflammation and oxidative stress [75]. Inflammation is considered

a hallmark of cancer in the tumor microenvironment. Indeed, cancer is viewed as a wound that does not heal [76], inducing persistent activation of inflammatory signals and releasing proinflammatory cytokines. Thus, cancer recruits inflammatory cells and stimulates them to generate ROS, reactive nitrogen intermediates, and cytokines [77, 78], that is, like a bridge, ROS plays a critical role in the close association between inflammation and cancer [79]. Therefore, during tumor development, upregulation of THSD7A and persistent expression of pathogenic epitopes triggers an immune response. In the first step, regionally expressed THSD7A, due to oncogenesis, is released and taken up by dendritic cells (DCs), which coordinate specific immune signals to lose peripheral tolerance to THSD7A. Such immunogenic signals might include proinflammatory cytokines and factors, such as TNF- α , IL-1, IFN- α , and CD40L/CD40, to promote immunity. DCs present a THSD7A antigen peptide to T cells in the form of antigen peptide MHC molecular complex, resulting in the activation of cytotoxic T lymphocytes and helper T cells (Th) against the THSD7A antigen. Developed mature Th cells and numerous cytokines drive the differentiation of activated B cells into plasma cells, which produce high-affinity antibodies [80].

5.2. Change in Expression of Podocyte Target Antigens and Other Potential Antigens. Circulating antibodies produced by extrarenal antigen exposure can specifically bind to podocyte target antigens through endothelial cells and GBM. In addition, the anti-PLA2R1 and anti-THSD7A antibodies initially produced against nonpodocyte antigens exclusively bind with podocyte antigen epitopes determined by the presence of disulfide bonds in a nonreducing state [4]. The role of antigen conformational changes in extrarenal tissue has been suggested in anti-GBM disease [81]. Exactly as that in Goodpasture's disease, MN may also be considered an autoimmune "conformeropathy" involving pathogenic conformational changes. Interestingly, air pollution and malignancy both cause oxidative stress and inflammation, which trigger the release of secondary mediators. The resulting cytokines and oxygen free radicals may exert distant effects in other organs, such as the kidneys. A study in China confirmed renal injury after consecutive exposure to PM2.5 and revealed that it occurred via inflammatory cytokine and chemokine expression and reduced antioxidant activity [73]. Analysis of renal biopsies in THSD7A-associated MN with malignancy revealed that more inflammatory cells infiltrated the glomeruli in patients with no malignancy [64, 82]. Therefore, both PM2.5 and malignancy may contribute to the nonreducing state in the renal microenvironment, enabling circulating antibodies to bind to cryptic epitopes that may be hidden in healthy individuals.

Antibodies against cytoplasmic podocyte proteins, including α -enolase, aldose reductase, and manganese superoxide dismutase 2, have been detected in the sera of patients with primary and secondary MN [83, 84]. However, these cytoplasmic antigens are not accessible to circulating antibodies under normal conditions. Oxidative stress caused by PM2.5 and tumors may be a primary insult to podocytes, which is responsible for the novel membrane expression of

cytoplasmic antigens, which triggers the formation of new antibodies [85, 86]. Although intriguing, the role of oxidative stress in the initiation and/or maintenance of the disease has not been firmly established.

6. Disparate Paths to the Same Disease

The initiation of MN is the result of a multihit mechanism. Based on the current understanding, we recognize the possibility that associated factors, including malignancy, chronic infection, or environmental factors, may represent a disease-precipitating "second hit" in a patient with genetic and immune predisposition to develop MN [87]. Through a large number of high-quality research [15, 64, 66, 69, 88], we discuss the similarities between PLA2R and THSD7A, focus on the effect of PM2.5 and tumor in MN, and allow to better identify the potential pathogenic factors in MN (Figure 4).

IgG4 is the most prevalent subclass in most cases of PLA2R- and THSD7A-related MN. IgM > IgG3 > IgG1 > IgG2 > IgG4 is considered the temporal model sequence of Ig class switching in the germinal center reaction [89]. To note, in the progress of MN, Ig subclasses switch from IgG1 at the early stage to IgG4 at all later stages [90]. Induced by environmental stimuli or other causes, the PLA2R1 antigen and/or THSD7A antigen constant is exposed to extrarenal tissues. During prolonged disease activity, high-affinity IgG4 often formed by following repeated or long-term exposure to antigen [91–93]. Based on this understanding, we have further speculated that the occurrence of MN is due to prolonged exposure of some factors. PLA2R and THSD7A expressed in extrarenal tissues and presenting pathogenic epitopes are necessary to elicit autoimmune responses. It should be noted that both PM2.5 and malignancy may induce extrarenal antigen exposure to immune cells through conformational changes, molecular mimicry, or upregulated expression and directly damage the kidneys. Inflammation enhances the immunogenicity of autoantigens and affects the antigen processing capacity of APCs, which contributes to the autoimmune response. Undoubtedly, genetic susceptibility influences the development of MN, and other pathogenic factors exert an additive effect in determining whether the genetic potential is manifested [94]. Immunization can be augmented by the unmasking of hidden cryptic epitopes undergoing conformational changes upon exposure to environmental stimuli [95]. The MN may appear to be primary but in fact represent occult secondary disease. The discovery of other factors that promote antigen recognized by the immune system is worthy of further exploration and confirmation. In addition to PM2.5 and tumor being clearly related to the occurrence of MN, dysbiosis of the gut microbiota could be another factor. Indeed, the existing studies indicate that patients with MN exhibited gut microbial signatures distinct from healthy controls, which suggests the potential of gut microbiota as a contributor in the pathogenesis of MN [96, 97]. However, the direct evidence for the relationship between dysbiosis of the gastrointestinal flora and the development of MN is lacking and needs to be further enriched.

In addition, PLA2R and THSD7A expressed in podocytes play an indispensable role in maintaining the integrity of podocyte function, which may determine why the disease mainly affects podocytes and the pathological features are limited to the kidney. The location of autoantigenic proteins is restricted to the space between podocytes and the GBM. The clearance of immune complexes under the glomerular epithelium may be blocked; however, the bronchial epithelium is in direct contact with the environment and the cell turnover rate is high, which may promote the clearance of immune deposits through the sputum. Moreover, the biology of autoantigenic proteins in podocytes is another key precondition. Fresquet et al. [98] offered insights into the role of PLA2R in podocytes through PLA2R and the A2t complex. They found that PLA2R may be at the heart of actin cytoskeleton reorganization and tight junction assembly. *In vitro*, anti-PLA2R antibodies interfere with the adhesion of podocytes to collagen type IV in MN [99]. As mentioned above, THSD7A plays an important role in the integrity of the glomerular filtration barrier. Autoantibodies to THSD7A might alter the structural and functional permeability of the slit diaphragm to proteins.

In conclusion, the discovery of PLA2R and THSD7A as two autoantigens in MN has been a “game changer” that has fundamentally changed our approach toward diseases. However, many questions remain unsolved. In this review, we analyzed the similarities in the pathological mechanisms triggered by disparate antigens and their associated diseases resulting in the same renal phenotype to explore the triggers of MN. Further research is required to reveal the molecular pathogenesis of MN in the lungs and tumors and investigate innovative therapeutic strategies targeting MN-specific pathological mechanisms.

Conflicts of Interest

The authors declare that they have no conflicts of interest.

Acknowledgments

This study was supported by funds from the National Natural Science Foundation of China (grant number 8207151173) and Horizontal Subject (HX-DZM-202018).

References

- [1] W. G. Couser, “Primary membranous nephropathy,” *Clinical Journal of the American Society of Nephrology*, vol. 12, no. 6, pp. 983–997, 2017.
- [2] P. Ronco and H. Debiec, “Pathophysiological advances in membranous nephropathy: time for a shift in patient’s care,” *The Lancet*, vol. 385, no. 9981, pp. 1983–1992, 2015.
- [3] L. H. Beck Jr., R. G. B. Bonegio, G. Lambeau et al., “M-type phospholipase A2 receptor as target antigen in idiopathic membranous nephropathy,” *The New England Journal of Medicine*, vol. 361, no. 1, pp. 11–21, 2009.
- [4] N. M. Tomas, L. H. Beck Jr., C. Meyer-Schwesinger et al., “Thrombospondin type-1 domain-containing 7A in idiopathic membranous nephropathy,” *The New England Journal of Medicine*, vol. 371, no. 24, pp. 2277–2287, 2014.
- [5] Y. du, J. Li, F. He et al., “The diagnosis accuracy of PLA2R-AB in the diagnosis of idiopathic membranous nephropathy: a meta-analysis,” *PLoS One*, vol. 9, no. 8, article e104936, 2014.
- [6] L. H. Beck Jr., F. C. Fervenza, D. M. Beck et al., “Rituximab-induced depletion of anti-PLA2R autoantibodies predicts response in membranous nephropathy,” *Journal of the American Society of Nephrology*, vol. 22, no. 8, pp. 1543–1550, 2011.
- [7] J. M. Hofstra, H. Debiec, C. D. Short et al., “Antiphospholipase A2 receptor antibody titer and subclass in idiopathic membranous nephropathy,” *Journal of the American Society of Nephrology*, vol. 23, no. 10, pp. 1735–1743, 2012.
- [8] E. Hoxha, S. Harendza, H. Pinnschmidt, U. Panzer, and R. A. K. Stahl, “M-type phospholipase A2 receptor autoantibodies and renal function in patients with primary membranous nephropathy,” *Clinical Journal of the American Society of Nephrology*, vol. 9, no. 11, pp. 1883–1890, 2014.
- [9] A. P. Bech, J. M. Hofstra, P. E. Brenchley, and J. F. M. Wetzels, “Association of anti-PLA2R antibodies with outcomes after immunosuppressive therapy in idiopathic membranous nephropathy,” *Clinical Journal of the American Society of Nephrology*, vol. 9, no. 8, pp. 1386–1392, 2014.
- [10] P. Ruggenenti, H. Debiec, B. Ruggiero et al., “Anti-phospholipase A2 receptor antibody titer predicts post-rituximab outcome of membranous nephropathy,” *Journal of the American Society of Nephrology*, vol. 26, no. 10, pp. 2545–2558, 2015.
- [11] A. E. van de Logt, K. Dahan, A. Rousseau et al., “Immunological remission in PLA2R-antibody-associated membranous nephropathy: cyclophosphamide versus rituximab,” *Kidney International*, vol. 93, no. 4, pp. 1016–1017, 2018.
- [12] J. Wang, Z. Cui, J. Lu et al., “Circulating antibodies against thrombospondin type-I domain-containing 7A in Chinese patients with idiopathic membranous nephropathy,” *Clinical Journal of the American Society of Nephrology*, vol. 12, no. 10, pp. 1642–1651, 2017.
- [13] C. Zaghrini, B. Seitz-Polski, J. Justino et al., “Novel ELISA for thrombospondin type 1 domain-containing 7A autoantibodies in membranous nephropathy,” *Kidney International*, vol. 95, no. 3, pp. 666–679, 2019.
- [14] S. A. Ritz, “Air pollution as a potential contributor to the ‘epidemic’ of autoimmune disease,” *Medical Hypotheses*, vol. 74, no. 1, pp. 110–117, 2010.
- [15] X. Xu, G. Wang, N. Chen et al., “Long-term exposure to air pollution and increased risk of membranous nephropathy in China,” *Journal of the American Society of Nephrology*, vol. 27, no. 12, pp. 3739–3746, 2016.
- [16] O. Llorca, “Extended and bent conformations of the mannose receptor family,” *Cellular and Molecular Life Sciences*, vol. 65, no. 9, pp. 1302–1310, 2008.
- [17] L. East and C. M. Isacke, “The mannose receptor family,” *Biochimica et Biophysica Acta (BBA) - General Subjects*, vol. 1572, no. 2-3, pp. 364–386, 2002.
- [18] E. Zvaritch, G. Lambeau, and M. Lazdunski, “Endocytic properties of the M-type 180-kDa receptor for secretory phospholipases A₂,” *The Journal of Biological Chemistry*, vol. 271, no. 1, pp. 250–257, 1996.
- [19] Y. Dong, L. Cao, H. Tang, X. Shi, and Y. He, “Structure of human M-type phospholipase A2 receptor revealed by cryo-electron microscopy,” *Journal of Molecular Biology*, vol. 429, no. 24, pp. 3825–3835, 2017.
- [20] B. Seitz-Polski, G. Dolla, C. Payré et al., “Epitope spreading of autoantibody response to PLA2R associates with poor

- prognosis in membranous nephropathy," *Journal of the American Society of Nephrology*, vol. 27, no. 5, pp. 1517–1533, 2016.
- [21] M. Fresquet, T. A. Jowitt, J. Gummadova et al., "Identification of a major epitope recognized by PLA2R autoantibodies in primary membranous nephropathy," *Journal of the American Society of Nephrology*, vol. 26, no. 2, pp. 302–313, 2015.
- [22] L. Kao, V. Lam, M. Waldman, R. J. Glasscock, and Q. Zhu, "Identification of the immunodominant epitope region in phospholipase A2 receptor-mediated autoantibody binding in idiopathic membranous nephropathy," *Journal of the American Society of Nephrology*, vol. 26, no. 2, pp. 291–301, 2015.
- [23] C. Meyer-Schwesinger, N. M. Tomas, S. Dehde et al., "A novel mouse model of phospholipase A2 receptor 1-associated membranous nephropathy mimics podocyte injury in patients," *Kidney International*, vol. 97, no. 5, pp. 913–919, 2020.
- [24] C. Cornaby, L. Gibbons, V. Mayhew, C. S. Sloan, A. Welling, and B. D. Poole, "B cell epitope spreading: mechanisms and contribution to autoimmune diseases," *Immunology Letters*, vol. 163, no. 1, pp. 56–68, 2015.
- [25] P. Shah, A. Tramontano, and S. P. Makker, "Intramolecular epitope spreading in Heymann nephritis," *Journal of the American Society of Nephrology*, vol. 18, no. 12, pp. 3060–3066, 2007.
- [26] D. J. Salant, "Does epitope spreading influence responsiveness to rituximab in PLA2R-associated membranous nephropathy?," *Clinical Journal of the American Society of Nephrology*, vol. 14, no. 8, pp. 1122–1124, 2019.
- [27] B. Seitz-Polski, K. Dahan, H. Debiec et al., "High-dose rituximab and early remission in PLA2R1-related membranous nephropathy," *Clinical Journal of the American Society of Nephrology*, vol. 14, no. 8, pp. 1173–1182, 2019.
- [28] K. Dahan, H. Debiec, E. Plaisier et al., "Rituximab for severe membranous nephropathy: a 6-month trial with extended follow-up," *Journal of the American Society of Nephrology*, vol. 28, no. 1, pp. 348–358, 2017.
- [29] B. Seitz-Polski, H. Debiec, A. Rousseau et al., "Phospholipase A2 receptor 1 epitope spreading at baseline predicts reduced likelihood of remission of membranous nephropathy," *Journal of the American Society of Nephrology*, vol. 29, no. 2, pp. 401–408, 2018.
- [30] L. Seifert, E. Hoxha, A. M. Eichhoff et al., "The most N-terminal region of THSD7A is the predominant target for autoimmunity in THSD7A-associated membranous nephropathy," *Journal of the American Society of Nephrology*, vol. 29, no. 5, pp. 1536–1548, 2018.
- [31] S. V. Stoddard, C. L. Welsh, M. M. Palopoli et al., "Structure and function insights garnered from in silico modeling of the thrombospondin type-1 domain-containing 7A antigen," *Proteins*, vol. 87, no. 2, pp. 136–145, 2019.
- [32] N. M. Tomas, E. Hoxha, A. T. Reinicke et al., "Autoantibodies against thrombospondin type 1 domain-containing 7A induce membranous nephropathy," *The Journal of Clinical Investigation*, vol. 126, no. 7, pp. 2519–2532, 2016.
- [33] N. M. Tomas, C. Meyer-Schwesinger, H. von Spiegel et al., "A heterologous model of thrombospondin type 1 domain-containing 7A-associated membranous nephropathy," *Journal of the American Society of Nephrology*, vol. 28, no. 11, pp. 3262–3277, 2017.
- [34] J. Herwig, S. Skuza, W. Sachs et al., "Thrombospondin type 1 domain-containing 7A localizes to the slit diaphragm and stabilizes membrane dynamics of fully differentiated podocytes," *Journal of the American Society of Nephrology*, vol. 30, no. 5, pp. 824–839, 2019.
- [35] T. B. Huber, B. Schermer, and T. Benzing, "Podocin organizes ion channel-lipid supercomplexes: implications for mechanosensation at the slit diaphragm," *Nephron. Experimental Nephrology*, vol. 106, no. 2, pp. e27–e31, 2007.
- [36] P. W. Mathieson, "What has the immune system got against the glomerular podocyte?," *Clinical and Experimental Immunology*, vol. 134, no. 1, pp. 1–5, 2003.
- [37] C. C. Silliman, E. E. Moore, G. Zallen et al., "Presence of the M-type sPLA(2) receptor on neutrophils and its role in elastase release and adhesion," *American Journal of Physiology. Cell Physiology*, vol. 283, no. 4, pp. C1102–C1113, 2002.
- [38] F. Granata, A. Petraroli, E. Boilard et al., "Activation of cytokine production by secreted phospholipase A2 in human lung macrophages expressing the M-type receptor," *Journal of Immunology*, vol. 174, no. 1, pp. 464–474, 2005.
- [39] W. Liu, C. Gao, H. Dai et al., "Immunological pathogenesis of membranous nephropathy: focus on PLA2R1 and its role," *Frontiers in Immunology*, vol. 10, p. 1809, 2019.
- [40] V. Papayannopoulos, "Neutrophil extracellular traps in immunity and disease," *Nature Reviews. Immunology*, vol. 18, no. 2, pp. 134–147, 2018.
- [41] S. Verstraelen, R. van den Heuvel, I. Nelissen, H. Witters, G. Verheyen, and G. Schoeters, "Flow cytometric characterisation of antigen presenting dendritic cells after in vitro exposure to diesel exhaust particles," *Toxicology In Vitro*, vol. 19, no. 7, pp. 903–907, 2005.
- [42] S. Becker and J. Soukup, "Coarse(PM(2.5-10)), fine(PM(2.5)), and ultrafine air pollution particles induce/increase immune costimulatory receptors on human blood-derived monocytes but not on alveolar macrophages," *Journal of Toxicology and Environmental Health. Part A*, vol. 66, no. 9, pp. 847–859, 2003.
- [43] B. Bleck, D. B. Tse, I. Jaspers, M. A. Curotto de Lafaille, and J. Reibman, "Diesel exhaust particle-exposed human bronchial epithelial cells induce dendritic cell maturation," *Journal of Immunology*, vol. 176, no. 12, pp. 7431–7437, 2006.
- [44] R. F. Hamilton Jr., A. Holian, and M. T. Morandi, "A comparison of asbestos and urban particulate matter in the in vitro modification of human alveolar macrophage antigen-presenting cell function," *Experimental Lung Research*, vol. 30, no. 2, pp. 147–162, 2004.
- [45] S. Kantengwa, L. Jornot, C. Devenoges, and L. P. Nicod, "Superoxide anions induce the maturation of human dendritic cells," *American Journal of Respiratory and Critical Care Medicine*, vol. 167, no. 3, pp. 431–437, 2003.
- [46] F. D. Batista and N. E. Harwood, "The who, how and where of antigen presentation to B cells," *Nature Reviews. Immunology*, vol. 9, no. 1, pp. 15–27, 2009.
- [47] B. Granum, P. I. Gaarder, E. C. Groeng, R. B. Leikvold, E. Namork, and M. Løvik, "Fine particles of widely different composition have an adjuvant effect on the production of allergen-specific antibodies," *Toxicology Letters*, vol. 118, no. 3, pp. 171–181, 2001.
- [48] H. Takano, T. Yoshikawa, T. Ichinose, Y. Miyabara, K. Imaoka, and M. Sagai, "Diesel exhaust particles enhance antigen-induced airway inflammation and local cytokine expression in mice," *American Journal of Respiratory and Critical Care Medicine*, vol. 156, no. 1, pp. 36–42, 1997.

- [49] J. M. Brown, J. C. Pfau, and A. Holian, "Immunoglobulin and lymphocyte responses following silica exposure in New Zealand and mixed mice," *Inhalation Toxicology*, vol. 16, no. 3, pp. 133–139, 2004.
- [50] P. Ronco and H. Debiec, "Molecular pathogenesis of membranous nephropathy," *Annual Review of Pathology*, vol. 15, no. 1, pp. 287–313, 2020.
- [51] P. T. Klouda, E. J. Acheson, F. S. Goldby et al., "Strong association between idiopathic membranous nephropathy and HLA-DRW3," *The Lancet*, vol. 314, no. 8146, pp. 770–771, 1979.
- [52] H. C. Stanescu, M. Arcos-Burgos, A. Medlar et al., "Risk HLA-DQA1 and PLA2R1 alleles in idiopathic membranous nephropathy," *The New England Journal of Medicine*, vol. 364, no. 7, pp. 616–626, 2011.
- [53] M. J. Coenen, J. M. Hofstra, H. Debiec et al., "Phospholipase A2 receptor (PLA2R1) sequence variants in idiopathic membranous nephropathy," *Journal of the American Society of Nephrology*, vol. 24, no. 4, pp. 677–683, 2013.
- [54] K. Z. Latt, K. Honda, M. Thiri et al., "Identification of a two-SNP PLA2R1 haplotype and HLA-DRB1 alleles as primary risk associations in idiopathic membranous nephropathy," *Scientific Reports*, vol. 8, no. 1, article 15576, 2018.
- [55] P. Sekula, Y. Li, H. C. Stanescu et al., "Genetic risk variants for membranous nephropathy: extension of and association with other chronic kidney disease aetiologies," *Nephrology, Dialysis, Transplantation*, vol. 32, no. 2, pp. 325–332, 2017.
- [56] R. Ramachandran, V. Kumar, A. Kumar et al., "PLA2R antibodies, glomerular PLA2R deposits and variations in PLA2R1 and HLA-DQA1 genes in primary membranous nephropathy in South Asians," *Nephrology, Dialysis, Transplantation*, vol. 31, no. 9, pp. 1486–1493, 2016.
- [57] J. Lv, W. Hou, X. Zhou et al., "Interaction between PLA2R1 and HLA-DQA1 variants associates with anti-PLA2R antibodies and membranous nephropathy," *Journal of the American Society of Nephrology*, vol. 24, no. 8, pp. 1323–1329, 2013.
- [58] M. Saeed, M. L. Beggs, P. D. Walker, and C. P. Larsen, "PLA2R-associated membranous glomerulopathy is modulated by common variants in PLA2R1 and HLA-DQA1 genes," *Genes and Immunity*, vol. 15, no. 8, pp. 556–561, 2014.
- [59] D. Kanigicherla, J. Gummadova, E. A. McKenzie et al., "Anti-PLA2R antibodies measured by ELISA predict long-term outcome in a prevalent population of patients with idiopathic membranous nephropathy," *Kidney International*, vol. 83, no. 5, pp. 940–948, 2013.
- [60] Z. Cui, L. J. Xie, F. J. Chen et al., "MHC class II risk alleles and amino acid residues in idiopathic membranous nephropathy," *Journal of the American Society of Nephrology*, vol. 28, no. 5, pp. 1651–1664, 2017.
- [61] W. B. Le, J. S. Shi, T. Zhang et al., "HLA – DRB1 * 15 : 01 and HLA – DRB3 * 02 : 02 in PLA2R-related membranous nephropathy," *Journal of the American Society of Nephrology*, vol. 28, no. 5, pp. 1642–1650, 2017.
- [62] K. J. Robson, J. D. Ooi, S. R. Holdsworth, J. Rossjohn, and A. R. Kitching, "HLA and kidney disease: from associations to mechanisms," *Nature Reviews. Nephrology*, vol. 14, no. 10, pp. 636–655, 2018.
- [63] D. Vindrieux, A. Augert, C. A. Girard et al., "PLA2R1 mediates tumor suppression by activating JAK2," *Cancer Research*, vol. 73, no. 20, pp. 6334–6345, 2013.
- [64] E. Hoxha, L. H. Beck Jr., T. Wiech et al., "An indirect immunofluorescence method facilitates detection of thrombospondin type 1 domain-containing 7A-specific antibodies in membranous nephropathy," *Journal of the American Society of Nephrology*, vol. 28, no. 2, pp. 520–531, 2017.
- [65] N. Hanset, S. Aydin, N. Demoulin et al., "Podocyte antigen staining to identify distinct phenotypes and outcomes in membranous nephropathy: a retrospective multicenter cohort study," *American Journal of Kidney Diseases*, vol. 76, no. 5, pp. 624–635, 2020.
- [66] E. Hoxha, T. Wiech, P. R. Stahl et al., "A mechanism for cancer-associated membranous nephropathy," *The New England Journal of Medicine*, vol. 374, no. 20, pp. 1995–1996, 2016.
- [67] F. Lin, D. Zhang, J. Chang et al., "THSD7A-associated membranous nephropathy in a patient with neurofibromatosis type 1," *European Journal of Medical Genetics*, vol. 61, no. 2, pp. 84–88, 2018.
- [68] Z. Zhang, T. Gong, H. G. Rennke, and R. Hayashi, "Duodenal schwannoma as a rare association with membranous nephropathy: a case report," *American Journal of Kidney Diseases*, vol. 73, no. 2, pp. 278–280, 2019.
- [69] P. R. Stahl, E. Hoxha, T. Wiech, C. Schröder, R. Simon, and R. A. K. Stahl, "THSD7A expression in human cancer," *Genes, Chromosomes & Cancer*, vol. 56, no. 4, pp. 314–327, 2017.
- [70] T. E. Danciu and M. Whitman, "Oxidative stress drives disulfide bond formation between basic helix-loop-helix transcription factors," *Journal of Cellular Biochemistry*, vol. 109, no. 2, pp. 417–424, 2010.
- [71] K. H. Kim, E. Kabir, and S. Kabir, "A review on the human health impact of airborne particulate matter," *Environment International*, vol. 74, pp. 136–143, 2015.
- [72] N. Li, C. Sioutas, A. Cho et al., "Ultrafine particulate pollutants induce oxidative stress and mitochondrial damage," *Environmental Health Perspectives*, vol. 111, no. 4, pp. 455–460, 2003.
- [73] M. X. Xu, Y. T. Qin, C. X. Ge et al., "Activated iRhom2 drives prolonged PM2.5 exposure-triggered renal injury in Nrf2-defective mice," *Nanotoxicology*, vol. 12, no. 9, pp. 1045–1067, 2018.
- [74] S. Chakravarthi, C. E. Jessop, and N. J. Bulleid, "The role of glutathione in disulfide bond formation and endoplasmic-reticulum-generated oxidative stress," *EMBO Reports*, vol. 7, no. 3, pp. 271–275, 2006.
- [75] S. I. Grivennikov, F. R. Greten, and M. Karin, "Immunity, inflammation, and cancer," *Cell*, vol. 140, no. 6, pp. 883–899, 2010.
- [76] H. F. Dvorak, "Tumors: wounds that do not heal. Similarities between tumor stroma generation and wound healing," *The New England Journal of Medicine*, vol. 315, no. 26, pp. 1650–1659, 1986.
- [77] M. Valko, C. J. Rhodes, J. Moncol, M. Izakovic, and M. Mazur, "Free radicals, metals and antioxidants in oxidative stress-induced cancer," *Chemico-Biological Interactions*, vol. 160, no. 1, pp. 1–40, 2006.
- [78] E. Shacter, E. J. Beecham, J. M. Covey, K. W. Kohn, and M. Potter, "Activated neutrophils induce prolonged DNA damage in neighboring cells," *Carcinogenesis*, vol. 9, no. 12, pp. 2297–2304, 1988.
- [79] C. Tabolacci, C. Forni, R. N. Jadeja, and F. Facchiano, "Natural compounds against cancer, inflammation, and oxidative

- stress," *BioMed Research International*, vol. 2019, Article ID 9495628, 2 pages, 2019.
- [80] D. S. Chen and I. Mellman, "Oncology meets immunology: the cancer-immunity cycle," *Immunity*, vol. 39, no. 1, pp. 1–10, 2013.
- [81] V. Pedchenko, O. Bondar, A. B. Fogo et al., "Molecular architecture of the Goodpasture autoantigen in anti-GBM nephritis," *The New England Journal of Medicine*, vol. 363, no. 4, pp. 343–354, 2010.
- [82] C. Lefaucheur, B. Stengel, D. Nochy et al., "Membranous nephropathy and cancer: epidemiologic evidence and determinants of high-risk cancer association," *Kidney International*, vol. 70, no. 8, pp. 1510–1517, 2006.
- [83] Y. Kimura, N. Miura, H. Debiec et al., "Circulating antibodies to α -enolase and phospholipase A2 receptor and composition of glomerular deposits in Japanese patients with primary or secondary membranous nephropathy," *Clinical and Experimental Nephrology*, vol. 21, no. 1, pp. 117–126, 2017.
- [84] M. Prunotto, M. L. Carnevali, G. Candiano et al., "Autoimmunity in membranous nephropathy targets aldose reductase and SOD2," *Journal of the American Society of Nephrology*, vol. 21, no. 3, pp. 507–519, 2010.
- [85] A. Pozdzik, I. Brochériou, C. David, F. Touzani, J. M. Goujon, and K. M. Wissing, "Membranous nephropathy and anti-podocytes antibodies: implications for the diagnostic workup and disease management," *BioMed Research International*, vol. 2018, Article ID 6281054, 19 pages, 2018.
- [86] A. Pozdzik, F. Touzani, I. Brochériou, and F. Corazza, "Molecular classification of membranous nephropathy," *Current Opinion in Nephrology and Hypertension*, vol. 28, no. 4, pp. 336–344, 2019.
- [87] L. H. Beck Jr., "PLA2R and THSD7A: disparate paths to the same disease?," *Journal of the American Society of Nephrology*, vol. 28, no. 9, pp. 2579–2589, 2017.
- [88] J. Li, Z. Cui, J. Long et al., "Primary glomerular nephropathy among hospitalized patients in a national database in China," *Nephrology, Dialysis, Transplantation*, vol. 33, no. 12, pp. 2173–2181, 2018.
- [89] A. M. Collins and K. J. Jackson, "A temporal model of human IgE and IgG antibody function," *Frontiers in Immunology*, vol. 4, p. 235, 2013.
- [90] C. C. Huang, A. Lehman, A. Albawardi et al., "IgG subclass staining in renal biopsies with membranous glomerulonephritis indicates subclass switch during disease progression," *Modern Pathology*, vol. 26, no. 6, pp. 799–805, 2013.
- [91] G. Vidarsson, G. Dekkers, and T. Rispen, "IgG subclasses and allotypes: from structure to effector functions," *Frontiers in Immunology*, vol. 5, p. 520, 2014.
- [92] P. Bruhns, "Properties of mouse and human IgG receptors and their contribution to disease models," *Blood*, vol. 119, no. 24, pp. 5640–5649, 2012.
- [93] R. C. Aalberse, S. O. Stapel, J. Schuurman, and T. Rispen, "Immunoglobulin G4: an odd antibody," *Clinical and Experimental Allergy*, vol. 39, no. 4, pp. 469–477, 2009.
- [94] X. D. Zhang, Z. Cui, and M. H. Zhao, "The genetic and environmental factors of primary membranous nephropathy: an overview from China," *Kidney Diseases (Basel)*, vol. 4, no. 2, pp. 65–73, 2018.
- [95] H. Debiec and P. Ronco, "Immune response against autoantigen PLA2R is not gambling: implications for pathophysiology, prognosis, and therapy," *Journal of the American Society of Nephrology*, vol. 27, no. 5, pp. 1275–1277, 2016.
- [96] J. Zhang, D. Luo, Z. Lin et al., "Dysbiosis of gut microbiota in adult idiopathic membranous nephropathy with nephrotic syndrome," *Microbial Pathogenesis*, vol. 147, article 104359, 2020.
- [97] R. Dong, M. Bai, J. Zhao, D. Wang, X. Ning, and S. Sun, "A comparative study of the gut microbiota associated with immunoglobulin a nephropathy and membranous nephropathy," *Frontiers in Cellular and Infection Microbiology*, vol. 10, article 557368, 2020.
- [98] M. Fresquet, T. A. Jowitt, E. A. McKenzie et al., "PLA₂R binds to the annexin A2-S100A10 complex in human podocytes," *Scientific Reports*, vol. 7, no. 1, article 7028, p. 6876, 2017.
- [99] A. Škoberne, A. Behnert, B. Teng et al., "Serum with phospholipase A2 receptor autoantibodies interferes with podocyte adhesion to collagen," *European Journal of Clinical Investigation*, vol. 44, no. 8, pp. 753–765, 2014.

Research Article

Predictive Significance of the Prognostic Nutritional Index (PNI) in Patients with Severe COVID-19

Wei Wei ¹, Xingyue Wu ^{1,2}, Chaoyuan Jin ¹, Tong Mu ³, Guorong Gu ¹, Min Min ¹,
Sucheng Mu ¹ and Yi Han ¹

¹Department of Emergency Medicine, Zhongshan Hospital, Fudan University, Shanghai, China

²Shanghai Medical College, Fudan University, Shanghai, China

³Nanjing Sport Institute, Nanjing, China

Correspondence should be addressed to Min Min; min.min@zs-hospital.sh.cn, Sucheng Mu; 18111210085@fudan.edu.cn, and Yi Han; han.yi@zs-hospital.sh.cn

Received 17 March 2021; Accepted 28 June 2021; Published 13 July 2021

Academic Editor: Francois Meurens

Copyright © 2021 Wei Wei et al. This is an open access article distributed under the Creative Commons Attribution License, which permits unrestricted use, distribution, and reproduction in any medium, provided the original work is properly cited.

Background. The prognostic nutritional index (PNI) has been reported to significantly correlate with poor survival and postoperative complications in patients with various diseases, but its relationship with mortality in COVID-19 patients has not been addressed. **Method.** A multicenter retrospective study involving patients with severe COVID-19 was conducted to investigate whether malnutrition and other clinical characteristics could be used to stratify the patients based on risk. **Results.** A total of 395 patients were included in our study, with 236 patients in the training cohort, 59 patients in the internal validation cohort, and 100 patients in the external validation cohort. During hospitalization, 63/236 (26.69%) and 14/59 (23.73%) patients died in the training and validation cohorts, respectively. PNI had the strongest relationships with the neutrophil-lymphocyte ratio (NLR) and lactate dehydrogenase (LDH) level but was less strongly correlated with the CURB65, APACHE II, and SOFA scores. The baseline PNI score, platelet (PLT) count, LDH level, and PaO₂/FiO₂ (P/F) ratio were independent predictors of mortality in COVID-19 patients. A nomogram incorporating these four predictors showed good calibration and discrimination in the derivation and validation cohorts. A PNI score less than 33.405 was associated with a higher risk of mortality in severe COVID-19 patients in the Cox regression analysis. **Conclusion.** These findings have implications for predicting the risk of mortality in COVID-19 patients at the time of admission and provide the first direct evidence that a lower PNI is related to a worse prognosis in severe COVID-19 patients.

1. Introduction

By the end of 19th June 2021, more than 177,833,450 confirmed coronavirus disease 2019 (COVID-19) cases had been documented worldwide, with more than 3,851,736 deaths [1]. Unlike patients with other common infectious diseases, patients with COVID-19 have a wide range of clinical manifestations, including complex and mixed pulmonary conditions and multiorgan failure that can lead to death. However, not all patients develop a poor clinical outcome. Given the large number of COVID-19 cases, we need to pay more attention to those who are likely to progress to death.

Recent evidence has shown that malnutrition is a critical prognostic factor in many diseases, including autoimmune

diseases [2], cardiovascular diseases [3], lung diseases [4, 5], and malignancies [6]. Chronic inflammatory diseases are associated with the increased production of catabolic cytokines, muscle catabolism, appetite suppression, and lower albumin levels [7]. High degrees of malnutrition correlate with high levels of inflammation [8]. Malnutrition is a modifiable risk factor [9].

The prognostic nutritional index (PNI) is calculated based on the serum albumin concentration and lymphocyte count in the peripheral blood. Previously, the PNI was reported to correlate significantly with poor survival and postoperative complications in patients with various malignant digestive system tumors [10, 11]. A previous study indicated that a lower PNI in patients with a decreased left atrial

ejection fraction tended to be associated with a higher risk of mortality in a retrospective study [12]. Once they have been infected with severe acute respiratory syndrome coronavirus 2 (SARS-CoV-2), patients, particularly elderly patients, often develop cardiovascular dysfunction due to the widespread expression of angiotensin-converting enzyme 2 (ACE2) in the heart and blood vessels [13]. Therefore, the prognostic value of the PNI in patients with COVID-19 is worth further investigation. However, to date, the relevant studies have mainly focused on crude analyses rather than establishing a systematic, quantified model; hence, the application value of the present PNI is extremely limited [14, 15].

As current evidence regarding the prognostic impact of malnutrition on severe COVID-19 is limited and the relationship between malnutrition and mortality in COVID-19 patients has not been addressed, we aimed to identify the prevalence, clinical associations, and prognostic consequences of malnutrition in a retrospective cohort of patients with severe COVID-19 and establish a novel prognostic nomogram for the early prediction and modification of the disease outcome.

2. Materials and Methods

2.1. Data Source. The medical records and compiled data used in this retrospective study were collected from COVID-19 patients in Renmin Hospital of Wuhan University and Jin Yin Tan Hospital in Wuhan City. All patients had a clear clinical outcome of either hospital discharge or death. Data were reviewed by a trained team of physicians [16]. The study was approved by the Ethics Committee of Renmin Hospital of Wuhan University.

2.2. Laboratory Confirmation. Laboratory confirmation of SARS-CoV-2 infection was obtained with patients' throat swab specimens and was conducted in Renmin Hospital of Wuhan University and Jin Yin Tan Hospital. The severity of COVID-19 was defined at the time of admission, according to American Thoracic Society guidelines for community-acquired pneumonia (CAP) [17]. All laboratory tests were performed according to the clinical care needs of the patients. The laboratory assessments consisted of a complete blood count, liver function assessment, and arterial blood gas measurements. To minimize sampling bias, the data on admission were obtained, by communicating effectively with medical workers and double-checking.

The neutrophil-lymphocyte ratio (NLR) was defined by dividing the neutrophil count by the lymphocyte count. The prognostic nutritional index (PNI) score was calculated using the formula $10 \times \text{serum albumin (g/dL)} + 0.005 \times \text{total lymphocyte count (mm}^3\text{)}$ [18]. A score greater than 38 is considered normal; scores of 35 to 38 and less than 35 reflect moderate and severe malnutrition, respectively.

2.3. Statistical Analysis. Continuous variables are expressed as the medians with interquartile ranges (IQRs) as well as mean with standard deviation, while categorical variables are presented as frequencies and percentages (%). To determine differences between the two groups, chi-squared tests

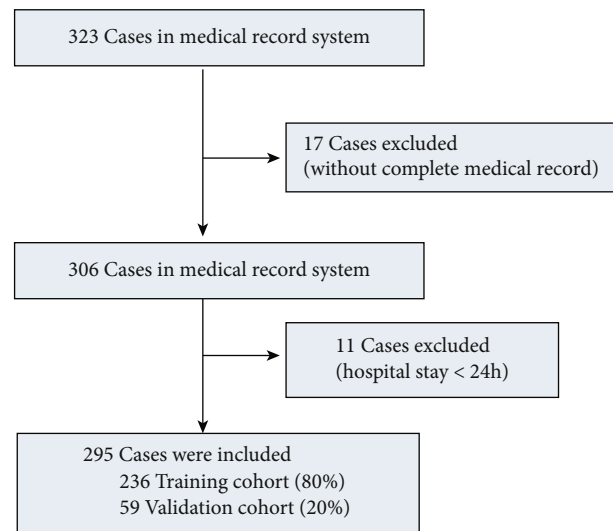


FIGURE 1: Flowchart of patient recruitment in the internal cohort.

were performed for categorical variables, and Wilcoxon rank-sum and one-way ANOVA tests were performed for continuous variables [19].

A novel prognostic nomogram was constructed based on the results of multivariate analysis obtained with the rms package in R; the nomogram was developed based on 80% of the internal data and validated with the remaining 20% of internal data and another 100 external cases. The discrimination performance of the nomogram was quantified using the concordance index (C-index) and calibration curve analysis. The C-index value ranges from 0.5 to 1.0, with 0.5 indicating random chance and 1.0 demonstrating perfect discrimination.

To evaluate the discriminatory ability of the prognostic nomogram, receiver operating characteristic (ROC) curves were generated, and differences among the areas under the curve (AUCs) were compared. Correlations were assessed with Kendall's tau-b analysis, and survival probability was evaluated by Cox analysis.

All analyses were conducted using R (version 3.6.3) and SPSS (version 25). *P* values less than 0.05 were considered statistically significant in each statistical analysis.

3. Results

3.1. Clinical Characteristics of Patients with COVID-19. A total of 323 patients with severe COVID-19 were identified according to the inclusion criteria, of whom 28 patients were excluded for having (1) incomplete medical records ($n = 17$) or (2) hospital stays less than 24 h ($n = 11$). Finally, 295 patients were included in our study, with 236 patients in the training cohort and 59 patients in the validation cohort (Figure 1). The clinical characteristics of the patients included in the training and validation cohorts are presented in Table 1. Among them, 116 (49.15%) and 37 (62.71%) patients were male, with a median age of 61 years and 60 years in the training and validation cohorts, respectively. There were no significant differences in clinical characteristics or disease severity scores (using the Acute Physiology

TABLE 1: Clinical characteristics of patients with COVID-19 in the training and validation cohorts.

	Training cohort (N = 236)	Validation cohort (N = 59)	P value
Gender (N, %)			0.062
Male	116 (49.15%)	37 (62.71%)	
Female	120 (50.85%)	22 (37.29%)	
Age (years)	61 (48.71)	60 (47.69)	0.550
History (N, %)			
Hypertension	70 (29.67%)	15 (25.42%)	0.520
DM	36 (15.25%)	8 (13.56%)	0.744
Symptoms (N, %)			
Fatigue	104 (44.07%)	27 (45.76%)	0.815
Headache	15 (6.36%)	3 (5.08%)	0.952
Cough	152 (64.41%)	42 (71.19%)	0.326
Dyspnea	67 (28.39%)	19 (32.20%)	0.564
Diarrhea	27 (11.44%)	6 (10.17%)	0.774
Signs			
Temperature	36.70 (36.50, 37.00)	36.60 (36.40, 37.00)	0.548
HR (bpm)	86 (80, 98)	88 (81, 98)	0.336
RR (/min)	20 (19, 24)	20 (20, 25)	0.552
Laboratory indices			
WBC counts (10 ⁹ /L)	6.29 (4.46, 9.37)	5.37 (3.96, 8.02)	0.105
NEU counts (10 ⁹ /L)	6.51 (3.56, 50.3)	5.14 (3.12, 29.41)	0.244
LYM counts (10 ⁹ /L)	1.21 (0.72, 5.33)	1.16 (0.72, 2.77)	0.886
MON counts (10 ⁹ /L)	0.53 (0.37, 2.33)	0.53 (0.33, 1.15)	0.764
NLR	4.62 (2.32, 10.02)	3.78 (1.79, 9.11)	0.406
HGB (g/L)	125.00 (115.00, 137.00)	130.00 (119.00, 143.00)	0.088
PLT (10 ⁹ /L)	199.50 (141.80, 262.30)	205.00 (156.00, 252.00)	0.529
ALB (g/L)	35.10 (32.00, 39.40)	37.00 (32.30, 40.00)	0.308
PNI	36.19 (33.23, 39.78)	37.00 (32.30, 40.00)	0.916
ALT (U/L)	26.50 (17.30, 43.00)	27.00 (16.50, 41.50)	0.689
AST (U/L)	31.00 (22.00, 46.00)	30.00 (21.00, 38.50)	0.460
GLU (mmol/L)	5.90 (5.02, 7.79)	5.56 (4.77, 6.79)	0.059
LDH (U/L)	296.50 (211.00, 432.50)	273.00 (220.00, 420.00)	0.825
P/F ratio (mmHg)	168.85 (100.42, 289.75)	231.42 (131.11, 342.00)	0.120
CURB65	1.0 (0, 1.0)	1.0 (0, 1.0)	0.931
APACHE II	6.0 (3.0, 10.0)	6.0 (3.0, 10.0)	0.600
SOFA	2.0 (1.0, 4.0)	1.0 (0, 3.0)	0.143
Death (N, %)	63 (26.69%)	14 (23.73%)	0.643

Abbreviations: DM; diabetes mellitus; WBC: white blood cells; NEU: neutrophils; LYM: lymphocytes; MON: monocytes; NLR: neutrophil-lymphocyte ratio; HGB: hemoglobin; PLT: platelet; ALB: albumin; PNI: prognostic nutritional index; ALT: alanine transaminase; AST: aspartate aminotransferase; LDH: lactic dehydrogenase; P/F ratio: PaO₂/FiO₂ ratio; CURB65: confusion, uremia, respiratory rate, blood pressure; APACHE II: Acute Physiology and Chronic Health Evaluation II; SOFA: sequential organ failure assessment.

and Chronic Health Evaluation II (APACHE II), sequential organ failure assessment (SOFA), and CURB65 scores) between the two cohorts (Table 1). During hospitalization, 63/236 (26.69%) and 14/59 (23.73%) patients died in the training and validation cohorts, respectively. In addition, 218 (73.90%) patients recovered and had been discharged at the time of analysis.

3.2. Comparison between Surviving and Nonsurviving Patients in the Training Cohort.

Surviving and nonsurviving patients with COVID-19 had significant differences in many clinical characteristics and laboratory indicators on admission. Patients in the nonsurviving group were significantly older (74 years, IQR 63-81) than surviving patients (55 years, IQR 44-66). Although many studies have indicated that male patients with COVID-19 had a higher risk of mortality, in the current study, 37 of the 63 (58.73%) patients in the nonsurviving group were male, which was not different from the proportion in the surviving group (79/173, 45.66%, $P > 0.05$). Patients with hypertension were more likely to die, and those

TABLE 2: Clinical characteristics of surviving and nonsurviving patients in the training cohort.

	Surviving patients (N = 173)	Nonsurviving patients (N = 63)	P value
Gender (N, %)			0.076
Male	79 (45.66%)	37 (58.73%)	
Female	94 (54.34%)	26 (41.27%)	
Age (years)	55 (44, 66)	74 (63, 81)	<0.001
History (N, %)			
Hypertension	40 (23.12%)	30 (47.62%)	<0.001
DM	25 (14.45%)	11 (17.46%)	0.569
Symptoms (N, %)			
Fatigue	63 (36.42%)	41 (65.08%)	<0.001
Headache	13 (7.51%)	2 (3.17%)	0.227
Cough	115 (66.47%)	37 (58.73%)	0.272
Dyspnea	36 (20.81%)	31 (49.21%)	<0.001
Diarrhea	20 (11.56%)	7 (11.11%)	0.925
Signs			
T	36.70 (36.50, 37.00)	36.70 (36.40, 36.90)	0.543
HR	86 (80, 98)	86 (77,102)	0.898
RR	20 (19, 22)	20 (19, 28)	0.052
Laboratory indices			
WBC counts (10 ⁹ /L)	5.65 (4.28, 8.10)	8.49 (5.61, 11.98)	<0.001
NEU counts (10 ⁹ /L)	5.51 (3.02, 61.85)	7.89 (4.62, 13.16)	0.259
LYM counts (10 ⁹ /L)	1.53 (0.9, 11.2)	0.60 (0.41, 1.13)	<0.001
MON counts (10 ⁹ /L)	0.57 (0.39, 4.8)	0.42 (0.28, 0.65)	<0.001
NLR	3.41 (1.89, 7.16)	12.51 (7.22, 18.83)	<0.001
HGB (g/L)	125.00 (116.50, 136.00)	122.00 (111.00, 137.50)	0.560
PLT (10 ⁹ /L)	214.00 (157.00, 287.00)	155.00 (114.50, 208.50)	<0.001
ALB	35.90 (32.60, 39.90)	33.40 (31.40, 36.60)	0.004
PNI	37.21 (34.07, 40.56)	33.41 (31.46, 36.63)	<0.001
ALT (U/L)	27.00 (16.50, 43.00)	25.00 (20.00, 45.00)	0.708
AST (U/L)	30.00 (22.00, 42.00)	41.00 (24.00, 63.00)	0.001
GLU (mmol/L)	5.60 (4.96, 7.13)	7.00 (5.78, 10.30)	<0.001
LDH (U/L)	263.00 (195.00, 355.00)	493.00 (362.50, 611.50)	<0.001
P/F ratio	257.58 (168.85, 314.75)	104.44 (75.56, 150.00)	<0.001

Abbreviations: DM: diabetes mellitus; WBC: white blood cells; NEU: neutrophils; LYM: lymphocytes; MON: monocytes; NLR: neutrophil/lymphocyte ratio; HGB: hemoglobin; PLT: platelet; ALB: albumin; PNI: prognostic nutritional index; ALT: alanine transaminase; AST: aspartate aminotransferase; LDH: lactic dehydrogenase; P/F ratio: PaO₂/FiO₂ ratio; CURB65: confusion, uremia, respiratory rate, blood pressure; APACHE II: Acute Physiology and Chronic Health Evaluation II; SOFA: sequential organ failure assessment.

TABLE 3: Univariate and multivariate logistic analysis of potential prognostic factors.

Factors	Univariate analysis		Multivariate analysis	
	OR (95% CI)	P value	OR (95% CI)	P value
Age	1.089 (1.060, 1.119)	<0.001		0.105
Hypertension	3.023 (1.646, 5.551)	<0.001		0.165
Fatigue	3.254 (1.780, 5.950)	<0.001		0.666
Dyspnea	3.687 (1.992, 6.822)	<0.001		0.373
WBC count	1.197 (1.101, 1.301)	<0.001		0.696
NLR	1.155 (1.101, 1.212)	<0.001		0.805
PLT count	0.991 (0.987, 0.995)	<0.001	0.984 (0.974, 0.993)	0.001
PNI	0.839 (0.774, 0.911)	<0.001	0.853 (0.740, 0.983)	0.028
LDH	1.009 (1.006, 1.011)	<0.001	1.005 (1.001, 1.009)	0.012
P/F ratio	0.986 (0.981, 0.992)	<0.001	0.988 (0.981, 0.995)	0.001

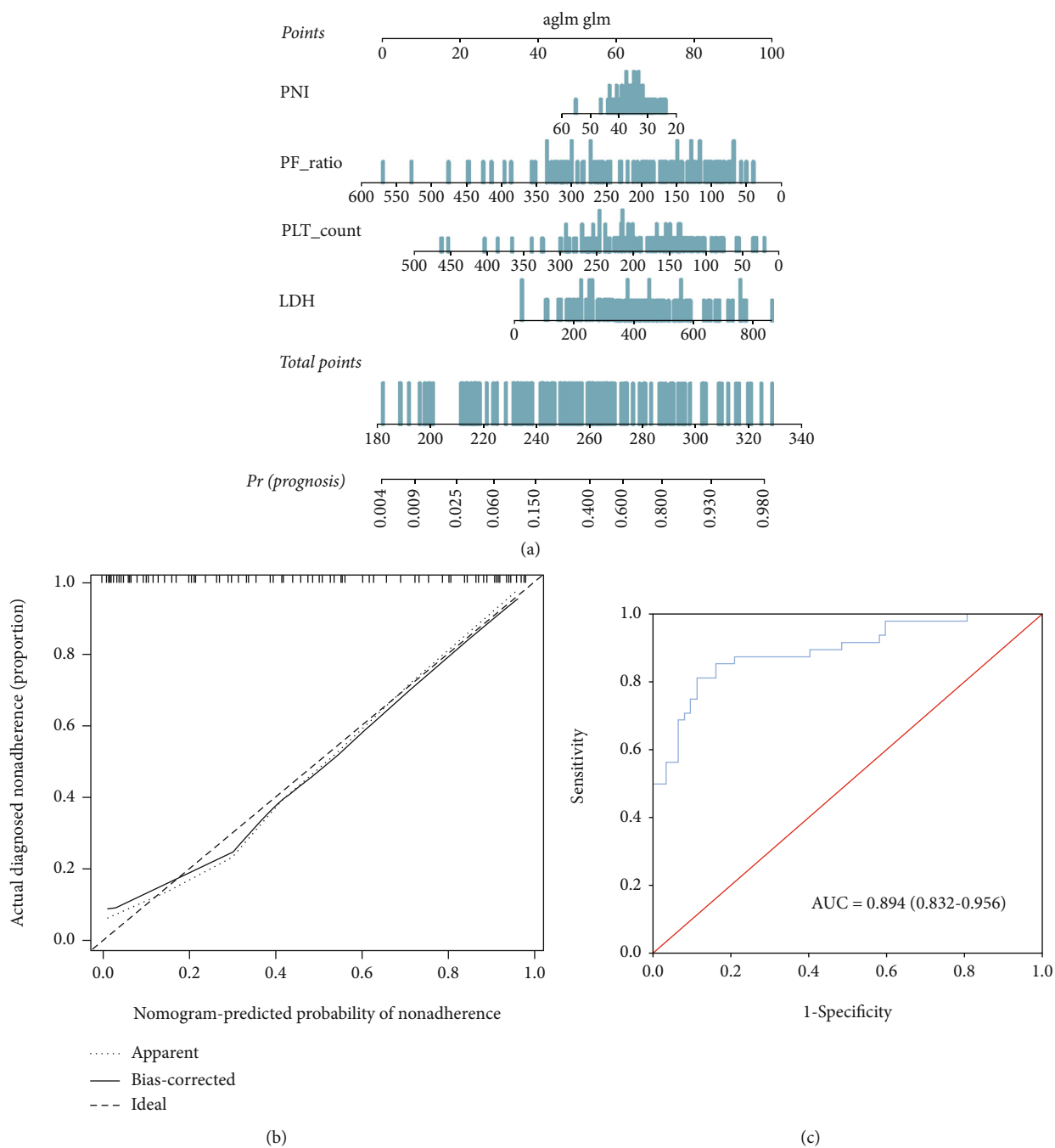
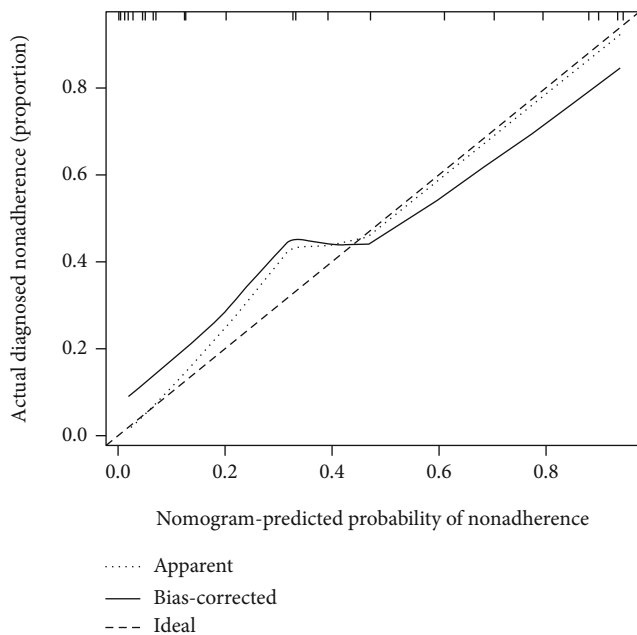


FIGURE 2: Development and performance of the nomogram in the training cohort. (a) A nomogram for predicting the prognosis of patients with severe COVID-19; (b) calibration curve of the nomogram in the training cohort, which depicts the calibration of the nomogram in terms of the agreement between the predicted risk of death and observed outcomes. The 45° dotted line represents an ideal prediction, and the solid line represents the bias-corrected predictive performance of the nomogram. The closer the solid line fits the ideal line, the better the predictive accuracy of the nomogram; (c) ROC curve of the nomogram in the training cohort.

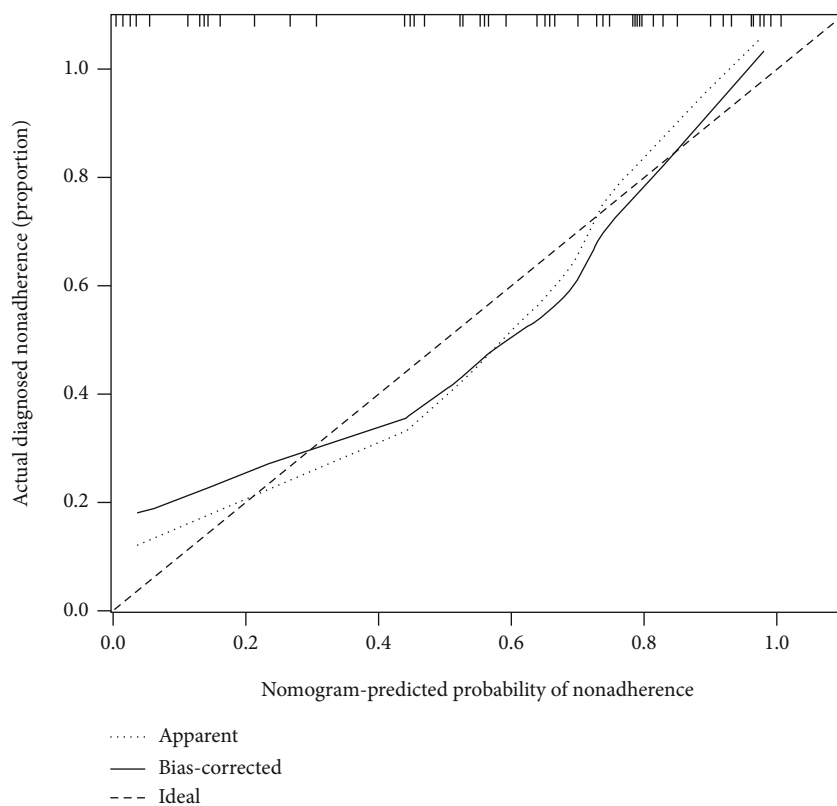
with dyspnea before admission tend to have a poor outcome ($P < 0.001$), with a history of hypertension in 41/63 (65.08%) of nonsurviving patients and 63/171 (36.84%) of surviving patients and dyspnea in 31/63 (49.21%) of nonsurviving patients and 36/171 (21.05%) of surviving patients. No differences were observed in headache, cough, and diarrhea.

In addition, the white blood cell count ($10^9/L$) was 8.49 (IQR 5.61-11.98) in nonsurviving patients, which was dra-

matically higher than that in surviving patients (5.65 (IQR 4.28-8.10)). Meanwhile, the lymphocyte count ($10^9/L$) was 0.60 (IQR 0.41-1.13) in nonsurviving patients, which was dramatically lower than that in surviving patients (1.53 (IQR 0.90-11.2)). The monocyte count ($10^9/L$) was 0.42 (IQR 0.28-0.65) in nonsurviving patients, which was dramatically lower than that in surviving patients (0.57 (IQR 0.39-4.8)) (Table 2, $P < 0.001$). As an indicator of the



(a)



(b)

FIGURE 3: Continued.

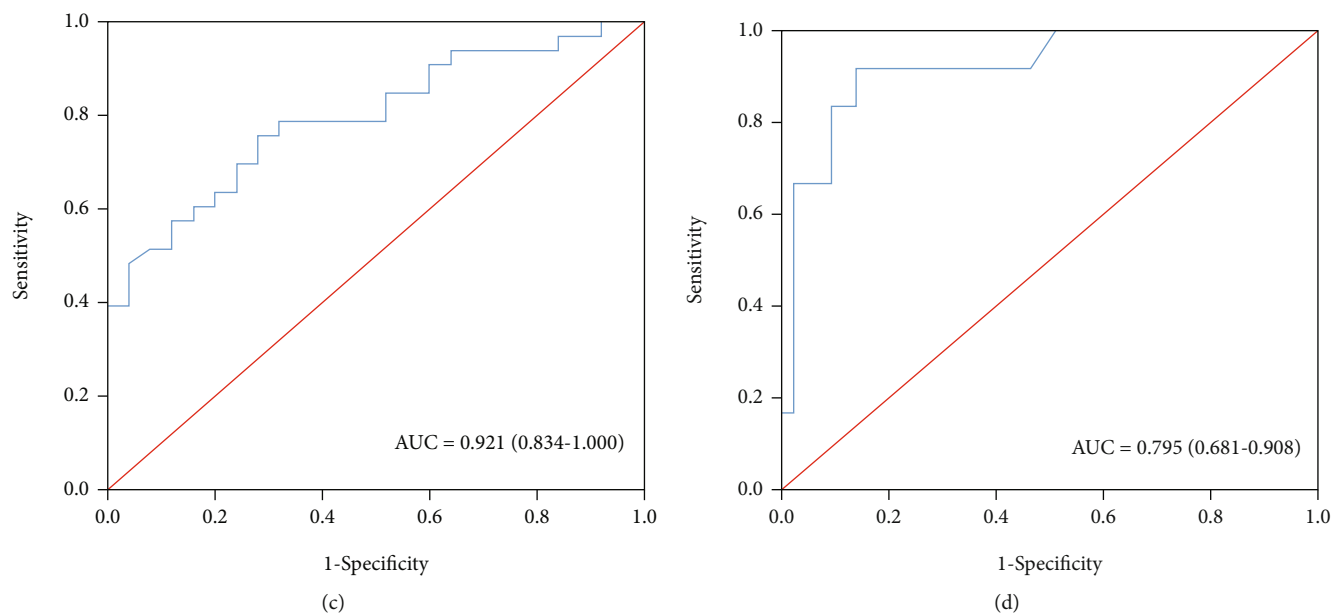


FIGURE 3: Performance of the nomogram in the validation cohorts. Calibration curve of the nomogram in the internal (a) and external (b) validation cohorts. The 45° dotted line represents an ideal prediction, and the solid line represents the bias-corrected predictive performance of the nomogram. The closer the solid line fits the ideal line, the better the predictive accuracy of the nomogram; ROC curves of the nomogram in the internal (c) and external (d) validation cohorts, respectively.

response to an infection, the neutrophil/lymphocyte ratio (NLR) was also higher in nonsurviving patients (12.51, IQR 7.22-18.83) than in surviving patients (3.41, IQR 1.89-7.16). The blood platelet count represents coagulation function and was dramatically reduced in nonsurviving patients (155.00 (IQR 114.50-208.50) vs. 35.90 (IQR 157.00-287.00)) ($P < 0.001$). Moreover, the serum levels of AST and GLU were also higher in patients with poor outcomes than in the other group (41.00 (IQR 24.00-63.00) vs. 30.00 (IQR 22.00-42.00), $P < 0.001$; 7.00 (IQR 5.80-10.30) vs. 5.60 (IQR 4.96-7.13), $P < 0.001$). COVID-19 damages respiratory function, and the $\text{PaO}_2/\text{FiO}_2$ (P/F) ratio in nonsurviving patients was markedly lower than that in surviving patients (104.44 (IQR 75.56-150.0) vs. 257.58 (IQR 168.85-314.75)). The PNI score in nonsurviving patients on admission was 33.41 (IQR 31.46-36.63), which was significantly lower than that in surviving patients (37.21 (IQR 34.07-40.56)) (Table 2).

3.3. Logistic Regression Analysis and Nomogram Establishment. Multivariate logistic regression analysis showed that the PLT count (odds ratio (OR) and 95% confidence interval (CI), 0.984 (0.974, 0.993); $P = 0.001$), baseline PNI score (OR and 95% CI, 0.853 (0.740, 0.983); $P = 0.028$), lactate dehydrogenase (LDH) level (OR with 95% CI, 1.005 (1.001, 1.009); $P = 0.012$), and P/F ratio (OR with 95% CI, 0.988 (0.981, 0.995); $P = 0.001$) were independent predictors of mortality in COVID-19 patients (Table 3).

A nomogram incorporating these four predictors was then constructed (Figure 2(a)) and showed good reliability (C-index: 0.959). The calibration curve for the nomogram (Figure 2(b)) showed good calibration in the training cohort. Then, the favorable calibration of the nomogram was confirmed in the validation cohort (Figure 3(a)). The AUCs of

the nomogram in the training and validation cohorts were 0.894 (95% CI, 0.832-0.956; Figure 2(c)) and 0.921 (95% CI, 0.834-1.000; Figure 3(c)), respectively, which revealed good discrimination. Furthermore, our nomogram also performed well in an external validation cohort (Figure 3(b)), with an AUC of 0.795 (95% CI, 0.681-0.908, Figure 3(d)).

3.4. Correlation between the PNI Score and Other Biomarkers of Disease Severity. The AUC for the PNI score was 0.711 (95% CI, 0.628-0.793), with a cutoff value of 33.405 (Figure 4(a)). We then divided the enrolled data into two groups based on the cutoff value of the PNI score. Cox analysis showed a significant reduction in the survival probability in the patients with a PNI score less than 33.405 on admission (Figure 4(b)). Furthermore, the correlation between the PNI score and disease severity was evaluated with Kendall's tau-b analysis. The results showed that the PNI score had the strongest negative relationships with the NLR and LDH level ($R = -0.458$, $P < 0.001$ and $R = -0.414$, $P < 0.001$) but was less strongly correlated with the CURB65 ($R = -0.303$, $P < 0.001$), APACHE II ($R = -0.313$, $P < 0.001$), and SOFA ($R = -0.256$, $P < 0.001$) scores (Figure 4(c)).

4. Discussion

In this study, we retrospectively assessed the clinical characteristics of severe COVID-19 patients from multiple hospitals and identified the baseline risk factors for mortality. Our results indicated that the PLT count, PNI score, P/F ratio, and LDH level on admission were independent predictors of mortality. The nomogram based on these risk factors showed good calibration and discrimination in the training and validation cohorts.

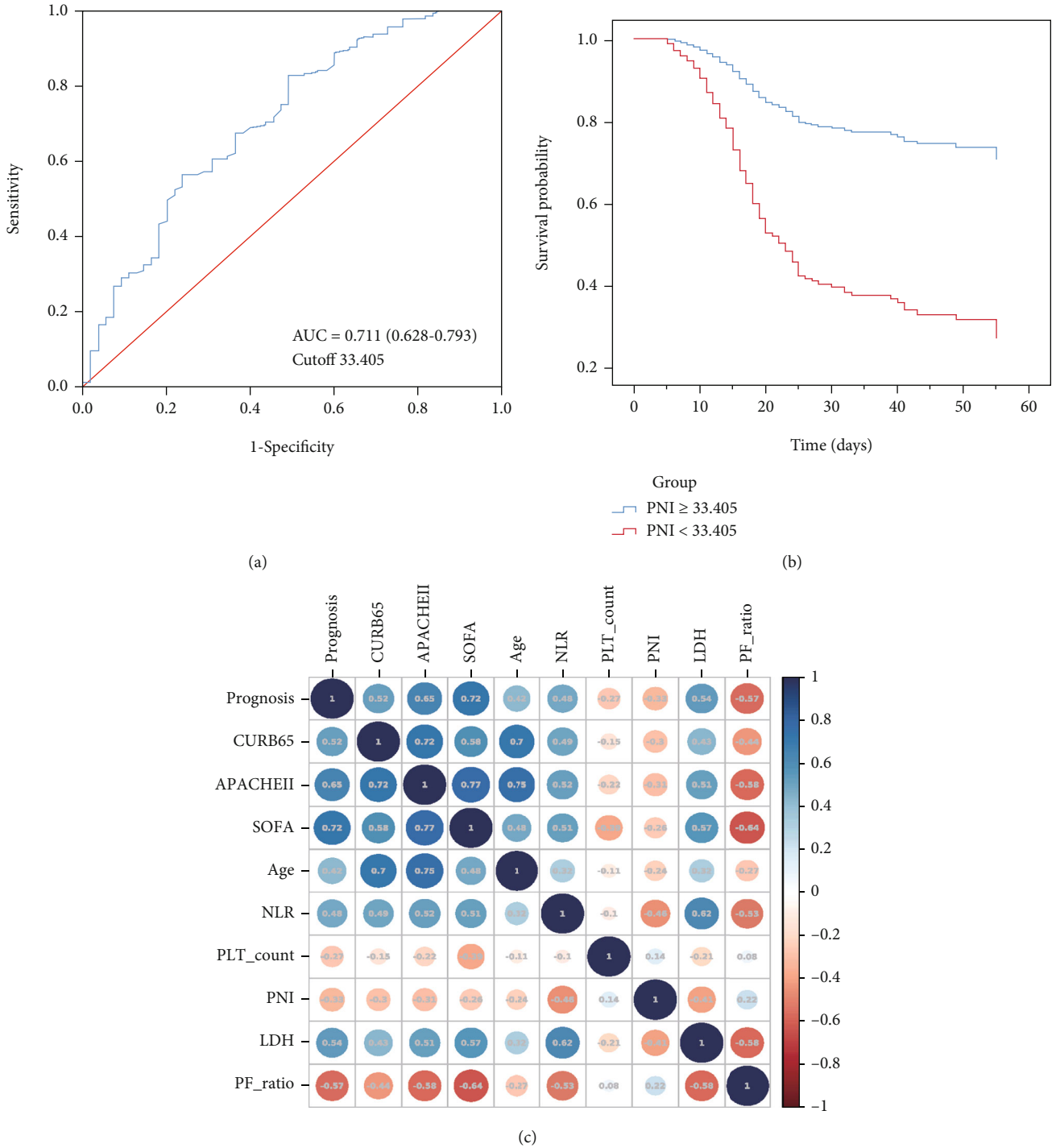


FIGURE 4: The significance of the PNI score for the prediction of mortality in patients with severe COVID-19. (a) ROC curve of PNI; (b) Cox analysis of COVID-19 patients based on the cutoff value of the PNI score; (c) correlation between the PNI score and other indicators of disease severity.

With the rapid increase in newly confirmed and severe cases, the management of patients with severe cases has become a challenging issue during the COVID-19 outbreak. The timely identification of patients at a high risk of developing acute respiratory distress syndrome (ARDS), multiorgan failure, and death might help clinicians develop individual treatment plans and rationally allocate medical resources.

In our cohorts, the mortality of patients with severe COVID-19 was 26.70%, which was higher than that in some large-scale reports [20] and slightly lower than that in Washington state in February [21]. This might be because we enrolled patients with COVID-19 during the early phase of the pandemic in Wuhan City, China. In addition, we found that nonsurviving patients were more likely to be older and

have underlying hypertension than surviving patients, which is in agreement with recent reports, which have suggested that age and hypertension may be risk factors for progression to severe COVID-19 [22, 23].

In our study, the patients with severe COVID-19 who died had lower baseline platelet counts, PNI scores, and P/F ratios and higher LDH levels, and these variables were independent risk factors for mortality. Previous studies showed that thrombocytopenia in COVID-19 patients was not a significant predictor of disease progression or adverse outcomes [24, 25]. Studies in consecutive patients with COVID-19 have reported that only approximately 5% of patients present with a platelet count less than 100×10^9 cells/L. Mild thrombocytopenia (a platelet count $< 150 \times 10^9$ cells/L) is identified in 70-95% of patients with severe COVID-19 [20]. The P/F ratio, which directly reflects lung oxygenation, represents the severity of ARDS in COVID-19 patients. In our study, the P/F ratio in nonsurviving patients was twofold lower than that in surviving patients, which was similar to the findings in Arentz et al.'s study [21]. Furthermore, in our previous study, the area under the curve (AUC = 0.878) implied that a serum LDH level greater than 344.5 U/L was strongly predictive of severe COVID-19, with high specificity (96.9%) and sensitivity (68.8%), further confirming that the LDH level is a strong predictive factor that can be used for the early detection of lung injury and severe COVID-19 cases [26].

Interestingly, we found that the prognostic nutritional index (PNI), which was initially used to assess patients' immune and nutritional statuses during the perioperative period and is calculated based on the serum albumin concentration and lymphocyte count in the peripheral blood, was also associated with mortality in patients with severe COVID-19. Previously, PNI was reported to be significantly correlated with poor survival and postoperative complications in patients with various malignant digestive system tumors [10, 11]. However, no studies have explored the association between the immunonutritional status and prognosis in COVID-19 patients.

Albumin is a widely used indicator of nutrition and has been shown to be associated with a poor outcome in critically ill patients. Growing evidence has shown that COVID-19 is associated with a strong cytokine storm [27] and, consequently, the consumption of albumin. Hypoalbuminemia is a typical clinical manifestation of various critical illnesses [28-31]. In our study, we found that the PNI score was significantly lower in nonsurviving patients and was most strongly negatively related to the NLR. The NLR is a reliable marker of systemic inflammation. A higher NLR has been widely reported to be a predictive indicator of poor survival in patients with many different diseases [32, 33]. The PNI score involves a combination of the albumin level and lymphocyte count in the peripheral blood, whereas the NLR can only reflect the inflammation status. In recent studies, the PNI was superior to the NLR as a prognostic marker in many cancer patients [34-36].

Furthermore, we also showed that the PNI score was negatively correlated with the LDH level. The LDH level was found to be positively associated with the C-reactive protein (CRP) level and negatively associated with the lymphocyte count [26]. Therefore, the PNI has been confirmed to be a

marker of the immunonutritional status of critically ill patients. The PNI was less strongly correlated with the CURB65, APACHE II, and SOFA scores in our study. The PNI score is a new biomarker of critical illness.

A combination of nutrition and inflammation can better predict the disease progression than an individual predictor. However, studies on the PNI score in COVID-19 patients are extremely limited. We evaluated the clinical characteristics and prognostic importance of the PNI score in severe COVID-19 patients, providing the first direct evidence that a lower PNI score is related to a worse prognosis. Furthermore, our nomogram, which includes the PNI score, had a higher AUC than the PNI score alone for predicting disease prognosis, which provides a new method of evaluating disease outcomes with good predictive accuracy.

However, there are still some limitations of our study. Our study was a retrospective study. The characteristics of the enrolled patients were imbalanced, and approximately 26.70% of the patients died. Second, the sample size was limited, and adjuvant treatments during hospitalization were thought to be similar but were not analyzed. A larger global cohort study of patients with COVID-19 would help further validate the nomogram model and identify the risk factors for severe COVID-19 and mortality.

5. Conclusion

In conclusion, our results provide the first direct evidence that a lower PNI score is related to a worse prognosis in patients with severe COVID-19. We also found that a lower PLT count, PNI, and P/F ratio and a higher LDH level on admission are independent predictors of mortality in patients with severe COVID-19, and the nomogram based on these four risk factors showed good predictive accuracy in the training and validation cohorts.

Abbreviations

PNI:	Prognostic nutritional index
COVID-19:	Coronavirus disease 2019
SARS-CoV-2:	Severe acute respiratory syndrome coronavirus 2
CAP:	Community-acquired pneumonia
NLR:	Neutrophil-lymphocyte ratio
IQR:	Interquartile range
C-index:	Concordance index
ROCs:	Receiver operating characteristics
AUC:	Areas under the curve
APACHE II:	Acute Physiology and Chronic Health Evaluation II
SOFA:	Sequential organ failure assessment
WBC:	White blood cell
AST:	Aspartate aminotransferase
LDH:	Lactic dehydrogenase
P/F:	PaO ₂ /FiO ₂
PLT:	Lower platelet
OR:	Odds ratio
ARDS:	Acute respiratory distress syndrome
CI:	Confidence interval
CRP:	C-reactive protein.

Data Availability

You could find these data in our results.

Ethical Approval

The study was approved by the Ethics Committee of Renmin Hospital of Wuhan University. And the judgement's reference number was WDRY2020-K048.

Conflicts of Interest

All authors declared that they had no conflict of interest.

Authors' Contributions

W. W. analyzed data and drafted the manuscript; X. W. organized, analyzed, and interpreted the data; the order of the authorship was based on their contributions to this study. Y. H. acquired data, designed the study, and took responsibility for data integrity and the accuracy of data analysis; S. M. helped revise the manuscript. M.M. organized data and helped with data analysis. Y. H., S. M., and M. M. are cocorresponding authors. C. J., T. M., and G. G. helped with data collections and performed the literature search. Wei Wei and Xingyue Wu are co-first authors.

Acknowledgments

We are grateful to all the patients, doctors, and nurses who participated in the study. We also would like to thank Dr. Peiyun Zhou from Shanghai Medical College of Fudan University for his help in practical questions and insightful discussions. His help was invaluable. This study was financially supported by Shanghai Pujiang Program (2020PJD011).

References

- [1] Organization, WH, "Coronavirus disease (COVID-19) outbreak 2020," 2020, <https://www.who.int>.
- [2] R. Dupont, M. Longué, A. Galinier et al., "Impact of micronutrient deficiency & malnutrition in systemic sclerosis: cohort study and literature review," *Autoimmunity Reviews*, vol. 17, no. 11, pp. 1081–1089, 2018.
- [3] S. Raposeiras Roubín, E. Abu Assi, M. Cespón Fernandez et al., "Prevalence and prognostic significance of malnutrition in patients with acute coronary syndrome," *Journal of the American College of Cardiology*, vol. 76, no. 7, pp. 828–840, 2020.
- [4] N. Lelijveld, M. Kerac, A. Seal et al., "Long-term effects of severe acute malnutrition on lung function in Malawian children: a cohort study," *European Respiratory Journal*, vol. 49, no. 4, p. 1601301, 2017.
- [5] S. E. Torrisi, B. Ley, M. Kreuter et al., "Reply to: Malnutrition in idiopathic pulmonary fibrosis: the great forgotten comorbidity," *European Respiratory Journal*, vol. 53, no. 5, p. 1900615, 2019.
- [6] U. Capitanio and F. Montorsi, "Does preoperative nutritional status affect survival in renal cell carcinoma? The debate continues," *European Urology*, vol. 59, no. 6, pp. 929–930, 2011.
- [7] M. Merker, M. Felder, L. Gueissaz et al., "Association of baseline inflammation with effectiveness of nutritional support among patients with disease-related malnutrition: a secondary analysis of a randomized clinical trial," *JAMA Network Open*, vol. 3, no. 3, article e200663, 2020.
- [8] D. Sueta, S. Hokimoto, K. Sakamoto et al., "Validation of the high mortality rate of malnutrition-inflammation-atherosclerosis syndrome," *International Journal of Cardiology*, vol. 230, pp. 97–102, 2017.
- [9] A. M. Freeman, P. B. Morris, N. Barnard et al., "Trending cardiovascular nutrition controversies," *Journal of the American College of Cardiology*, vol. 69, no. 9, pp. 1172–1187, 2017.
- [10] D. J. Pinato, B. V. North, and R. Sharma, "A novel, externally validated inflammation-based prognostic algorithm in hepatocellular carcinoma: the prognostic nutritional index (PNI)," *British Journal of Cancer*, vol. 106, no. 8, pp. 1439–1445, 2012.
- [11] C. Wang, W. He, Y. Yuan et al., "Comparison of the prognostic value of inflammation-based scores in early recurrent hepatocellular carcinoma after hepatectomy," *Liver International*, vol. 40, no. 1, pp. 229–239, 2020.
- [12] Y. L. Cheng, S. H. Sung, H. M. Cheng et al., "Prognostic nutritional index and the risk of mortality in patients with acute heart failure," *Journal of the American Heart Association*, vol. 6, no. 6, 2017.
- [13] E. Driggin, M. V. Madhavan, B. Bikdeli et al., "Cardiovascular considerations for patients, health care workers, and health systems during the COVID-19 pandemic," *Journal of the American College of Cardiology*, vol. 75, no. 18, pp. 2352–2371, 2020.
- [14] T. Çınar, M. Hayıroğlu, V. Çiçek et al., "Is prognostic nutritional index a predictive marker for estimating all-cause in-hospital mortality in COVID-19 patients with cardiovascular risk factors?," *Heart & lung : the journal of critical care*, vol. 50, no. 2, pp. 307–312, 2021.
- [15] X. Hu, H. Deng, Y. Wang, L. Chen, X. Gu, and X. Wang, "Predictive value of the prognostic nutritional index for the severity of coronavirus disease 2019," *Nutrition*, vol. 84, p. 111123, 2021.
- [16] S. Mu, W. Wei, C. Jin et al., "Risk factors for COVID-19 patients with cardiac injury: pulmonary ventilation dysfunction and oxygen inhalation insufficiency are not the direct causes," *Aging*, vol. 12, no. 23, pp. 23464–23477, 2020.
- [17] J. P. Metlay, G. W. Waterer, A. C. Long et al., "Diagnosis and treatment of adults with community-acquired pneumonia. An official clinical practice guideline of the American Thoracic Society and Infectious Diseases Society of America," *American Journal of Respiratory and Critical Care Medicine*, vol. 200, no. 7, pp. e45–e67, 2019.
- [18] G. P. Buzby, J. L. Mullen, D. C. Matthews, C. L. Hobbs, and E. F. Rosato, "Prognostic nutritional index in gastrointestinal surgery," *American Journal of Surgery*, vol. 139, no. 1, pp. 160–167, 1980.
- [19] R. L. Baker, B. L. Jamison, T. A. Wiles et al., "CD4 T cells reactive to hybrid insulin peptides are indicators of disease activity in the NOD mouse," *Diabetes*, vol. 67, no. 9, pp. 1836–1846, 2018.
- [20] W. J. Guan, Z. Y. Ni, Y. Hu et al., "Clinical characteristics of coronavirus disease 2019 in China," *The New England Journal of Medicine*, vol. 382, no. 18, pp. 1708–1720, 2020.
- [21] M. Arentz, E. Yim, L. Klaff et al., "Characteristics and outcomes of 21 critically ill patients with COVID-19 in Washington State," *JAMA*, vol. 323, no. 16, pp. 1612–1614, 2020.
- [22] C. Wu, X. Chen, Y. Cai et al., "Risk factors associated with acute respiratory distress syndrome and death in patients with

- coronavirus disease 2019 pneumonia in Wuhan, China,” *JAMA Internal Medicine*, vol. 180, no. 7, pp. 934–943, 2020.
- [23] F. Zhou, T. Yu, R. du et al., “Clinical course and risk factors for mortality of adult inpatients with COVID-19 in Wuhan, China: a retrospective cohort study,” *Lancet*, vol. 395, no. 10229, pp. 1054–1062, 2020.
- [24] C. Huang, Y. Wang, X. Li et al., “Clinical features of patients infected with 2019 novel coronavirus in Wuhan, China,” *Lancet*, vol. 395, no. 10223, pp. 497–506, 2020.
- [25] J. Thachil, N. Tang, S. Gando et al., “ISTH interim guidance on recognition and management of coagulopathy in COVID-19,” *Journal of Thrombosis and Haemostasis*, vol. 18, no. 5, pp. 1023–1026, 2020.
- [26] Y. Han, H. Zhang, S. Mu et al., “Lactate dehydrogenase, an independent risk factor of severe COVID-19 patients: a retrospective and observational study,” *Aging*, vol. 12, no. 12, pp. 11245–11258, 2020.
- [27] J. B. Moore and C. H. June, “Cytokine release syndrome in severe COVID-19,” *Science*, vol. 368, no. 6490, pp. 473–474, 2020.
- [28] G. Chen, D. Wu, W. Guo et al., “Clinical and immunological features of severe and moderate coronavirus disease 2019,” *The Journal of Clinical Investigation*, vol. 130, no. 5, pp. 2620–2629, 2020.
- [29] A. Y. Liu, C. S. Nabel, B. S. Finkelman et al., “Idiopathic multicentric Castleman’s disease: a systematic literature review,” *Lancet Haematol*, vol. 3, no. 4, pp. e163–e175, 2016.
- [30] A. Nowak-Węgrzyn, Y. Katz, S. S. Mehr, and S. Koletzko, “Non-IgE-mediated gastrointestinal food allergy,” *The Journal of Allergy and Clinical Immunology*, vol. 135, no. 5, pp. 1114–1124, 2015.
- [31] F. Violi, G. Ceccarelli, R. Cangemi et al., “Hypoalbuminemia, coagulopathy, and vascular disease in COVID-19,” *Circulation Research*, vol. 127, no. 3, pp. 400–401, 2020.
- [32] E. Cataudella, C. M. Giraffa, S. di Marca et al., “Neutrophil-to-lymphocyte ratio: an emerging marker predicting prognosis in elderly adults with community-acquired pneumonia,” *Journal of the American Geriatrics Society*, vol. 65, no. 8, pp. 1796–1801, 2017.
- [33] A. Haram, M. R. Boland, M. E. Kelly, J. C. Bolger, R. M. Waldron, and M. J. Kerin, “The prognostic value of neutrophil-to-lymphocyte ratio in colorectal cancer: a systematic review,” *Journal of Surgical Oncology*, vol. 115, no. 4, pp. 470–479, 2017.
- [34] T. Oba, K. Maeno, M. Ono, T. Ito, T. Kanai, and K. I. Ito, “Prognostic nutritional index is superior to neutrophil-to-lymphocyte ratio as a prognostic marker in metastatic breast cancer patients treated with Eribulin,” *Anticancer Research*, vol. 41, no. 1, pp. 445–452, 2021.
- [35] J. Wang, Y. Liu, X. Mi, M. Shao, and L. Liu, “The prognostic value of prognostic nutritional index (PNI) and neutrophil to lymphocyte ratio (NLR) for advanced non-small cell lung cancer treated with platinum-based chemotherapeutics,” *Ann Palliat Med*, vol. 9, no. 3, pp. 967–978, 2020.
- [36] C. Mirili, A. Yilmaz, S. Demirkan, M. Bilici, and S. Basol Tekin, “Clinical significance of prognostic nutritional index (PNI) in malignant melanoma,” *International Journal of Clinical Oncology*, vol. 24, no. 10, pp. 1301–1310, 2019.

Research Article

HMSC-Derived Exosome Inhibited Th2 Cell Differentiation via Regulating miR-146a-5p/SERPINB2 Pathway

Jing Zhou,¹ Yi Lu,² Wei Wu,² and Yunhai Feng¹ 

¹Department of Otorhinolaryngology, Head & Neck Surgery, Dahua Hospital, Shanghai 200237, China

²Department of Pharmaceutics School of Pharmacy, Fudan University, Shanghai 201203, China

Correspondence should be addressed to Yunhai Feng; fengyunhaient@sina.com

Received 14 December 2020; Revised 1 February 2021; Accepted 27 April 2021; Published 15 May 2021

Academic Editor: Ran Wang

Copyright © 2021 Jing Zhou et al. This is an open access article distributed under the Creative Commons Attribution License, which permits unrestricted use, distribution, and reproduction in any medium, provided the original work is properly cited.

Background. Allergic rhinitis (AR) is a global disease without specific treatment. Human mesenchymal stem cell- (HMSC-) derived exosomes (HMSC-exos) have been implicated for the amelioration of allergic inflammation by delivering miR-146a-5p in a mouse asthma model. However, the anti-allergic activity and the underlying mechanism of HMSC-exos in AR remain unclear. The present study aimed to investigate the role of HMSC-exos in the pathogenesis of AR. **Materials and Methods.** Blood specimens were collected from AR patients and healthy donors for investigation. HMSC and CD4⁺ T cells were used in the present study. Flow cytometry was used to characterize the population of Type 1 helper T (Th1) and Th2 cells. Specific siRNA and overexpressed plasmids were designed to silence or overexpress the expressions of miR-146a-5p and SERPINB2. Luciferase reporter assay was adopted to explore the binding site of miR-146a-5p and SERPINB2. Quantitative real-time PCR and immunoblots were performed to estimate the expression of target genes. **Results.** The population of Th2 cells was significantly elevated in AR patients as compared with that in healthy donors. HMSC-exos could decrease the expression of SERPINB2 and the differentiation of Th2 cells. miR-146a-5p in HMSC-exos exhibited consistent effects and lowered the expression of SERPINB2 by binding on its 3'UTR region. Moreover, the differentiation of Th2 cells was promoted by SERPINB2 that could be reversed by HMSC-exos. Additionally, the miR-146a-5p expression was negatively associated with the SERPINB2 expression in the serum of AR patients. **Conclusion.** HMSC-exos could inhibit the differentiation of Th2 cells via the regulation of the miR-146a-5p/SERPINB2 pathway. miR-146a-5p and SERPINB2 could be applied as potential targets for AR treatment.

1. Introduction

Allergic rhinitis (AR) is a type of nasal mucosal disease characterized by overreacted immune responses. It is a global disease that affects approximately 20%–30% of the world population [1]. Although AR is not fatal, patients usually experience physical discomfort and psychological stress that heavily impairs their quality of life. The pathogenesis of AR is associated with the activation of immunoglobulin E (IgE) and the release of inflammatory components, such as histamine in response to specific allergens [2]. Our previous study revealed that the reduction of inflammatory responses using taurine could ameliorate the symptoms of AR in a mouse model [3]. Therefore, strategies to inhibit the inflammation in the nasal mucosa are potential therapeutics for AR treatment.

Type 1 helper T (Th1) and Th2 cells are two subtypes of helper T cells. Th1 cells are activated by IL-12 and marked by T-bet. Th1 cells can secrete IFN- γ and IL-2 and stimulate the activities of macrophages and CD8⁺ T cells that mediate cell-mediated immune responses against intracellular antigens [4]. By contrast, Th2 cells are activated by IL-4 and IL-2 and marked by GATA-3. Th2 cells can stimulate B cells and mediate humoral immune responses against extracellular antigens [4]. The imbalance of Th1 and Th2 cells is considered to be a pathogenic factor of allergic diseases, such as AR [5]. During AR, the CD4⁺ T cells are more likely to differentiate into Th2 cells that reduce the population of Th1 cells and result in the imbalance of Th1/Th2 cells. Moreover, the inhibition of Th2 cells was a potential approach for AR treatment [6]. Therefore, therapeutics targeting Th1 and Th2 cells are promising approaches for AR treatment.

Exosomes are believed to play a critical role in the orchestration of immune responses. Previous studies have indicated that cell-derived exosomes could trigger proinflammatory responses by the transportation of molecules contained in the exosomes [7, 8]. Additionally, the released exosomes and microRNAs (miRNAs) are detected in bronchoalveolar lavage fluids from patients with respiratory diseases, such as asthma and AR, indicating that exosomes and miRNAs are involved in AR pathogenesis [9]. A previous study showed that exosomes derived from the human mesenchymal stem cell (HMSC) could ameliorate inflammation by delivering miR-146a-5p that was abundantly expressed in HMSC-derived exosomes (HMSC-exos) [10].

Serpin family B member 2 (SERPINB2), a member of the serine protease inhibitor family, is predicted as a potential target of miR-146a-5p that can stimulate inflammation. Moreover, SERPINB2 was highly expressed in nasal brushings of AR patients and played a crucial role in Th2-mediated immune responses [11]. By searching the predicting miRNA for SERPINB2 using the TargetScan database (<http://www.targetscan.org>), SERPINB2 is predicted as a potential target of miR-146a-5p. However, the regulatory mechanisms of miR-146a-5p and SERPINB2 in AR remain unclear. Furthermore, their role in the differentiation of Th1 and Th2 cells remains unclear. Therefore, our study was conducted to explore the role of the miR-146a-5p/SERPINB2 signaling pathway in the differentiation of Th1 and Th2 cells, aiming to provide novel strategies for AR treatment.

2. Materials and Methods

2.1. Sample Collection. The blood specimens of AR patients and healthy donors were collected from Dahua Hospital, Shanghai, China, after written informed consent was obtained from all the subjects ($n = 25$ for each group). All blood samples were subpacked in 500 μ L sodium citrate (3.2%) tubes, centrifuged, and the plasma snap-frozen in liquid N_2 and stored at -80°C for further analysis. These AR patients, aged 20–50 years, do not have any other chronic medical conditions or allergic disorders except AR. The inclusion and exclusion criteria were as per those mentioned in a previous report [12]. Briefly, the inclusion criteria were as follows: age 20–50 years, daytime fatigue, daytime somnolence, nasal congestion, perennial AR with a positive skin test response for perennial allergen (wheal diameter equal to 3 mm or greater), and a negative skin test response for seasonal allergens. The exclusion criteria included seasonal allergies, known sleep apnea, obesity, nasal polyps, recent upper respiratory tract infection, deviated septum, asthma, and other respiratory diseases. Age-matched healthy individuals without chronic medical conditions or allergic disorders were selected as controls.

2.2. Cell Culture. The HMSC and 293T cells were obtained from Shanghai Biology Institute (Shanghai, China). HMSC was obtained by density centrifugation isolation from bone marrow, then cultured and expanded. Cells were cultured in DMEM medium with 10% fetal bovine serum (FBS, Gibco, USA) and were maintained in 5% CO_2 at 37°C . Flow cytometry

was used to detect biomarkers of HMSC, including positive biomarkers (CD90 and CD105) and negative biomarkers (CD34 and CD45).

2.3. Exosomes Isolation. Exosomes were precipitated using exosome precipitation solution (Exo-Quick; System Bioscience) as per the manufacturer's instructions with some modifications. HMSC exosomes were collected from approximately 3.2×10^7 cells at early passages (passages 2–3). Once the HMSC cultures reached 70% confluence, the cells were cultured for 24–48 h in α -MEM containing exosome-depleted FBS or PL. Exosome-depleted FBS and PL were obtained with overnight centrifugation at $70,000 \times g$ at 4°C . Briefly, the HMSC conditioned medium was centrifuged twice at $500 \times g$ for 10 min, twice at $2000 \times g$ for 15 min, and twice at $10,000 \times g$ for 30 min. The supernatant was then transferred to Ultra-Clear tubes and centrifuged at $70,000 \times g$ for 1 h at 4°C in an SW32Ti rotor (Beckman Coulter Inc., Woerden, The Netherlands). The exosome-containing pellet was washed with PBS and centrifuged at $70,000 \times g$ for 1 h. The pellet was then carefully suspended in 200 μ L PBS and used immediately or stored at -80°C . Exosome protein markers, CD63 (Ab134045, Abcam, UK), CD81 (ab109201, Abcam, UK), and TSG101 (ab125011, Abcam, UK), were determined using immune blotting. The morphology of the exosomes was examined using transmission electron microscopy. The size analysis of the exosome was provided in supplementary material file 1.

2.4. Exosome Uptake Assay. Exosomes were stained with PKH67 (Sigma) as per previously reported protocols [13]. The exosomes were incubated with PKH67 solution for 4 min at room temperature. Then, exosomes were isolated via centrifugation at $100,000 \times g$ for 1 h. When the exosomes were cocultured with CD4^+ T cells, the uptake of exosomes was detected using confocal microscopy.

2.5. Isolation of CD4^+ T Cells. In the present study, the blood samples from AR patients or normal corresponding donors were diluted with PBS solution (1:1). Peripheral blood mononuclear cells were obtained via centrifugation on a lymphocyte separation medium. Then, the cell concentration of lymphocytes was adjusted to $1 \times 10^6/\text{mL}$. The human CD4^+ T cells were isolated with CD4^+ T cell isolation kits (130-096-533, Miltenyi Biotec, Germany). All the procedures were performed as per the manufacturer's instructions.

2.6. RNA Isolation and qRT-PCR Analysis. Total RNA of samples was extracted using TRIzol (Invitrogen) as per the manufacturer's protocol from different CD4^+ T cells from AR patients. RNA was transcribed into cDNA using a cDNA synthesis kit (RR047A, Takara). Quantitative real-time PCR was performed using SYBR green (RR820A, Takara) as per the three-step amplification procedure. Gene expression was calculated using the $2^{-\Delta\Delta\text{Ct}}$ method. All the data represent the average of three replicates. The detection of genes was performed using the following primers: hsa-miR-146a-5p, F: CGCGTGAG AACTGAATTCCA, R: AGTGCA GGGTCCGAGGTATT; SERPINB2, F: CGAGGAGAGGA GAT TGAAC, R: GGATCTGCTG CATGAAC-; T-bet, F:

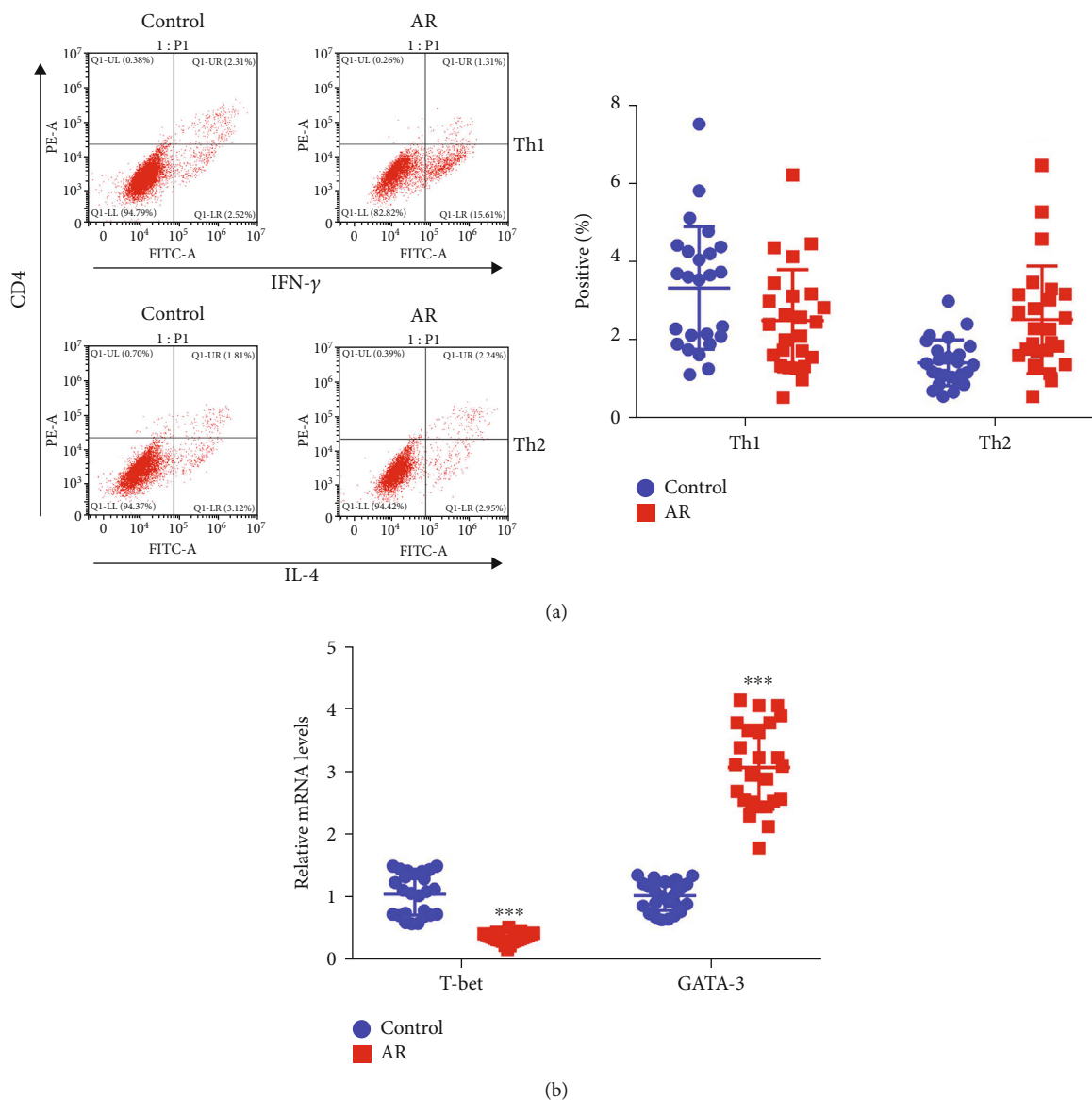


FIGURE 1: The population of Th2 cells was upregulated in the blood samples of allergic rhinitis (AR) patients. (a) Flow cytometry was used to examine the distribution of Th1 (CD4⁺IFN- γ ⁺) or Th2 (CD4⁺IL-4⁺) cells in the blood samples of allergic rhinitis patients and corresponding donors. * $p < 0.05$ vs. control, ** $p < 0.01$ vs. control. (b) qRT-PCR was used to examine the relative mRNA levels of T-bet (Th1 marker) and GATA-3 (Th2 marker) in the blood-derived mononuclear cells of allergic rhinitis patients and corresponding donors. *** $p < 0.001$ vs. control.

TTGAGGTGAACGACGGAGAG, R: TGGGTAGGAGAGGAGAGTAGTG; GATA-3, F: GAGCGAGCAACGCAATCTGAC, R: AGGCTGGGAAGCAAAGGTGAG; β -actin, F: GATGACCCAGATCATGTTTGAG, R: TAATGTCACGCACGATTTCC'; U6, F: CTCGCTTCGGCAGCACA, R: AACGCTTCACGAATTTGCGT.

2.7. Western Blot Analyses. Different CD4⁺ T cells, as indicated above, were lysed using RIPA lysis buffer with a protease inhibitor to obtain total proteins (Beyotime, China). The protein was separated in SDS-PAGE and transferred to a polyvinylidene fluoride membrane. Thereafter, the primary antibody was applied at 4°C overnight. The secondary antibody (Beyotime, Shanghai, China) was applied for 1 h

at 37°C. The protein expression was detected after the application of ECL substrate. All the data represent the average of three replicates. Our study used the following primary antibodies: TSG101 (Ab125011, Abcam), CD63 (Ab59479, Abcam), CD81 (Ab109201, Abcam), SERPINB2 (Ab269275, Abcam), T-bet (Ab91109, Abcam), GATA-3 (Ab106625, Abcam), and β -actin (20536-1-AP, Proteintech).

2.8. Flow Cytometry. The population of Th1 and Th2 cells was estimated using Th1/Th2/Th17 PhenotypingKit (560758, BD Biosciences). Total 1×10^5 CD4⁺ T cells were collected and stained with PerCP-Cy5.5-labeled anti-IFN γ and APC-anti-IL-4 for 30 min at room temperature. Th1 cells were marked as CD4⁺IFN- γ ⁺, whereas Th2 cells were marked as CD4⁺IL-

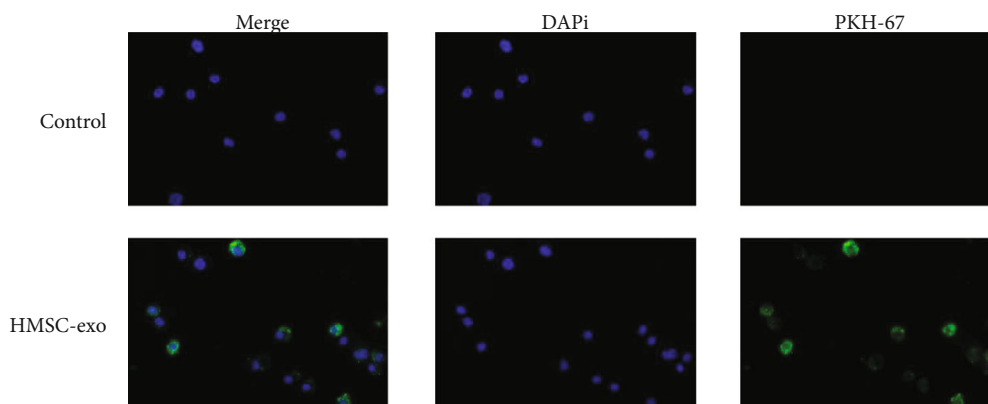


FIGURE 2: The HMSC-exo was able to uptake by AR CD4⁺ cells through endocytosis. The PKH67-labeled (green) immature HMSC-exos were cocultured with CD4⁺ cells. Then, the AR CD4⁺ cells were fixed and stained with DAPI (blue). The uptake of HMSC-exos by AR CD4⁺ cells was observed under a confocal microscope.

4⁺. The populations of Th1 and Th2 cells were calculated using the FACSDiva 7.0 software. All the data represent the average of three replicates.

2.9. Knockdown and Overexpression of SERPINB2. Cells were transfected with three siRNAs targeting at SERPINB2 (RiboBio, Guangzhou, China) and a plasmid containing the coding sequence of human SERPINB2 (Major, Shanghai, China). Two negative control (NC) plasmids were applied as the control group of the siRNA and overexpression plasmid. Lipofectamine 3000 (Thermo Fisher Scientific) was used for the transfection. The sequence of SERPINB2 plasmids was provided as follows: siSERPINB2-1: 5'-CCTTATACAAGTTACTTAA-3'; siSERPINB2-2: 5'-GGCACAAGCTGCAGATAAAA-3'; siSERPINB2-3: 5'-GGTCAAGACTCAAACC AAA-3'; siNC: 5'-CAGUACUUUUGUGUAGUACAA-3'.

2.10. Dual-Luciferase Reporter Gene Assay. Human embryonic kidney cells (HEK 293T) are widely used for determining the dual-luciferase reporter gene assay [14]. Wildtype and mutant sequences of SERPINB2 were cloned to luciferase reporter vectors (pGL3-Basic). Then, 293T cells were transfected with vectors and miR-146a-5p inhibitor or mimics. After 48 h, a dual-luciferase reporter gene kit (Beijing Yuanpinghao Biotechnology Co., Ltd.) was used to detect and analyze the luciferase activity. All the data represent the average of three replicates.

2.11. Statistical Analyses. Statistical analyses were conducted using GraphPad Prism version 7.0. The experimental data are presented as mean \pm SD for at least three samples. Comparison between two groups was performed using the *T*-test, whereas comparison among multiple groups was performed with one-way analysis of variance. A two-sided *p* value of <0.05 was considered to indicate statistical significance.

3. Results

3.1. The Population of Th2 Cells Was Elevated in the CD4⁺ T Cells of AR Patients. To verify the ratio of Th1 and Th2 cells in AR, we collected blood specimens from AR patients for

analyses. The CD4⁺ T cells were isolated from the blood specimens. Flow cytometry showed that the quantity of Th1 (CD4⁺IFN- γ ⁺) was significantly decreased, whereas that of Th2 (CD4⁺IL-4⁺) was significantly increased in AR patients as compared with that in healthy donors (*p* < 0.05) (Figure 1(a)). Moreover, the expression of T-bet (the marker of Th1 cells) was significantly decreased, whereas that of GATA-3 (the marker of Th2 cells) was significantly elevated in AR patients as compared with that in healthy donors (*p* < 0.05) (Figure 1(b)). These results indicated that the elevation of Th2 might be associated with the development of AR.

3.2. Exosomes of HMSC Could Be Absorbed by CD4⁺ T Cells through Endocytosis in AR. Furthermore, we explored the interaction between HMSC-exos and CD4⁺ T cells. The HMSC-exos were isolated, as described previously. We verified the isolated HMSC using flow cytometry that revealed that the positive rate of negative biomarkers (CD34 and CD45) for HMSC was <1.0%, whereas that of positive biomarkers (CD90 and CD105) for HMSC was >90% (Figure S1A). Transmission electron microscopy validated the morphology of the isolated HMSC-exos (Figure S1B). Then, the markers of exosomes, including TSG101, CD63, and CD81, were detected in isolated exosomes that indicated the successful isolation of HMSC-exos (Figure S1C). When CD4⁺ T cells were cocultured with PKH67-labeled HMSC-exos, we found that CD4⁺ T cells could absorb HMSC-exos via endocytosis (Figure 2). These results suggested that HMSC could interact with CD4⁺ T cells via the secretion of exosomes.

3.3. HMSC-Exos Decreased the Expression of SERPINB2 and Differentiation of Th2 Cells after Coculture with CD4⁺ T Cells. To understand the effects of HMSC-exos on CD4⁺ T cells, we detected the expression of several genes, including T-bet and GATA-3 of CD4⁺ T cells after coculture with HMSC-exos. GW4869 was added to inhibit the secretion of exosomes as an NC. The expression of T-bet was significantly elevated after coculture with GW4869-exos and HMSC-exos, whereas that of GATA-3 was significantly decreased after

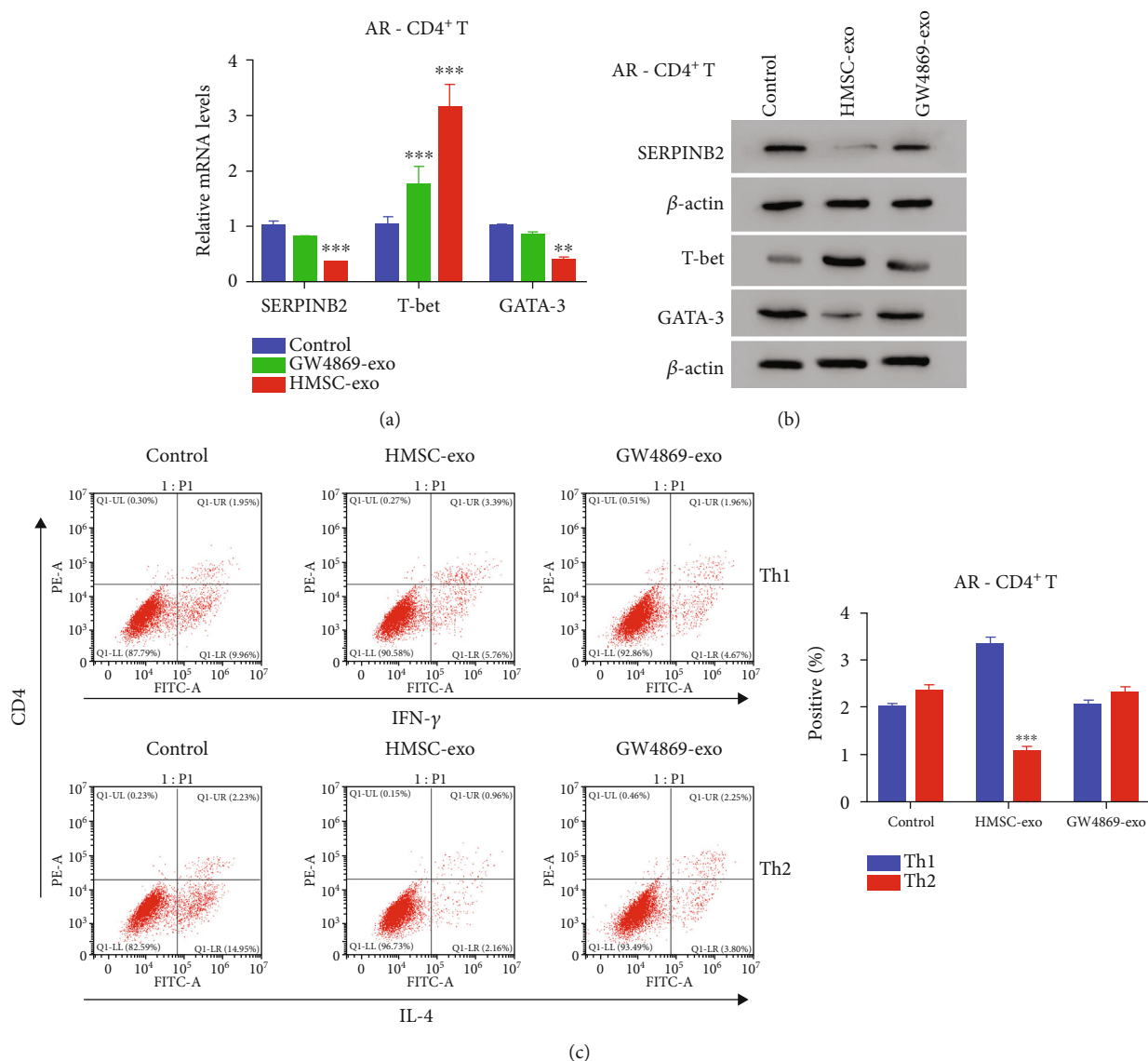


FIGURE 3: The differentiation of AR CD4⁺ cells into Th2 type was downregulated after co-culture with HMSC-exo. (a, b) qRT-PCR and western blot analysis were used to examine the relative mRNA and protein levels of SERPINB2, T-bet, and GATA-3 in AR CD4⁺ after coculture with GW4869-exo or HMSC-exo. ** $p < 0.01$ vs. control, *** $p < 0.001$ vs. control. (c) The AR CD4⁺ cells differentiated into Th2 type cells were deeply suppressed after co-cultured with HMSC-exo. *** $p < 0.001$ vs. Th1.

coculture with HMSC-exos ($p < 0.05$) (Figures 3(a) and 3(b)). In the meantime, the SERPINB2 expression was significantly reduced after coculture with HMSC-exos, consistent with that in GATA-3 ($p < 0.05$). Moreover, flow cytometry revealed that the population of Th2 cells was significantly decreased after coculture with HMSC-exos ($p < 0.05$) (Figure 3(c)). However, the population of Th2 cells was not significantly altered when they were cocultured with GW4869-exos ($p < 0.05$). These results indicated that HMSC-exos could reduce the expression of SERPINB2 and differentiation of Th2 cells.

3.4. HMSC-Exos Inhibited the Differentiation of Th2 Cells via Delivery of miR-146a-5p. Furthermore, we explored the underlying mechanism of HMSC-exos in the differentiation of Th1 and Th2 cells. The mimics and inhibitor of miR-

146a-5p were used to induce the upregulation and downregulation of miR-146a-5p in HMSC ($p < 0.05$) (Figure 4(a)). miR-146a-5p mimics exosomes (mimic-exo) significantly elevated, whereas miR-146a-5p inhibitor exosomes (inhibitor-exo) significantly decreased the expression of miR-146a-5p as compared with the control group ($p < 0.05$) (Figure 4(b)). Moreover, SERPINB2 was significantly decreased by miR-146a-5p mimic-exo, whereas inhibitor-exo significantly promoted the SERPINB2 expression ($p < 0.05$). Furthermore, we confirmed the alteration of SERPINB2 induced by mimic-exo using immunoblots (Figure 4(c)). The expression of T-bet was markedly decreased after coculture with inhibitor-exo; the expression of GATA-3 was notably decreased after coculture with mimic-exo. Additionally, flow cytometry showed that the population of Th1 cells was significantly reduced by inhibitor-exo, whereas that of Th2 cells was significantly reduced by

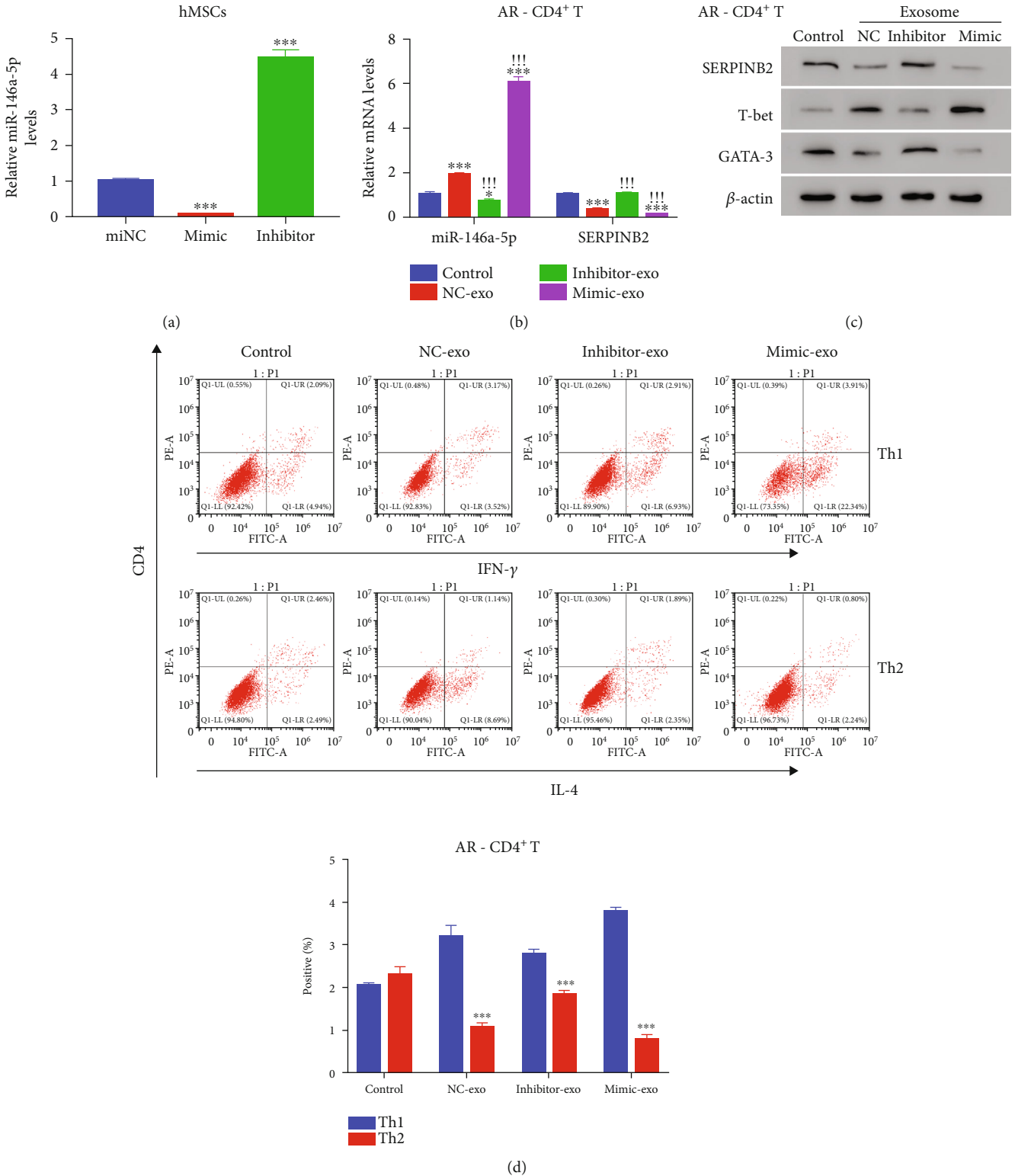


FIGURE 4: HMSC-derived exosome inhibited the AR CD4⁺ cells differentiated into Th2 type cells through delivering miR-146a-5p. (a) miR-146a-5p induced silencing and overexpression using corresponding mimic and inhibitor in hMSCs. ****p* < 0.001 vs. miNC (b). The relative levels of miR-146a-5p and SERPINB2 in AR CD4⁺ cells after coculture with NC-exo, inhibitor-exo, and mimic-exo. **p* < 0.05 vs. control, ****p* < 0.001 vs. control; !!! **p* < 0.05 vs. NC-exo. (c) Western blot analysis was used to quantify the protein contents of SERPINB2, T-bet, and GATA-3 in AR CD4⁺ cells after co-culture with NC-exo, inhibitor-exo, and mimic-exo. (d) The distribution of Th1 and Th2 cells in AR CD4⁺ T cells after co-culture with NC-exo, inhibitor-exo, and mimic-exo. ****p* < 0.001 vs. control.

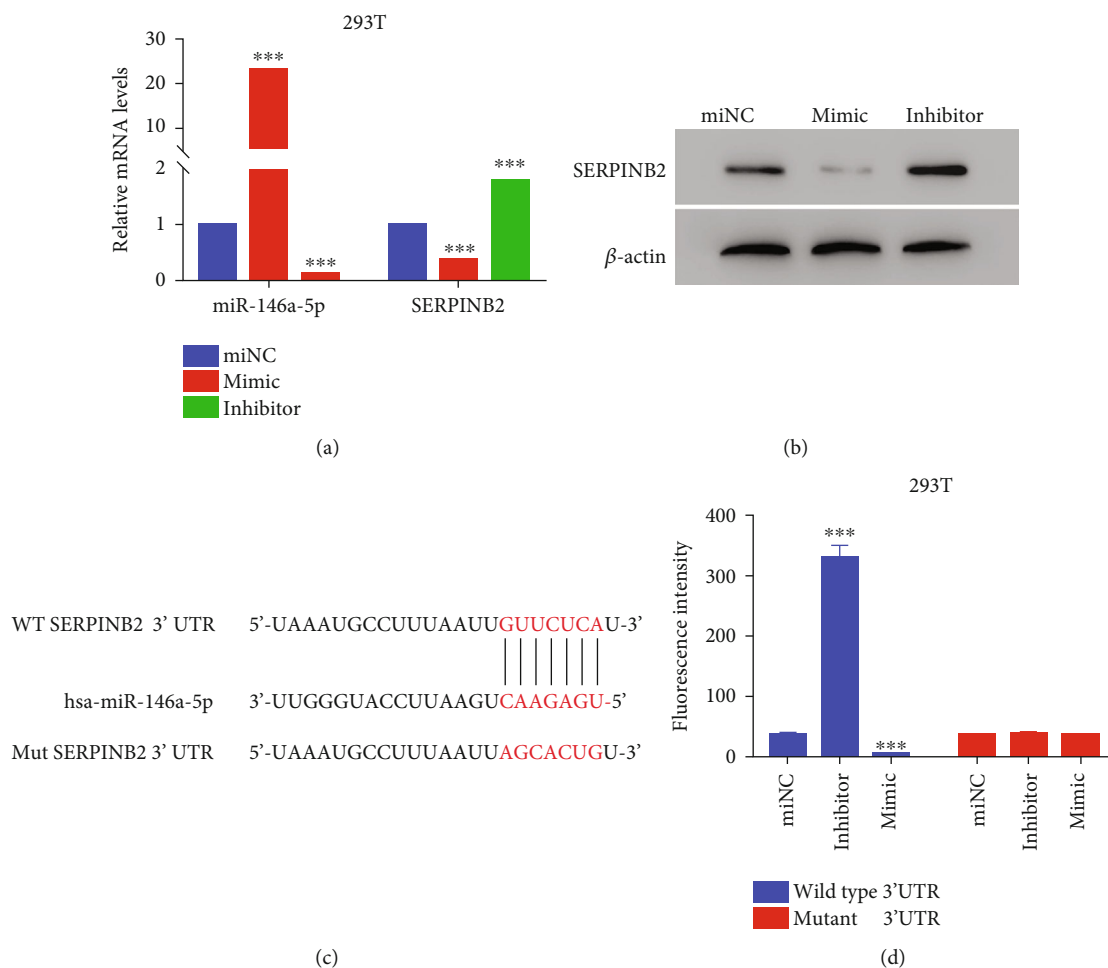


FIGURE 5: miR-146a-5p inhibited the transcription of SERPINB2 by binding on its 3' UTR. (a) qRT-PCR was used to examine the relative levels of miR-146a-5p and SERPINB2 in 293T cells after coculture with miR-146a-5p miNC, mimic, and inhibitor. *** $p < 0.001$ vs. miNC. (b) The protein level of SERPINB2 was examined in 293T cells after coculture with miR-146a-5p miNC, mimic, and inhibitor. (c) The wild type and mutant binding site in the 3' UTR of SERPINB2 for miR-146a-5p. (d) Dual-luciferase report vector was used to determine the relationship between miR-146a-5p and SERPINB2 in 293T cells. *** $p < 0.001$ vs. miNC.

mimic-exo. These results indicated that HMSC-exos could inhibit the differentiation of Th2 cells by delivering miR-146a-5p.

3.5. miR-146a-5p Inhibited SERPINB2 by Binding on Its 3' UTR Region. SERPINB2 was significantly reduced with the elevated level of miR-146a-5p; therefore, we explored the correlation between miR-146a-5p and SERPINB2. The mimics and inhibitor of miR-146a-5p were used to induce the upregulation and downregulation of miR-146a-5p ($p < 0.05$) (Figure 5(a)). The expression of SERPINB2 was significantly elevated with miR-146a-5p inhibitor that was reversed by miR-146a-5p mimics ($p < 0.05$) (Figures 5(a) and 5(b)). The binding region of SERPINB2 and miR-146a-5p was predicted using online databases (Figure 5(c)). Dual-luciferase report vectors with wildtype and mutant sequences of 3' UTR of SERPINB2 were transfected in 293T cells. Results showed that the fluorescence intensity of the wildtype vector was significantly affected ($p < 0.05$), whereas the mutant vector exhibited no significant change ($p > 0.05$), indicating that

miR-146a-5p could directly bind to the 3' UTR region of SERPINB2 (Figure 5(d)). These results suggested that SERPINB2 was involved in the biological activities of miR-146a-5p.

3.6. SERPINB2 Promoted the Differentiation of Th2 Cells and Was Suppressed by HMSC-Exos. Furthermore, we explored the role of SERPINB2 in the differentiation of Th2 cells. Specific siRNAs and overexpression plasmids were designed to inhibit and elevate the SERPINB2 expression that was significantly inhibited by three siRNAs ($p < 0.05$) (Figure S2A–B). Moreover, SERPINB2 knockdown could significantly elevate the population of Th1 cells and diminish Th2 cells ($p < 0.05$) (Figure 6(a)). Moreover, T-bet was notably increased, and GATA-3 was decreased after SERPINB2 inhibition (Figure 6(b)). Additionally, the SERPINB2 expression was significantly increased after transfecting with SERPINB2-overexpressed plasmid ($p < 0.05$) (Figure S2C–D). HMSC-exos significantly reduced the SERPINB2 expression ($p < 0.05$) (Figure 7(a)). Additionally, the HMSC-exos markedly reduced

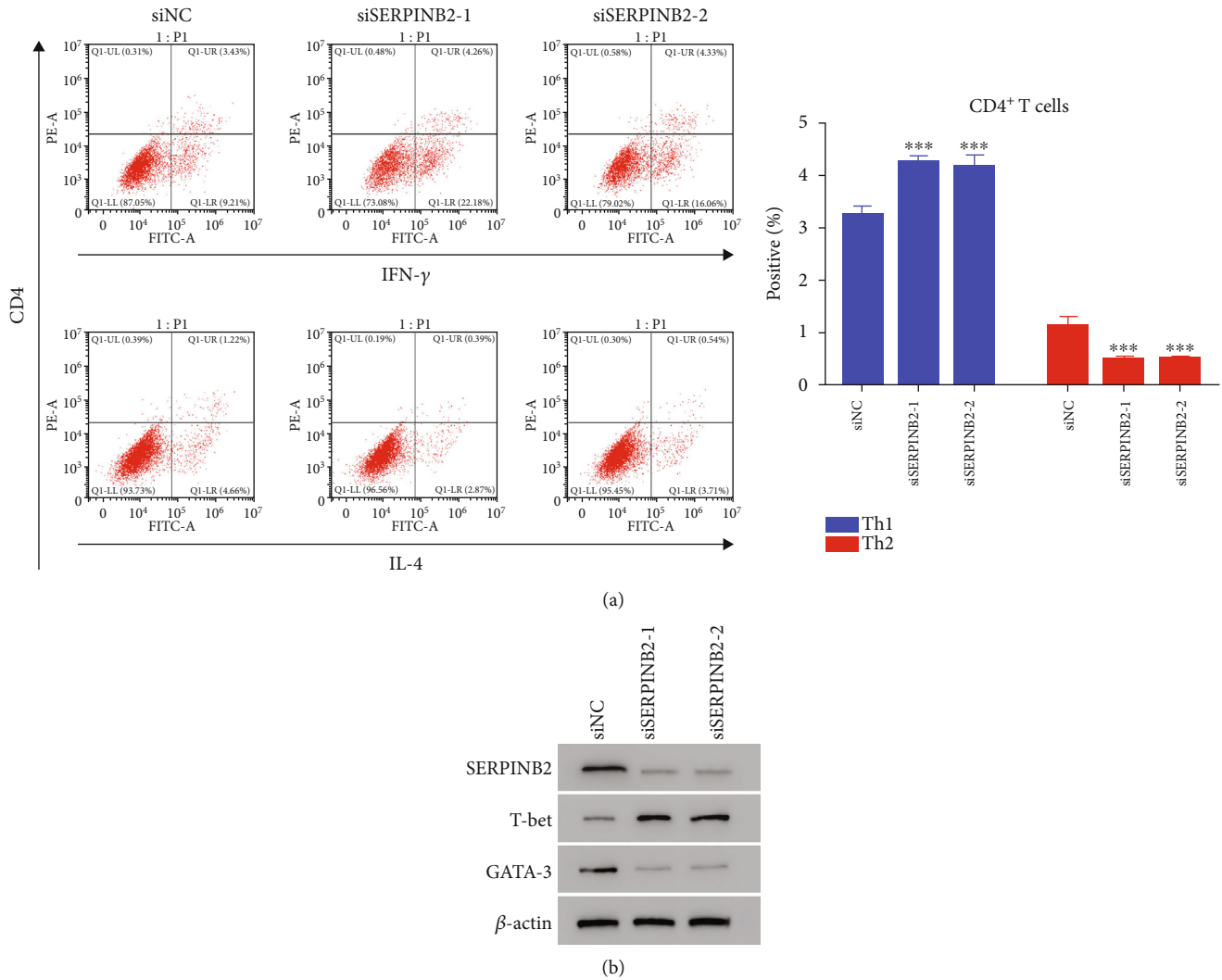


FIGURE 6: Knockdown of SERPINB2 inhibited the CD4⁺ T cells differentiated into Th2 type cells. (a) The differentiation of CD4⁺ T cells into Th2 type cells was deeply suppressed after transfection with siSERPINB2-1 or siSERPINB2-2. *** $p < 0.001$ vs. siNC. (b) Western blot analysis was used to examine the protein levels of SERPINB2, T-bet, and GATA-3 in the CD4⁺ T cells after transfection with siSERPINB2-1 or siSERPINB2-2.

the GATA-3 expression and increased the T-bet expression in CD4⁺ T cells ($p < 0.05$) (Figure 7(b)). Moreover, the population of Th1 cells did not change significantly, whereas that of Th2 cells decreased significantly after coculture with HMSC-exos ($p < 0.05$) (Figure 7(c)). These results indicated that SERPINB2 could promote the differentiation of Th2 cells, which was suppressed by HMSC-exos.

3.7. miR-146a-5p Was Negatively Associated with SERPINB2. To validate the association between miR-146a-5p and SERPINB2 in AR, we detected their expressions in AR patients and the corresponding donors. miR-146a-5p was significantly suppressed, whereas SERPINB2 was highly expressed in AR patients ($p < 0.05$) (Figure 8(a)). Moreover, miR-146a-5p was negatively associated with the SERPINB2 expression ($r = -0.81$, $p < 0.05$) (Figure 8(b)). These results suggested that miR-146a-5p and SERPINB2 were involved in the same signaling pathway.

4. Discussion

Our study investigated a novel miR-146a-5p/SERPINB2 signaling pathway in AR pathogenesis. The imbalance of Th1/Th2 cells was associated with AR pathogenesis. Exosomes derived from HMSC could inhibit the differentiation of Th2 cells via the delivery of miR-146a-5p. Moreover, SERPINB2 could promote the differentiation of Th2 cells that was suppressed by miR-146a-5p in HMSC-exos. These findings revealed a novel regulatory mechanism of HMSC-exos in the differentiation of CD4⁺ T cells and provided potential therapeutic targets for AR treatment.

AR is an allergic disease with overreacted immune responses in the nasal mucosa, wherein the generation of IgE and the recruitment of immune cells are involved in allergic responses [15]. The excessive activation of Th2 cells and the induction of eosinophilic-dependent inflammation are associated with AR symptoms [16]. Th2 cells are capable of

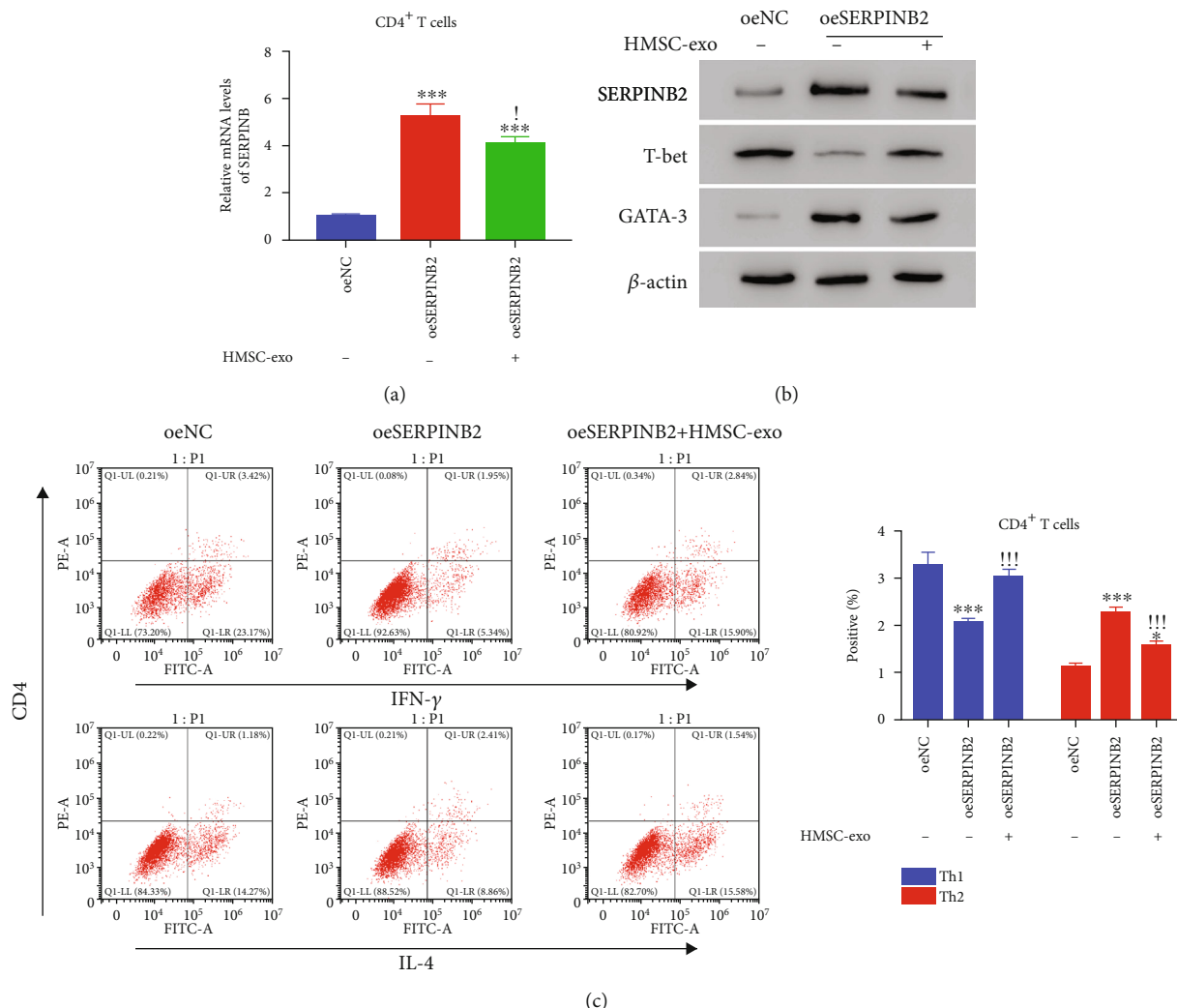


FIGURE 7: HMSC-derived exosome suppressed the effects of oeSERPINB2 in normal CD4⁺ T cells. (a) The level of SERPINB2 was downregulated in oeSERPINB2 cells after coculture with HMSC-exo. (b) Western blot analysis was used to examine the protein contents of SERPINB2, T-bet, and GATA-3 in oeSERPINB2 cells with or without coculture with HMSC-exo. (c) The differentiation of CD4⁺ T cells into Th2 cells was suppressed after coculture with HMSC-exo. **p* < 0.05 vs. oeNC, ****p* < 0.001 vs. oeNC; !!!*p* < 0.001 vs. oeSERPINB2.

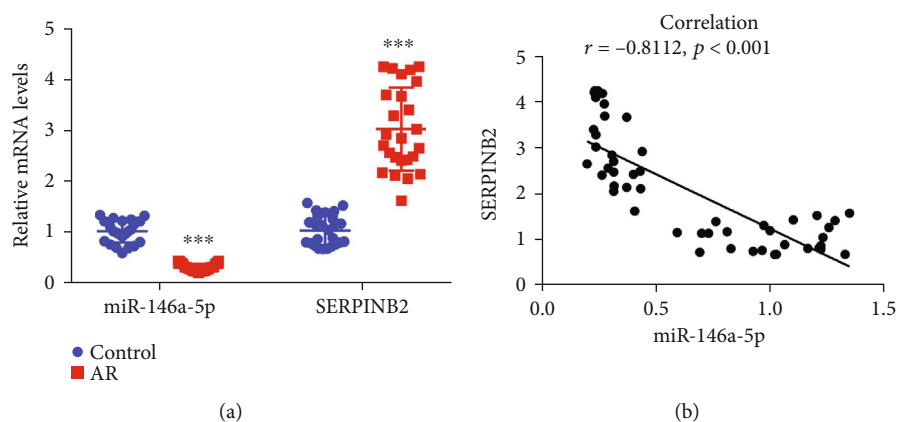


FIGURE 8: miR-146a-5p was negatively correlated with SERPINB2. (a) The relative levels of miR-146a-5p and SERPINB2 were examined in the serum-derived mononuclear cells of allergic rhinitis patients and corresponding donors, *n* = 25 for each group. (b) Correlation analysis between miR-146a-5p and SERPINB2.

releasing cytokines, including IL-4, IL-10, and IL-13, to stimulate the activities of different immune cells. IL-4 can stimulate the production of IgE antibodies by B cells that subsequently activates mast cells to produce histamine [17]. A previous study showed that these cytokines were elevated in the serum of AR patients [18]. In our study, the population of Th2 cells was significantly elevated in AR patients as compared with that in healthy donors. Thus, the elevation of Th2 cells was associated with AR pathogenesis.

Exosomes are crucial regulators of intercellular communications. The contents of the exosomes are believed to play key roles in allergic diseases. Exosomes derived from bronchial epithelial cells can stimulate chemotaxis and monocyte proliferation [19]. Additionally, macrophages can release exosomes to stimulate the inflammatory responses in response to intracellular pathogens [20]. Mast cells are critical for Th2- and IgE-mediated immune responses and can secrete histamine to stimulate inflammation [21]. A previous study has demonstrated that exosomes derived from mast cells could stimulate the secretion of inflammatory cytokines and induce airway inflammation and allergic symptoms [22]. Our study showed that HMSC-exos could be absorbed by CD4⁺ T cells and diminishes the Th2 cell population, indicating that HMSC-exos might be associated with the differentiation of CD4⁺ T cells during AR pathogenesis.

miR-146a-5p was first reported by Taganov et al. in 2006 and was associated with the NF- κ B pathway [23]. TRAF6 and IRAK1 were predicted as potential targets of miR-146a-5p, and their expressions were suppressed by miR-146a-5p. Moreover, miR-146a-5p in the HMSC-exos could significantly inhibit the infiltration of immune cells, reduce the levels of Th2-related cytokines, and alleviate overreacted responses of the airway in a mouse asthma model [10]. Consequently, miR-146a-5p was considered to negatively regulate the immune responses. In our study, miR-146a-5p in the HMSC-exos was demonstrated to decrease the population of Th2 cells, consistent with previous hypotheses. Moreover, SERPINB2 was predicted as a potential target of miR-146a-5p. SERPINB2 is highly expressed during inflammation, infection, and tissue damage, indicating its immune features [24, 25]. A previous study revealed that SERPINB2 and miR-146a-5p are highly expressed in psoriatic skin and SERPINB2 was suppressed by miR-146a-5p [26]. Our study revealed that SERPINB2 inhibition could reduce the differentiation of Th2 cells, whereas its overexpression exhibited reversed effects. Moreover, the regulation by SERPINB2 could be reversed after coculture with HMSC-exos. These results indicated that HMSC-exos could inhibit Th2 cell differentiation via the miR-146a-5p/SERPINB2 pathway.

There are certain limitations of this study. Our results were mainly obtained from in vitro experiments. The construction of an AR mouse model will further help us investigate the biological activities of HMSC-exos in AR. However, our study still provides a novel molecular mechanism for AR pathogenesis.

5. Conclusions

In sum, our study showed that HMSC-exos could inhibit the differentiation of Th2 cells via the regulation of the miR-

146a-5p/SERPINB2 pathway. miR-146a-5p and SERPINB2 could be applied as potential targets for AR treatment.

Data Availability

The datasets used and/or analyzed during the current study are available from the corresponding author on reasonable request.

Conflicts of Interest

The authors declare that they have no competing interests.

Authors' Contributions

Yunhai Feng designed this project and revised the manuscript; Jing Zhou performed the experiments and wrote the draft; Yi Lu analyzed the data and edited diagrams. Wei Wu helped to technical assistance. All authors have contributed to read and agreed the final content of the manuscript for submission.

Acknowledgments

We sincerely acknowledged the assistance given by Dahua Hospital, Shanghai, 200237, China, and Fudan University, Shanghai, 201203, China for the present research. This research was financially supported by the Xuhui District Major Medical Research Project (NO.SHXU201804) and Shanghai Natural Science Foundation Project (NO.18ZR1435300).

Supplementary Materials

Supplementary materials: identification of HMSC-derived exosome. Figure S1: identification of human bone marrow mesenchymal stem cells (HMSC) and exosome. (a) Flow cytometer was used to examine the positive (CD90 and CD105) and negative biomarker (CD34 and CD45) for HMSC. (b) The morphology of exosome derived from HMSC. (c) Western blot was used to examine the protein levels of biomarker of exosome, including TSG101, CD63, and CD81. Figure S2: knockdown and overexpression of SERPINB2 in normal CD4⁺ T cells. A and B. The relative mRNA and protein levels of SERPINB2 were deeply suppressed in CD4⁺ T cells after transfecting with siSERPINB2-1, siSERPINB2-2, and siSERPINB2-3. *** $p < 0.001$ vs. siNC. (c, d) The relative mRNA and protein levels of SERPINB2 were significantly overexpressed in CD4⁺ T cells after transfecting with oeSERPINB2. *** $p < 0.001$ vs. oeNC. (*Supplementary Materials*)

References

- [1] A. N. Greiner, P. W. Hellings, G. Rotiroti, and G. K. Scadding, "Allergic rhinitis," *Lancet*, vol. 378, no. 9809, pp. 2112–2122, 2011.
- [2] L. M. Wheatley and A. Togias, "Allergic Rhinitis," *New England Journal of Medicine*, vol. 372, no. 5, pp. 456–463, 2015.
- [3] J. Zhou, Y. Lu, F. Li, W. Wu, D. Xie, and Y. Feng, "In vitro and in vivo anti-allergic effects of taurine on allergic rhinitis,"

- International Archives of Allergy and Immunology*, vol. 181, no. 6, pp. 404–416, 2020.
- [4] J. Zhu and W. E. Paul, “CD4 T cells: fates, functions, and faults,” *Blood*, vol. 112, no. 5, pp. 1557–1569, 2008.
- [5] C. Kirmaz, P. Bayrak, O. Yilmaz, and H. Yuksel, “Effects of glucan treatment on the Th1/Th2 balance in patients with allergic rhinitis: a double-blind placebo-controlled study,” *European Cytokine Network*, vol. 16, no. 2, pp. 128–134, 2005.
- [6] H. Shirasaki, E. Kanaizumi, N. Seki, and T. Himi, “Correlation of local FOXP3-expressing T cells and Th1-Th2 balance in perennial allergic nasal mucosa,” *New England Journal of Medicine*, vol. 2011, article 259867, pp. 1–6, 2011.
- [7] F. Huang, H. Jia, Y. Zou, Y. Yao, and Z. Deng, “Exosomes: an important messenger in the asthma inflammatory microenvironment,” *The Journal of International Medical Research*, vol. 48, no. 2, article 300060520903220, 2020.
- [8] C. Lässer, S. E. O’Neil, G. V. Shelke et al., “Exosomes in the nose induce immune cell trafficking and harbour an altered protein cargo in chronic airway inflammation,” *Journal of Translational Medicine*, vol. 14, no. 1, p. 181, 2016.
- [9] B. Sastre, J. A. Canas, J. M. Rodrigo-Munoz, and V. Del Pozo, “Novel modulators of asthma and allergy: exosomes and microRNAs,” *Frontiers in Immunology*, vol. 8, p. 826, 2017.
- [10] S. B. Fang, H. Y. Zhang, C. Wang et al., “Small extracellular vesicles derived from human mesenchymal stromal cells prevent group 2 innate lymphoid cell-dominant allergic airway inflammation through delivery of miR-146a-5p,” *Journal of Extracellular Vesicles*, vol. 9, no. 1, p. 1723260, 2020.
- [11] A. Zhao, Z. Yang, R. Sun et al., “SerpinB2 is critical to Th2 immunity against enteric nematode infection,” *Journal of Immunology*, vol. 190, no. 11, pp. 5779–5787, 2013.
- [12] T. J. Craig, S. Teets, E. B. Lehman, V. M. Chinchilli, and C. Zwillich, “Nasal congestion secondary to allergic rhinitis as a cause of sleep disturbance and daytime fatigue and the response to topical nasal corticosteroids,” *Journal of Allergy & Clinical Immunology*, vol. 101, no. 5, pp. 633–637, 1998.
- [13] G. Wei, Y. Jie, L. Haibo et al., “Dendritic cells derived exosomes migration to spleen and induction of inflammation are regulated by CCR7,” *Scientific Reports*, vol. 7, no. 1, p. 42996, 2017.
- [14] D. Wider and D. Picard, “Secreted dual reporter assay with Gaussia luciferase and the red fluorescent protein mCherry,” *PLoS One*, vol. 12, no. 12, article e0189403, 2017.
- [15] D. H. Broide, “Allergic rhinitis: pathophysiology,” *Allergy and Asthma Proceedings*, vol. 31, no. 5, pp. 370–374, 2010.
- [16] Q. L. Fu, Y. Y. Chow, S. J. Sun et al., “Mesenchymal stem cells derived from human induced pluripotent stem cells modulate T-cell phenotypes in allergic rhinitis,” *Allergy*, vol. 67, no. 10, pp. 1215–1222, 2012.
- [17] Y. Y. Wan, “GATA3: a master of many trades in immune regulation,” *Trends in Immunology*, vol. 35, no. 6, pp. 233–242, 2014.
- [18] H. Zhong, X. L. Fan, S. B. Fang, Y. D. Lin, W. Wen, and Q. L. Fu, “Human pluripotent stem cell-derived mesenchymal stem cells prevent chronic allergic airway inflammation via TGF- β 1-Smad2/Smad3 signaling pathway in mice,” *Molecular Immunology*, vol. 109, pp. 51–57, 2019.
- [19] A. Kulshreshtha, T. Ahmad, A. Agrawal, and B. Ghosh, “Proinflammatory role of epithelial cell-derived exosomes in allergic airway inflammation,” *Journal of Allergy and Clinical Immunology*, vol. 131, no. 4, pp. 1194–1203.e14, 2013.
- [20] S. Bhatnagar, K. Shinagawa, F. J. Castellino, and J. S. Schorey, “Exosomes released from macrophages infected with intracellular pathogens stimulate a proinflammatory response in vitro and in vivo,” *Blood*, vol. 110, no. 9, pp. 3234–3244, 2007.
- [21] S. Merluzzi, E. Betto, A. A. Ceccaroni, R. Magris, M. Giunta, and F. Mion, “Mast cells, basophils and B cell connection network,” *Molecular Immunology*, vol. 63, no. 1, pp. 94–103, 2015.
- [22] Y. C. Xia, T. Harris, A. G. Stewart, and G. A. Mackay, “Secreted factors from human mast cells trigger inflammatory cytokine production by human airway smooth muscle cells,” *International Archives of Allergy and Immunology*, vol. 160, no. 1, pp. 75–85, 2012.
- [23] K. D. Taganov, M. P. Boldin, K. J. Chang, and D. Baltimore, “NF-kappaB-dependent induction of microRNA miR-146, an inhibitor targeted to signaling proteins of innate immune responses,” *Proceedings of the National Academy of Sciences of the United States of America*, vol. 103, no. 33, pp. 12481–12486, 2006.
- [24] Q. Li, F. Ke, W. Zhang et al., “Plasmin plays an essential role in amplification of psoriasisiform skin inflammation in mice,” *PLoS One*, vol. 6, no. 2, article e16483, 2011.
- [25] M. Gliozzi, T. Greenwell-Wild, W. Jin et al., “A link between interferon and augmented plasmin generation in exocrine gland damage in Sjögren’s syndrome,” *Journal of Autoimmunity*, vol. 40, pp. 122–133, 2013.
- [26] H. Vaher, A. Kivihall, T. Runnel et al., “SERPINB2 and miR-146a/b are coordinately regulated and act in the suppression of psoriasis-associated inflammatory responses in keratinocytes,” *Experimental Dermatology*, vol. 29, no. 1, pp. 51–60, 2020.